NASA CR-72731

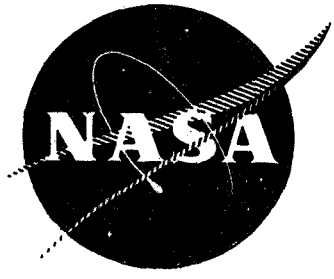

DEVELOPMENT OF HIGH-TEMPERATURE CHROMIUM ALLOYS

by

J.W. Clark

GENERAL ELECTRIC COMPANY

prepared for

NATIONAL AERONAUTICS AND SPACE ADMINISTRATION

NASA-Lewis Research Center
CONTRACT NAS 3-7260
John P. Merutka, Project Manager
William D. Klopp, Research Advisor

NASA CR-72731

FINAL REPORT

DEVELOPMENT OF HIGH-TEMPERATURE CHROMIUM ALLOYS

by

J.W. Clark
GENERAL ELECTRIC CO.
Evendale, Ohio 45215

prepared for

NATIONAL AERONAUTICS AND SPACE ADMINISTRATION

November 4, 1970

CONTRACT NAS 3-7260

Technical Management
NASA-Lewis Research Center
Cleveland, Ohio 44135
John P. Merutka, Project Manager
William D. Klopp, Research Advisor

TABLE OF CONTENTS

TABLE OF CONTENTS (Concl'd)

LIST OF TABLES

LIST OF TABLES (Concl'd)

LIST OF ILLUSTRATIONS

LIST OF ILLUSTRATIONS (CONCL'D)

ABSTRACT

Mechanical properties and air-oxidation behavior of some 400 chromium-base compositions were determined at temperatures up to 2400°F. W is superior to Mo and Re as a strengthening element, but it has an adverse effect on workability and low-temperature ductility. Carbides and borides strengthen without adversely affecting ductility. The air-oxidation resistance of Cr-Y alloys containing dispersions based on Cb, Ta, or Ti is markedly inferior to those with Hf-rich or Zr-rich secondary phases. Additions of La or of La plus Y were shown to be more effective than Y alone.

1. SUMMARY

Mechanical properties and air oxidation behavior of over 200 chromium-base alloys have been determined at test temperatures through 2400°F. Some 60 alloys were induction melted in ZrO_2 crucibles in an inert atmosphere, cast as ingots of about four pounds each, and processed by extrusion and swaging to small-diameter bar stock. Using hydrogen-reduced electrolytic chromium flake, oxygen, and nitrogen, levels were maintained below a total of 200 ppm. In addition, over 150 compositions were arc melted as 50- to 100-gram buttons or drop castings, and critical properties were evaluated.

Precipitation of metalloid phases based on Group IV-A and V-A metals was emphasized in this program. Several dilute alloys, dispersion strengthened by carbides or borides exhibited tensile ductility at sub-zero temperatures, combined with tensile strengths as high as 35,000 psi at 1900°F in the wrought condition and 6,000 to 10,000 psi at 2400°F. Addition of 4 atomic percent Mo (or Mo plus W) raises the tensile strength of the carbide-containing alloys to the range of 60,000 to 70,000 psi at 1900°F and about 20,000 psi at 2400°F, but the ductile-brittle transition temperature (DBTT) in tension increases to at least 350°F. Creep-rupture behavior is rather attractive through 2100°F (Cr-4Mo-Y alloys with CbC and TaC dispersions having 100-hour rupture strengths of 15,000 to 17,000 psi at this temperature).

Tungsten is a more effective solution strengthener than Mo, particularly at 2400°F, but concentrations of 4 atomic percent W raise the DBTT to at least 600°F. Rhenium was shown to be relatively ineffective in elevated-temperature strengthening, but room-temperature ductility was observed in a Cr-4Re-(Ta,Hf)C alloy and low Re levels were shown to have a beneficial effect on oxidation-nitridation behavior.

The air-oxidation resistance of Cr-Y alloys containing dispersions based on Cb, Ta, or Ti is markedly inferior to those with Hf-rich or Zr-rich secondary phases, which show no nitridation or drastic internal hardening after air exposure at temperatures through 2400°F. Additions of La or of La plus Y were shown to be more effective than Y alone in retarding nitridation of alloys with dispersions such as CbC, TaC, or TiC, at least through 100 hours at 2100°F.

2. INTRODUCTION

The sustained interest in chromium as a base for high-temperature structural components is founded on a number of factors. Chromium has a melting point advantage of 500° to 700°F over such more commonly used metals as iron, cobalt, and nickel, and its density is significantly lower than that of the latter two. The oxidation resistance of chromium is vastly superior to that of the heavier, more refractory metals such as columbium, tantalum, molybdenum, and tungsten. Hot corrosion by environments which contain sulfur or marine salts appears to be retarded in superalloys with only moderate additions of chromium, and chromium-base alloys have shown attractive behavior in limited hot-corrosion testing. The elastic modulus of chromium is higher by about 30% than that of most superalloys; the coefficient of thermal expansion is considerably lower, and the thermal conductivity higher by factors of two to five. These properties combine to offer the potential for much greater resistance to thermal shock or thermal fatigue than that exhibited by superalloys. In addition to the physical properties mentioned above, considerations of availability lend support to research on chromium alloys. The world reserves of chromium are estimated at about one billion tons. Chromium is thus more abundant than nickel, for example, by two orders of magnitude.

The use of chromium alloys as structural components in such applications as advanced air-breathing propulsion systems has been deterred by the lack of ductility at low temperatures, except in the purest forms of the unalloyed metal, in the optimum microstructural condition, and by the further embrittlement due primarily to reaction with nitrogen during extended exposure to air at elevated temperatures. There were also some early indications[1,2] that the potential strength advantage over superalloys, suggested by the increased melting point, could not be realized by "conventional" alloying approaches.

Several studies of chromium alloys over the past several years have identified alloy systems which not only have in fact achieved significant strength increases over the best currently available superalloys at temperatures above about 1800°F, but which also have given indications that the severity of the ductility and nitrogen-embrittlement problems could be greatly reduced. The alloying approach that has shown the most promise to date, and which has been emphasized in General Electric work[3-5] and by the Australian groups associated with the Department of Supply[6-8], is based on dispersion of carbides formed by the reactive metals of Group IV-A and V-A. Properties of one such alloy of this type, a rather complex carbide-strengthened Cr-W-Y alloy developed in this laboratory and designated C-207[9,10], have been investigated in some detail; and, the alloy has been developed to the point that turbine blading has been produced from 100-pound heats by forging. Based on creep-rupture characteristics, this alloy in the coated condition offers a temperature advantage of at least 100° to 150°F over the strongest

superalloys, with a 100-hour rupture strength of 16,000 psi at 2000°F. Other carbide-strengthened alloys (that contain no major substitutional solutes for solution strengthening) have shown considerable tensile ductility at sub-zero temperatures in both the wrought and recrystallized conditions, even when produced from chromium grades of only moderate purity.

The work summarized here was undertaken in an effort to make further improvements in the critical properties of chromium alloys beyond those offered by the compositions described above and more recently reported alloys identified by the Australians [7,8]. Not only were additional increases in accompanying improvements in the ductile-brittle transition temperature [which for C-207 is typically 400°F at slow (tensile) strain rates and 700°F under impact loading] were also sought. Although it is probable that long-time application of chromium alloys will require the successful development of protective coatings, a secondary objective of the present work has been the identification of more effective means of retarding reaction during air oxidation through minor alloying additions.

3. BACKGROUND

Several significant advances have been made in the technology of Cr alloys over the past several years. The addition of reactive elements such as yttrium was found to improve the resistance to nitrogen absorption [11,13]. The mechanism(s) by which reactive-metal additions improve the resistance to nitridation have not been completely defined, but the effect has been well documented and is reproducible. Combinations of Y with other reactive metal additions such as Th and Hf are more effective than single additions in improving both nitridation resistance and retention of ductility after high-temperature exposure. An alloy of Cr-Y-Th-Hf, where the total alloy content was less than 0.5 wt. percent, was resistant to nitridation for 100 hours at 2300°F in thin (0.022-inch) sections[14]. There was no evidence of incipient melting, and the ductile-brittle transition temperature (DBTT) in bending was about 300°F in the as-oxidized condition.

As a result of the improvement afforded by small amounts of Y, the Cr-Y system has been used as a base for several alloy development programs. It has made possible the induction melting process for primary consolidation and permitted use of Cr of only moderate purity. The melting process consists of melting hydrogen-reduced electrolytic flake in a Y_2O_3-stabilized ZrO_2 crucible in an inert atmosphere. Y was added to getter interstitial impurities from the melt and to provide a slight excess in the alloy for subsequent oxidation-nitridation resistance. The cost of the H_2-reduced flake is one-fourth to one-third the cost of high-purity crystals produced by the iodide process.

The addition of Groups VII and VIII metals to Cr in some cases results in a striking improvement in low-temperature ductility. Concentrations of about 35 atomic percent Re[15] and 20 atomic percent Ru[16] result in highly ductile Cr alloys. However, large amounts of each element are required to provide this high degree of ductility. A further disadvantage of Ru is a decrease in melting point to about 2900°F for a Cr-20Ru alloy compared to a melting point of about 4000°F in Cr-35Re. To date, the only relatively inexpensive metal which when added to Cr in moderate amounts causes ductility improvements similar to Re, is Co. Single-phase alloys containing 25 to 35% Co prepared by chill casting have exhibited considerable plasticity in room temperature rolling experiments[17]. Since the equilibrium solubility of Co in Cr is only about 10% at 1800°F, the alloys were supersaturated in the chill-casting process. It is clear that practical binary Cr-Co alloys will not be developed, since the terminal solubility drops rapidly with temperature, and such alloys are embrittled by sigma-phase formation during aging at 1500 to 2000°F. It is possible, however, that substitution of Co for part of the Re (or Ru) in ternary Cr-base alloys could result in useful materials.

One of the most significant developments in Cr alloy technology has been the improvement in strength and ductility afforded by carbide dispersions. Fine carbide dispersions have been shown to result in increased high-temperature strength while simultaneously increasing low-temperature ductility. It is reasoned that the carbide particles act as sinks for other interstitials, particularly nitrogen, and perhaps as sources of mobile dislocations[18], thereby improving ductility. Stress-rupture strengths of representative alloys are shown in Figure 1, with unalloyed Cr data included for comparison. Tensile properties of several alloys are compared in Table 1. Based on early data, the lower-C alloys with Zr or Hf-rich reactive metal additions were clearly superior to higher-C alloys. The normal structure of this type of alloy contained ZrC and (Zr,Ti)(C,N) phases of the NaCl type. Heat treatment at 2000-2250°F dissolved nonequilibrium $Cr_{23}C_6$ present in as-worked structures and precipitated dissolved interstitials as (Ti,Zr)(C,N) and/or ZrN. This removal of interstitials from solution, especially nitrogen, produced excellent ductility with DBTT values as low as -50°F. The low DBTT values could be retained even when the alloy was contaminated by 900-1000 ppm oxygen + nitrogen, provided that a sufficient reactive metal concentration was maintained to getter the contaminants.

The combination of solid-solution and carbide-dispersion mechanisms resulted in further advances in Cr-base alloys. Figure 2 summarizes the stress rupture properties of several alloys. The addition of W to a carbide-strengthened alloy resulted in significant strength increases. The C-207 alloy represents the best combination of strength, ductility, and oxidation resistance of any known Cr-base alloy at the outset of the present work, except perhaps the Cr-35Re alloy. The C-207 alloy has been prepared as 100-pound induction-melted heats, and its properties have been extensively investigated. It also has been successfully forged into turbine blades.

Utilizing the above background as a starting point, the present program was undertaken to further develop the potential of Cr-base alloys for use in advanced air-breathing engines.

4. TECHNICAL APPROACH

4.1 Alloy Design

In order to provide improvements in strength, ductility, and oxidation-nitridation resistance, five broad classes of alloys have been included in the study. These five types of alloy systems, with examples of the additions made, are:

1) Nitridation inhibitors (Y, Th, La)
2) Solid-solution strengtheners (Mo, W, V)
3) Solid-solution ductilizers (Re, Ru, Co)
4) Dispersion strengtheners (carbides, borides, intermetallics)
5) Complex combinations of above.

In several instances, sufficient data were available from prior work to specify compositions which merited full evaluation in this program. In other cases, this prior work had identified potentially fruitful alloying approaches, but had not proceeded to the point that exact compositions can be recommended with confidence. In the latter instances, it was considered more efficient to first conduct surveys of such alloy systems using heats of smaller size and confining the evaluation to the most critical characteristic(s) affected by the variable under study. This approach was adopted for this program, and four separate phases of alloy design were undertaken.

A) First series of induction-melted heats (3-4 pounds).
B) Small heats for system surveys (50-100 grams).
C) Series of induction-melted heats based on B.
D) Optimized compositions based on A through C.

Two somewhat arbitrary "standards" were employed in the initial phases. Briefly, the intent was to evaluate several alloying approaches using additions to or departures from the standard alloys. This standard could have been selected as unalloyed Cr or perhaps Cr-Y. Results from either of these would probably yield the same relative rating of the effectiveness of the further additions. The results would not, however, be likely to approach those required for the time/temperature/stress regime of interest here.

The standard solution-strengthened matrix, in atomic percent, is:

Cr-4Mo-.1Y (Cr-7.1Mo-.17Y in weight percent)

One of the basic guidelines in alloy design for high-temperature strength is, of course, the melting point, and the inter-related aspects of atomic mobility and attendant effects on creep. Although other factors such as differences in atomic size and elastic constants are also important, the melting characteristics assume added significance as the time/temperature conditions for stressed service are increased. A review of the effects of Re and other solutes with greater than six orbital electrons was presented in the preceding section. Of the remaining elements with melting points above 3000°F, only W, Mo, and V have extended solubility in Cr. The effects of these solutes on the high-temperature tensile strength of Cr alloys are compared in the following tabulation for concentrations of 3 to 6 atomic percent:

	Average Increase in Tensile Strength (psi/atom %)	
Solute	2000°F	2200°F
V	900	--
Mo	5700	4000
W	9900	8100

As might be expected, W has a considerably higher strengthening effect at these temperatures on an atomic basis. When the increase in strength per weight percent solute is considered, W and Mo are essentially equivalent at 2000°F and W is superior at the higher temperature. However, prior experience in these laboratories indicates that W additions are limited to about 4 atom percent by the solid-state miscibility gap in the Cr-W system[19]. More highly alloyed compositions reject a W-rich solid solution upon aging at temperatures below 1800°F and attempts to work such alloys have not been successful. Alloys with somewhat higher atomic concentrations of Mo have been reduced from ingot to bar stock and their strengths follow the trends shown in the tabulation above. Therefore, Mo alloys have been emphasized in preference to W in the initial phases of the study. The Cr-4Mo-.1Y alloy selected as the standard matrix will provide an increase of some 20,000 psi in the 2000°F tensile strength over that of Cr or Cr-Y, yet should permit processing without undue difficulty.

The standard reactive-metal/carbon alloy, in atomic percent, is:

Cr-.05Y-.4Zr-.2Ti-.4C
(Cr-.085Y-.7Zr-.2Ti-.09C in weight percent)

The use of a Zr-rich combination of Zr and Ti as the carbide-stabilizing addition represents the approach which has yielded the best balance of critical properties in our prior work. Although it is beyond the scope of this report to discuss the prior data in detail, a short review of conclusions is in order. Both Zr and Hf additions to Cr-Y-C alloys result in the formation of massive carbide particles. Although these large particles provide relatively little dispersion strengthening, the air oxidation behavior and resistance to embrittlement of such alloys is superior. Additions of Ta, Cb, and Ti result

in precipitation of fine, uniformly dispersed monocarbides with attractive thermal stability. The strengths of these types of alloys are considerably higher than those which form the coarse carbides, but they are more severely embrittled by air oxidation. Alloys with carbides based on a combination of Zr and Ti have structural, strength, and oxidation characteristics which are intermediate between the two groups described above and the thermal stability appears to be superior to either type, with little growth of the carbides observed upon 1000-hour exposure at 2000°F[4]. This type of carbide is used as the standard in Phases A and B of the program. Volume fractions of the dispersed phase, reactive-metal to interstitial ratios, and compositions of the compound-stabilizing elements have been varied with this standard as the basis for comparison. A limited evaluation of borides was also performed.

Finally, the desired level of retained yttrium is dependent on the type of alloy under consideration. Binary alloys with residual Y levels of 0.3% and higher are quite easy to work and have good oxidation resistance. Additions of substitutionally soluble elements do not appear to reduce the tolerance for Y, particularly in the case of non-reactive solutes. Carbide-strengthened alloys, on the other hand, are hot-short and suffer intermediate-temperature nitridation and consequent embrittlement at Y contents above 0.2% and most considerations indicate that the optimum level may be more nearly 0.1%. Microprobe scans of such alloys in the latter range and emission analyses of extracted phases show a lower solubility of Y and/or a tendency to segregate to the carbides. For these reasons, an intended Y level of .17% (.1 atom %) was used as a standard in the Phase A alloys which do not contain soluble second phases such as carbides, and a lower level of .085% Y (.05 atom %) was established as the standard in the dispersion-strengthened alloys.

Alloys selected for evaluation as four-pound heats contained solute concentrations of 4 to 8 atomic percent Mo, W, or Co and somewhat higher levels of V and Re. It was not considered necessary to investigate concentrations of the major solutes employed here at levels below 4 a/o since the strengthening at such levels would be inadequate in terms of the targets set for this work. With the exception of V, which has a relatively mild effect on hardness and strength, and of Re, which is known to promote excellent mechanical properties at about 35 a/o, it was felt to be inadvisable to include solution-strengthening additions above 8 a/o in this phase because of difficulties in working even more dilute alloys in prior studies.

Several other types of Cr alloys have been shown to offer promise of improvements in one or more of the critical properties. Insufficient data were initially available to justify the specification of exact compositions for full property screening. Consequently, these approaches were evaluated in the concurrent Phase B by surveys over broader ranges of solute concentration in small button heats from the pertinent alloy systems. A summary of the systems included in Phase B is shown in Table 2.

4.2 Outline of Evaluation Procedures

Some 60 compositions which represented the five general types of alloys described above were selected for screening as research heats of moderate size. Consolidation of these alloys has been performed primarily by induction melting of H_2-reduced chromium and casting as 2.125" diameter ingots. The ingots were processed by extrusion of Mo-canned or steel-canned billets followed by swaging to 0.25" diameter. Wrought bar stock from one representative alloy from each of the five types was subjected to:

1) A complete chemical analysis from three locations in the original ingot to document homogeneity.

2) A microstructural study of heat treatment response in the range 1400°F to values in excess of the solvus temperature of dispersed phases.

3) Low-temperature tensile tests in the three most attractive thermal conditions to determine the ductile-brittle transition temperature.

Heat treatment of the remaining induction-melted alloys was based on the above results. All the following were determined, provided that sufficient bar stock was available:

1) Analysis of wrought bar stock for interstitials and yttrium to insure the combined O_2 plus N_2 content does not exceed 300 ppm total and that the retained Y level is in the intended range.

2) The ductile-brittle transition temperature in tension.

3) Elevated-temperature tensile strength in vacuum (in the range 1900-2400°F) in one wrought and one fully recrystallized condition.

4) Air oxidation behavior in the range 1500-2400°F.

5) Metallographic evaluation of the above specimens.

In addition to the tests described above, creep-rupture strengths were determined at 2100 and 2400°F for those alloys which exhibited the best combination of other critical properties.

In Phase B, several different alloying approaches were studied in terms of specific effects on phase relationships, workability, low-temperature ductility, and resistance to nitrogen embrittlement. Consolidation of these compositions was by arc melting of small buttons or drop castings, and critical alloy interactions in each series were investigated by selective microstructural analyses, oxidation, forging, and rolling trials, and bend testing. The study of button heats and the initial work on induction melted alloys were conducted concurrently. Since the results from the buttons were used in the design of larger heats in later phases of the program, it will be more convenient to the reader to present the results from the smaller heats first.

5. EXPERIMENTAL RESULTS--ARC-MELTED BUTTONS

Data from a rather large number of arc-melted buttons from several alloy systems have been generated in this portion of the program. The ultimate goal was to select the most promising of the approaches surveyed here for incorporation in larger heats prepared in subsequent phases of the study. A summary of the alloy systems included in Phase B of the investigation is shown in Table 2. All of these alloys were arc melted as 50 to 100 gram heats using tungsten electrodes, water cooled copper button or drop-casting molds, and a helium-argon atmosphere gettered prior to preparation of the buttons by melting a titanium charge. Except where noted, the alloys were melted a minimum of three times to promote homogeneity.

5.1 Cr-W-V Alloys

Tungsten is one of the most effective solid-solution strengthening additions for chromium with complete solubility above 2750°F but, as a result of the miscibility gap in the Cr-W system[19], the solubility of W in Cr falls to only about 5 atomic percent at lower temperatures. Prior work indicates that vanadium exerts only a mild strengthening effect, but that it increases the solubility of W in ternary alloys[20]. Since available data were too limited to establish the solvus with any degree of accuracy, a series of alloys with 5, 7.5, and 10 atomic percent W was prepared with V additions ranging from 0 to 20%. The alloys were arc melted from iodide Cr crystals and drop-cast as 0.5" diameter cylinders. All alloys were single phase as-cast and after 2-hour annealing at both 2500 and 2900°F. The higher temperature was necessary for complete homogenization because traces of coring were present after 2 hours at 2500°F. Homogenized specimens were subsequently aged 230 hours at 1650°F and for 24 hours and 200 hours at 1800°F. The longer time at 1800°F was necessary to cause uniform precipitation in the two-phase alloys.

Cr-W-V alloy compositions and metallographic observations are given in Table 3. In the binary alloys, a sharp increase in hardness between 7.5 and 10% W was accompanied by irregular precipitation that was subsequently confirmed to be a W-rich solid solution. In the ternary alloys the precipitation was general and relatively uniform as indicated in Figure 3. It is difficult to determine whether the amount of precipitate is increased with increased V concentration. The precipitate particles are apparently very small and the difference in apparent precipitate density may be caused in part by the relative rates of etching of grains of differing orientations. In general, however, there appears to be an increase in degree of precipitation as the V concentration is increased.

In the more dilute ternary alloys a slight softening occurred upon first appearance of the precipitate, while in the more concentrated alloys hardening was observed. Location of the alloys in relation to the proposed ternary Cr-W-V equilibrium diagram[20] is shown in Figure 4. The metallographic results strongly indicate that V does not increase the solubility of W in Cr at low temperatures. It was not clear, however, whether a miscibility gap also exists in the Cr-V binary system or whether V simply increases the rate of precipitation of W from the Cr solid solution. Precipitation of a V-base solid solution would not be expected to result in the large hardness increase that has been noted in the Cr-W binary alloys when the W-rich solution precipitates.

The possibility that the second phase in the alloys with higher V contents could have resulted from interaction with residual interstitial impurities was also considered. X-ray diffraction data were obtained on residues from partial digestion of aged samples (1800°F-200 hours) of Cr-10W alloys with additions of 0, 10, and 20 atomic percent V, using a 10% H_2SO_4-C_2H_5OH electrolyte at a current density of about 0.2 amp/in^2. Only bcc phases were detected. The lattice parameter of the matrix increased from 2.916 A for the Cr-10W binary to 2.929 A in Cr-10W-10V and 2.939 A in Cr-10W-20V. The binary alloy also contained a second bcc phase with a lattice parameter of 3.125A, indicating the W-rich solid solution. No x-ray evidence of such a phase was observed in either of the alloys with ternary additions of V.

Whatever its nature, the uniformity and the apparent small size of the substructure in the V-rich alloys may provide a significant effect on the strength and/or ductility. A large heat of a ternary Cr-W-V alloy was produced in Phase C of this study to more fully evaluate the effects on mechanical properties.

5.2 Co Additions to Cr-Re and Cr-Ru Alloys

Concentrations of about 35 atomic percent Re[15] and 20 atomic percent Ru[16] result in highly ductile Cr alloys. Such compositions can be cold worked from the as-cast condition and retain their ductility after exposure at elevated temperatures. As outlined in a preceding section, prior General Electric experiments have shown that Co additions to Cr at levels of 25 to 30 atomic percent result in similar ductility improvements when the alloys are supersaturated by chill casting or by quenching from an annealing temperature above 2500°F. However, since the solubility of Co drops rapidly with decreasing temperature, these alloys are embrittled by sigma phase formation during aging in the temperature range of 1500 to 2000°F.

The approach adopted in the present series was to add Co to Cr-Re and Cr-Ru alloys in an attempt to decrease the amounts of Re or Ru required for significant ductility improvements. The alloys were prepared from iodide Cr crystals and Re, Co, and Ru powders which were hydrogen treated at 2550°F for 1/2 hour to deoxidize, and then arc melted. The ternary alloys were first melted as buttons and then drop cast into 1/2" diameter cylinders. Disks approximately 0.1" thick were cut from the cylinders and rolled at room temperature until excessive cracking occurred. Results of these rolling experiments are illustrated on the diagrams of the Cr-rich corners of the Cr-Re-Co and Cr-Ru-Co systems in Figures 5 and 6, respectively.

At the level of 11 a/o Re, the ductility shows a marked increase as the Co content increases. Little improvement in workability is noted at the lower Re content investigated. Similar behavior is observed in the Cr-Ru-Co system. Increasing the Co level results in a continuous improvement in cold rolling characteristics at the higher Ru content.

All the alloys shown in Figures 5 and 6 were single-phases in the as-cast condition. However, after heat treatment at 2550°F for 1 hour and then aging for 100 hours at 1650°F, precipitation of sigma phase occurred in most of the alloys. Aged structures of the more highly alloyed Cr-Re-Co compositions, those which in the cast condition exhibited the best cold workability, are shown in b and c of Figure 7. Based on similar metallographic observations from the two series, the tentative boundaries between the bcc solid solutions and the two-phase regions containing sigma are indicated on the ternary diagrams in Figures 5 and 6. Results indicate that Co can in fact be substituted for relatively large portions of the Re and Ru required to promote cold workability in cast Cr alloys. Thermal stability is impaired by such substitution, however, particularly at the higher Co levels.

In order to further define the Cr solid solution region in the Cr-Re-Co ternary system, an additional series of alloys located near the tentative 1650°F phase boundary was prepared. Alloy compositions and metallographic data from all alloys of this type are presented in Table 4. One of the alloys (30.2Re-5.7Co) contained a precipitate after 2-hour homogenization at 2750°F, but the remaining alloys were single phase. Only the alloys with combined Re and Co contents above about 27 atomic percent showed any significant enhancement of cold workability. After aging for 100 hours at 1650°F all of the alloys with Co concentrations above about 7.5 atomic percent exhibited a second phase, the more dilute showing only a grain boundary precipitate, presumably sigma phase. The microstructure of one such alloy is shown in Figure 7 along with the structures of alloys of higher Co contents which exhibit considerable ductility in the supersaturated condition but poorer stability at 1650°F. The extent of the Cr solid solution region in the Cr-Re-Co system at 1650°F is presented in Figure 8.

Alloys listed in Table 4 were forged at 2200°F but most, particularly those high in Co, fractured badly during forging. Attempts to cut bend test specimens from the forged alloys were not successful because of their brittleness except in the case of the Cr-2.5Co-25.6Re alloy. The latter composition exhibited ductility at room temperature (approximately 20° bend of a .050" thick specimen at a bend radius of .060" before fracture). The results indicate that the substitution of Co for Re in Cr alloys is possible but is not practical because of the instability of the alloys at intermediate temperatures (~ 1650°F). Co-rich alloys located near the solvus line, while relatively stable, are very brittle. No further work was performed on the ternary Cr-Co-Re or Cr-Co-Ru alloys.

5.3 Cr-Y Alloys with Dilute Re, Ru, and Co Additions

Aside from the improvement of ductility in concentrated solutions, Re has been shown in prior work to have a beneficial effect on air oxidation behavior of much more dilute Cr alloys containing Y[4,14]. Since Ru and Co are analogous to Re in other respects, the oxidation-nitridation resistance of a series of Cr-Y alloys with relatively small additions of these three elements was evaluated. The alloys were prepared from hydrogen-reduced Cr flake and purified Re, Ru, and Co. The Cr was alloyed first with the Re, Ru, or Co to insure homogeneity. These buttons were crushed to provide a master alloy to which the Y was added. The alloys were first melted as buttons and drop cast into 1/2" diameter cylinders. Disks approximately 0.1" thick were cut, ground through 600 grit paper, cleaned, and exposed to air at 1500° and 2100°F for 100 hours, and at 2400°F for 24 hours. Results are compiled in Table 5. In general, the combination of Y and Re results in improved oxidation-nitridation behavior. The Cr-Re-Y alloys exhibited better oxide adherence and less nitridation than similar compositions with either Ru or Co.

Photomicrographs of the representative specimens are presented in Figures 9 and 10. In none of the alloys was evidence of nitridation noted after 100 hours at 1500°F. Structures in each instance were similar to the as-cast structure. Alloys with 0.5 a/o Y contain second phase particles which are fairly uniformly distributed in an intergranular and inter-dendritic array. This distribution, as discussed in conjunction with the induction-melted heats in a later section, suggests that the particles are Y-rich. The alloys with 0.1 a/o Y also contain a second phase or phases but in greatly reduced quantity.

In the Cr-4Re-0.1Y alloy, precipitation of nitride needles occurred during oxidation at 2000 and 2400°F as shown in Figures 9A and 9B. The nitridation resistance appeared to be better than that of a Cr-4Mo-.1Y alloy which will be discussed later. Nitridation resistance, particularly at 2400°F, was improved as the Y content was increased to 0.5% as shown in Figures 9C and 9D. Some agglomeration of the dispersed phase occurred at the higher temperature. Increasing the Re to 8 a/o resulted in a further improvement in nitridation resistance, as indicated in Figures 10A and 10B. Again agglomeration of the second phase occurred at the higher test temperature, along with evidence of incipient melting.

The alloys with Ru and Co additions were much less resistant to air oxidation than the Re-containing alloys. Extensive nitridation occurred at 2400°F, as shown in Figures 10C and 10D. These results indicate that Re is beneficial with regard to nitridation resistance but that Ru and Co, at the 4 a/o level, are detrimental. Only Re-containing alloys were considered for extension of the work into Phases C and D of the program.

5.4 Cr-Y Alloys with Group IV-A and V-A Carbides

In order to provide the best possible combination of strength, ductility, and resistance to embrittlement during air oxidation in the design of dispersion strengthened alloys in succeeding phases of the work, a critical survey of the interactions between carbide-forming elements and nitridation-inhibiting additions was made in Phase B. Results from the first portion of that survey are presented in this section. Each of the Group IV-A and Group V-A metals were added at levels of 0.5 and 1.0 atomic percent to base compositions of Cr, Cr-Y, and Cr-Y-C. The alloys were arc melted as 60 gram buttons, sheathed in mild steel and drop-forged at 2200°F to a 60% reduction in thickness. The alloys with reactive metal additions of 1.0 atomic percent were rolled to .070 ± .010" strip at 2100°-1900°F, using initial reductions of 20% per pass at the higher temperature and finishing with 10% reductions at 1900°F.

Air oxidation tests were conducted at 2100°F on wrought samples of the entire series. Effects of oxidation on the lower-temperature mechanical properties of representative alloys with reactive metal additions of 1.0 atomic percent were compared by bend tests on sheet specimens. The as-rolled strip was cut into coupons, ground to remove surface defects and any interaction with the sheating material, annealed for one hour at 2000°F in vacuum of 10^{-5} torr, and electropolished at a current density of about 1 amp/in^2 in a 10% perchloric -90% acetic acid electrolyte maintained at or below 50°F. One sample was tested in this condition. Additional specimens were oxidized in static air for 100 hours at 2100°F, and if sufficient material was available, at 1500°F. The latter oxidation temperature was included since prior work has shown significant embrittlement of similar Cr alloys during air exposure at 1200 - 1600°F, even in compositions which have high resistance to nitridation at 2000°F and above[9,10]. Bend tests were made in an Instron machine at a ram speed of .05 ipm using a die radius of 4T where T is the sheet thickness. Ductile-brittle transition temperatures (DBTT) were approximated by a single specimen testing technique in which the sample was bent through an angle of 15° at the initial test temperature, then through additional bends of 15° at successively lower temperatures until fracture occurred. In the rolled and annealed condition, initial tests were made at 400°F and the temperature was lowered in decrements of 50° to 100°F. Tests of oxidized specimens were started at 800°F and decrements of 100° to 200°F were employed. The DBTT is here defined as the lowest temperature at which the specimen underwent a 15° bend without fracture. Values of the load at departure from linearity on automatically recorded load-time curves at the initial test temperature were used in the determination of flow stresses, which of course should not be considered as accurate measures of the proportional limit.

Results of 2100°F oxidation tests of the entire series are shown in Table 6 and mechanical properties of representative alloys are summarized in Table 7. Rather marked differences in both oxidation and mechanical behavior are observed between those alloys containing additions of Group IV-A metals (Ti, Zr, and Hf) and those with solutes from Group V-A (V, Cb, and Ta). Each of the elements in binary alloys with Cr at the level of 0.5 atomic percent results in an increase in the oxidation rate over that of the unalloyed metal at 2100°F. However, small additions of Y to the alloys with Group IV-A solutes are very effective in reducing oxidation, whereas Y is relatively ineffective when added to binary alloys with V, Cb, or Ta. The same trends are observed in similar alloys with C. Even without Y, the alloys with ZrC and HfC exhibit weight-gain values considerably below those with the other four carbides. Additions of Y in general result in lower oxidation rates in those compositions which contain carbides based on the Group IV-A metals, but have little effect on alloys with Group V-A carbides. The alloys with VC are an exception to this trend, in that quite low weight-gain values are obtained in the presence of Y, particularly at the higher nominal concentration of 0.2 atomic percent. It should also be noted that the alloys with carbides based on Group IV-A metals have somewhat lower rates of oxidation at the higher metal-to-carbon ratio, while the reverse appears to be the case for those with carbides of V, Cb, and Ta.

Differences in low-temperature mechanical properties and the effects of oxidation on ductility, which are summarized in Table 7, are also pronounced. Alloys with TiC, CbC, and TaC have considerably higher strengths and somewhat higher DBTT values in the rolled and annealed condition. Air exposure at 1500 and 2100°F results in a sharp decrease in ductility, particularly in the case of the CbC and TaC alloys. The compositions which contain ZrC, HfC, and VC are ductile near or below room temperature and the former two types exhibit much better retention of ductility after air oxidation. DBTT values of 200 to 400°F were measured in oxidized Cr-Y-C alloys with Zr or Hf, compared to greater than 800°F in similar compositions containing Cb or Ta.

Some of the factors which are involved in the differences in both mechanical and oxidation behavior can be illustrated by the photomicrographs in Figure 11. Carbides in the alloys with Zr, which are typical in this respect of those with Hf, are rather coarse and widely spaced. This morphology results from the restricted solubility of Zr and Hf in Cr[21]. Carbides are formed as grain boundary networks during solidification. These intergranular carbides are fragmented during processing, but are not appreciably altered by heat treatment. Such a coarse distribution does not have a large effect on either strength or ductility in the rolled and annealed condition. The particles are also too widely spaced to influence reaction during air exposure. Note in Figure 11A that only those few particles which intersect the surface appear to be affected by oxidation at 1500°F. At the higher oxidation temperature, the large carbides act as sinks for the gaseous contaminants as shown in Figure 11B, and no surface or intergranular nitrides are formed.

Carbides in the alloys with Cb or Ta additions are present in the form of fine, uniform dispersions which are much more effective in increasing the strength and result in somewhat lower ductility in the rolled and heat treated condition. The further losses in ductility during intermediate-temperature air exposure are probably related to additional precipitation of interstitials, both from the matrix and from inward diffusion of oxygen or nitrogen, and a resultant interaction with the dislocation array. Although essentially no subsurface hardening was observed at 1500°F in the Cr-Y alloys with ZrC or HfC additions, those containing Cb or Ta were hardened by 25-50 DPH to depths of 4 to 6 mils. Oxidation at the higher temperature results in accelerated reaction of alloys with CbC or TaC dispersions. The particles are closely enough spaced that they present a semi-continuous oxidation front. They are rapidly saturated by the gaseous contaminants, and both surface and intergranular nitrides are formed as illustrated in Figure 11D. Even in the absence of C, additions of Cb and Ta appear to at least partially negate the beneficial effects of Y on oxidation behavior, as indicated by the weight-gain data in Table 6. As noted previously, this is not the case with solutes from Group IV-A.

Alloys with VC appear to have the poor features of each type discussed above, without the attractive properties of either. A relatively fine dispersion is formed during cooling from high temperatures, but the thermal stability is quite low. Rapid agglomeration occurs upon heat treatment at temperatures as low as 2000°F. Although the ductility of the alloys with V is good, their strengths are not greatly different than those of a Cr-Y binary and they are severely embrittled by oxidation at 2100°F. Structures of the alloys with TiC are similar to those with CbC in that a fine dispersion is formed. Embrittlement due to oxidation is not as great, however, since Ti additions, unlike those of Group V-A solutes, do not interfere with the effects of Y.

Based on this survey, the choice of a combination of Zr and Ti as the "standard" carbide-stabilizing addition in the initial phases of the work on larger heats appears to be justified. Superior strengths, however, can be attained with Cb-rich or Ta-rich carbides. It is possible that embrittlement of such alloys can be minimized by the identification of an element which provides more effective resistance to oxidation and nitridation than does Y. Results of the study of this factor are presented in Section 5.6 through 5.9.

5.5 Intermetallic Dispersion Systems

Two binary systems and one ternary were surveyed to establish the efficacy of intermetallic compounds as dispersion strengtheners and to measure the oxidation-nitridation resistance of the resultant alloys. The Cr-Cb, the Cr-Si, and the ternary Cr-Cb-Si systems were selected for these purposes. In an effort to improve oxidation resistance, a Cr-0.1 Y base was used in most of the alloys. The elements were first added separately in arc melted buttons in sufficient amounts to produce $CbCr_2$ and Cr_3Si. Earlier work by Goldschmidt and Brand[22] had indicated that addition of the two elements in combination led to precipitation of $Cb_{0.6}Cr_{0.4}Si$, although the phase boundaries were not well established.

Observations made on these alloys are summarized in Table 8, and typical microstructures are shown in Figure 12. Reasonably fine and uniform dispersions were achieved in alloys with Cb levels of 3 atomic percent and above, and the precipitate appeared to be stable through 2200°F. However, when the Cb concentration is high enough to produce $CbCr_2$, the air oxidation behavior is particularly poor, as shown in Figure 12B. The Cr-Si buttons, although exhibiting considerably better oxidation behavior, were quite brittle and fractured rather badly during forging in spite of their relatively low hardnesses. The workability of ternary Cr-Cb-Si alloys proved to be somewhat improved over those of the Cr-Si system, but oxidation and nitridation rates are still unacceptably high, as shown in Table 8 and illustrated in Figure 12F. After subsequent work (described in following sections) showed that additions of La or of La plus Y were much more effective than Y alone in retarding nitridation, one alloy containing Cb and Si was prepared as a four-pound heat. However, this alloy could not be worked to small-diameter bar stock. No further work on these systems was recommended.

5.6 Alternate Nitridation Inhibitors in Cr-4Mo Alloys

In this group of alloys, several reactive metals were evaluated with respect to their effect on the nitridation resistance of the standard Cr-4Mo matrix. Since they closely resemble Y, emphasis was placed on the lighter rare earths from the lanthanide and actinide series, including mischmetal which is a naturally occurring mixture of the lighter elements in the former series. Additions of Be from Group II-A were also investigated. The alloys were prepared from hydrogen-reduced Cr flake. A master alloy of Cr-4Mo was first arc melted as 100-gram buttons, which were crushed and blended. The reactive additions were then added at levels of 0.1 and 0.5 atomic percent by arc melting and drop casting into 1/2"-diameter cylinders.

Oxidation tests were conducted in static air at 1500, 2100, and 2400°F. The weight change data are recorded in Table 9. Comparison of the total and net-weight-change values gives a good indication of the oxide adherence. In addition to considerable spalling at 2400°F in most of the alloys with reactive solute concentrations of 0.1 atomic percent, there was also evidence of volatile reaction products, particularly in the Cr-Mo and Cr-Mo-Be alloys. This behavior probably reflects formation of the volatile oxide CrO_3, as has been noted in a number of previous investigations at temperatures as low as 2000°F.

A summary of metallographic observations and hardness measurements of the oxidized specimens is presented in Table 10. No nitriding was detected after 1500°F exposure. In general, the alloys which exhibit a high degree of oxide adherence are also quite resistant to nitridation at the higher temperatures. Additions of La and Pr are more effective than Y in improving the air oxidation resistance of the Cr-4Mo base, and additions of mischmetal are at least equivalent. Photomicrographs of representative specimens are shown in Figures 13 and 14. The Cr-4Mo alloy is extensively nitrided at both 2100 and 2400°F. Addition of Y at the level of 0.1 atomic percent prevents the formation of continuous surface nitride layers, but as shown in 13C and 13D, some intergranular nitridation and precipitation of nitride needles within the grains is still observed at each temperature. Increasing the Y content to 0.5 atomic percent results in a further increase in nitridation resistance. Intergranular nitridation is virtually eliminated at 2400°F, but as shown in Figure 14A, there are some nitride needles evident and incipient melting occurs at this temperature. The same melting behavior was also noted at this concentration of Y in Cr alloys with Re, Ru, and Co, as illustrated earlier in Figure 9. The eutectic temperature of such Cr-rich alloys with Y is thus below 2400°F and the terminal solubility of Y at the eutectic is well below 0.5 atomic percent.

Structures of the alloys with the three most effective rare-earth solutes are shown in Figures 14B through 14D. The alloy with the higher concentration of mischmetal, which consists of 50% Ce plus approximately 25% La, 15% Nd, and 10% Pr by weight, exhibits very slight intergranular attack. Additions of 0.5 atomic percent lanthanum or praseodymium to the Cr-4Mo alloy completely prevent nitridation in 24-hour air exposure at 2400°F. Some minor agglomeration of the second phase, which is presumed to be rich in the rare earth metal, is observed in the alloys with Pr and mischmetal additions, but the Cr-Mo-La alloy is virtually unchanged from the as-cast condition. No evidence of incipient melting at 2400°F was detected in any of the three alloys.

5.7 Alternate Nitridation Inhibitors in Carbide-Containing Alloys

As noted above, La, Pr, and possibly mischmetal were found to be more effective nitridation inhibitors than Y in a Cr-4Mo matrix. Based on these results, the work was extended to more complex carbide-containing alloys. Emphasis was placed on those containing the (Zr,Ti)C dispersion, in which Y is relatively effective, and on alloys with CbC additions, in which Y does not prevent rather rapid reaction in air.

The first group of alloys containing various carbides and nitridation inhibitors are listed in Table 11 along with the oxidation test results. The alloys were drop cast from electrolytic Cr charges and then forged 50 to 75% at 2200°F. Oxidation test specimens were cut, polished, and exposed in the as-forged condition for 100 hours at 1500 and 2100°F and for 24 hours at 2400°F.

In general, the alloys containing carbides plus gettering additions exhibited hardening of 50 to 100 points DPH near the surface at 1500°F, although no evidence of nitride-layer formation was noted at this temperature. Some intergranular oxidation occurred in the Cr-TiC-La alloy, and most show spalling oxides.

At the higher temperatures, La appeared to be the most effective of the additions evaluated in preventing nitridation. The effects of only 0.2 atomic percent La in preventing nitridation at 2100 and 2400°F in the "standard" Cr-ZTC alloy are shown in Figure 15. Thick nitride layers were formed on the base Cr-ZTC alloy, while little or no nitridation occurred in the Cr-ZTC-0.2 La alloy. A concentration of 0.2% La was also effective in preventing nitridation in the Cr-TiC alloy, as shown in Figure 16, although the surface oxide was quite irregular. In the Cr-CbC alloy, additions of 0.2 La (or Pr) were not effective, but additions of 0.5 La resulted in significant improvement (as shown in Figure 16). Pr was similar to La in its effect on nitridation, and the Cr-CbC-0.2La was nearly identical in appearance to Figure 16B. It was not shown here because extensive cracking through the nitride layer into the matrix made it impossible to obtain a satisfactory metallographic polish.

In the binary Cr-La alloys, no evidence of incipient melting was detected at the level of 0.2 atomic percent La, but incipient melting did occur in the Cr-0.2% La alloy at 2100 and 2400°F. Available data on the Cr-La phase diagram indicate an eutectic temperature of about 1650 to 1700°F and the solubility of La at 2200°F is variously reported from 0.6 to less than 0.05 atomic percent[22,24]. In order to better establish the solubility of La and the melting relationships, additional Cr-La alloys were produced from high-purity (iodide) chromium. Alloys containing 0.1 to 0.5 atomic percent in increments of 0.1 atomic percent were drop cast, warm rolled at 1550°F, then annealed at 1650, 2000, and 2250°F. Metallographic examination indicated that the solubility of La in Cr is less than 0.1%, in that a second phase was present in all alloys, and agglomeration of this phase occurred in all the alloys at the higher temperatures. Incipient melting occurred at 2000 and 2250°F in alloys at and above a concentration of 0.2 atomic percent La.

In evaluating the effect of La on the structure, the purity of the starting materials must be considered. It appears likely that in the alloys made from the lower purity Cr, a large part of the La may be present as interstitial compounds, and thus does not result in incipient melting, but is still effective in inhibiting nitridation.

In an effort to establish the mechanisms through which La exerts its beneficial effects on air oxidation of Cr, warm-rolled specimens of a binary Cr-0.2La alloy were recrystallized by annealing in vacuum at 2100°F for 1 hour, then electropolished and exposed to air at 2100°F for 10 minutes, 1 hour, 10 hours, and 100 hours. The specimens were mounted and polished with a 5:1 taper such that an additional 5X magnification of the surface scale and subscale was imposed upon the optical magnification selected for examination. Taper sections after air exposures of 1 hour and 100 hours are shown in Figure 17. No evidence of a nitride layer was observed in any of the mounts. After the shorter time, there appears to be some porosity in the outer portions of the oxide, but that closest to the oxide-metal interface is quite dense and protrudes rather prominently into the matrix at more or less regular intervals. These cusps do not appear to be associated with grain boundaries, nor is there any evidence that they are related to pre-existing particles in the matrix. After 100 hours at 2100°F, two distinct oxide phases are observed, with much more porosity evident in the outer scale. In most regions, the darker underlying oxide seems to be continuous, but there are areas in which the lighter, porous oxide is in contact with the matrix. Back reflection X-ray patterns from the scale(s) in each specimen yielded only lines which could be indexed as slightly contracted Cr_2O_3, with a_o = 4.953A and c_o = 13.584A. However, in electron microprobe scans of the specimen exposed for 100 hours, the intensity of the La emission increased by a factor of 15 to 18 at the position of the darker phase in Figure 17C. This suggests, but of course does not establish, that formation of a complex oxide such as $LaCrO_3$ has taken place after 100 hours.

Whatever the mechanism, it is clear that La, as was shown for Y in earlier work[9,14], improves oxidation and nitridation resistance by promoting an adherent scale. Those alloys which undergo extensive nitride formation during air oxidation exhibit blistering or spalling oxide scales, while those which resist nitridation invariably show adherent, reasonably non-porous surface or subsurface oxides. This behavior can be rationalized by assuming that solution of lanthanum or yttrium in the oxide strengthens the surface scale. At temperatures near 1500°F, this would result in a loss of ductility in the surface scale in alloys with high rare-earth contents and promote spalling after formation of relatively thin surface oxides, thereby exposing the underlying alloy to nitrogen. Oxides on the compositions with low rare earth contents, on the other hand, would remain adherent at intermediate temperatures because they are not strengthened or embrittled

by dissolution of such elements. At the higher temperatures, where oxide plasticity is increased, the strengthening of the oxide due to rare earth in solution would become an advantage, inhibiting exfoliation or blistering of the scale. An alternative argument might involve the relative kinetics of 1) formation of a more protective subscale, perhaps a complex oxide such as $LaCrO_3$ or $YCrO_3$, which has been observed by Hagel in oxidation products from a binary Cr-Y alloy[25]; and 2) internal nitridation of La or Y. At 1500°F, if the latter were more rapid one would expect the observed detrimental effect of high rare earth contents. At 2000 to 2200°F development of a subsurface film which inhibits diffusion would preclude internal hardening in high rare earth alloys containing carbide dispersions as is noted in this work, but not in compositions with levels too low to form the complex oxide. This rationale suffers from the requirement that the rare earth must be more readily reactive with nitrogen than the other alloy constituents at intermediate temperatures. Thermodynamic functions indicate that any of the Group IV-A or V-A nitrides would form in preference to any known nitride of lanthanum or yttrium.

In either case, it might be expected that some structural changes would occur in the surface (or subsurface) scale, either formation of a new phase or changes in the lattice constants of Cr_2O_3, which should serve to help identify the role of the rare earth. No unequivocal evidence of a complex oxide is observed. There is no consistent change in the lattice constants of the surface scale with rare earth addition to the alloys, but the possibility of dissolution of small amounts of lanthanum or yttrium in the Cr_2O_3 is not necessarily ruled out since such solution might change the solubility of other impurities in the scale. It is also possible that the rare earth is internally oxidized, and La_2O_3 or Y_2O_3 particles which are formed promote adherence by "keying" the oxide, as suggested by Felten[26]. Although beyond the scope of the present program, considerably more work needs to be done to establish the mechanism(s) by which rare-earth type additions affect the oxidation behavior of complex chromium alloys. Recent studies by Seybolt[27] make an important contribution to this understanding.

5.8 Cr-Mo-La Alloys with Selected Carbides

An additional series of complex alloys containing 4% Mo, La, and various carbides was prepared and partially evaluated for oxidation resistance. The chemical compositions are given in Table 12 along with the results of air oxidation tests. An initial test at 2400°F was performed on as-cast specimens cut from the drop castings. The drop castings were then sheathed in Mo and swaged at 2400°F, but broke up badly. Sections of the swaged alloys were surface conditioned and oxidized at 2100°F for 100 hours. The specimens were irregular in shape so that weight-change data could not be obtained, but subsurface reactions were followed metallographically. Microstructures of several of the alloys after testing at 2100°F are shown in Figure 18.

In general, the alloys which contained carbides of Zr or Hf exhibited good resistance to nitridation in both the as-cast and hot-worked conditions. The alloys which contained Cb or Ta carbides exhibited very poor oxidation-nitridation resistance in the as-cast condition. In the alloys containing CbC the resistance apparently decreased as the La concentration was increased from 0.3 to 0.4 atomic percent. In the wrought condition, however, the reverse is true, apparently because working tends to break up the continuous Cb-rich carbide films in the grain boundary. The nitridation resistance of the wrought Cr-4Mo-CbC-0.4La alloy appeared similar to that of the Cr-CbC-0.5 La alloy (compare Figures 16D and 18D) except for some internal oxidation in the Cr-Mo composition.

The results obtained in these series indicate that in complex alloys containing Cb or Ta carbides, an addition of from 0.3 to 0.5 atomic percent La is required to provide nitridation resistance. In alloys containing carbides rich in Zr or Hf, 0.2 to 0.3% La is effective. The verification of the superiority of La as a nitridation inhibitor is considered to be potentially very important to the design of improved chromium alloys. This factor has been emphasized in Phases C and D of the present program, with only partially successful results that will be presented in following sections.

5.9 Combined Additions of La and Y to Cr-TaC Alloys

Analysis of the La-containing alloys listed in Tables 11 and 12 showed an average retention of 52% of the amount of La charged in these arc melted buttons. However, as will be described in more detail in the discussion of consolidation techniques used in making larger heats, excessive reaction with the ZrO_2 crucibles resulted in residual La levels of less than 0.1% in induction melted alloys. Since controlled retention of Y has proved to be more readily attained in induction melting, it was considered advisable to investigate the effects of combined additions of Y and La on resistance to nitridation. A base composition containing atomic concentrations of .6% Ta and 0.4% C, which is quite heavily attacked by nitrogen at 2100°F when additions of Y alone are employed, was selected for this study. Alloys were prepared by arc melting and drop casting as 60 gram cylinders and were tested in the as-cast condition. Results are summarized in Table 13.

Combined additions of Y and La, although not as effective as concentrations of 0.3 and 0.4% La alone in preventing subsurface attack during exposure to air at 2100°F, are nearly as beneficial at the combined level of 0.2 to 0.4%. Furthermore, if the La content in the combined addition is restricted to 0.2% or below, the incipient melting noted at this temperature in carbide-containing alloys with higher La concentrations appears to be eliminated or at least greatly reduced. These observations were subsequently employed in Phases C and D of the work on larger heats.

6. EXPERIMENTAL RESULTS -- INDUCTION-MELTED ALLOYS

6.1 Consolidation

Some 60 alloys were produced in this series in three separate phases. Analyses of raw materials used in melting the alloys are shown in Table 14. All of the induction melted heats were made from the hydrogen-reduced electrolytic flake. The analysis shown is the average of five separate lots of flake employed in this work, all of which had very closely similar chemistries. The maximum variation was noted in the iron content, which varied between 20 and 120 ppm, and in the carbon which ranged between 30 and 80 ppm. The iodide chromium described in Table 14 was used only in the preparation of wrought high-purity unalloyed chromium by extrusion and swaging of steel-sheathed crystals and in preparing several pounds of a Cr-35Re alloy by arc melting and drop casting followed by rod rolling and swaging.

In the initial phases of the induction melting work, four-pound alloy charges were melted in a 50 KW Stokes vacuum induction furnace with a capacity for 50-pound heats. A Y_2O_3-stabilized ZrO_2 crucible was packed inside the induction coil, with coarse ZrO_2 grit serving to insulate the crucible from the coil assembly. The briquetted charges which contained 0.3% Y and non-reactive solutes such as Mo and W were loaded into the crucible and the remainder of the Y (0.1 to 0.4% depending on the desired residual level) plus all reactive solutes such as carbon and Group IV-A and V-A metals were placed in a charging tray for addition to the melt later in the cycle. The furnace was then evacuated to about 10^{-3} torr. At this point a power setting of 1.5 ± 0.5 KW was applied to the induction coil, raising the charge temperature to 1200-1400°F, with the intention of facilitating removal of water vapor and other adsorbed gases. After this intermediate-temperature outgassing treatment, the power to the coil was shut off and the vacuum system continued to operate until the heat was scheduled to be melted, which was usually planned for the morning following the charging of the furnace during the previous afternoon.

Pressure in the furnace chamber was reduced to at least 10^{-4} torr by this practice, with a leak rate of $6 \pm 2 \times 10^{-4}$ torr per minute measured just before beginning the melting cycle. Initial heating was performed under vacuum, until the charge temperature reached about 2000°F. Purified argon was then admitted to the chamber to a pressure of 650-700 mm, and the remainder of the melting and casting cycle was conducted in this inert atmosphere to reduce vaporization of chromium. Power was increased to 15-18 KW until the charge was completely molten, which required 8 to 10 minutes from the time argon was introduced. After melting, the power was reduced to 11 ± 1 KW, resulting in a stable superheat of 100 to 150°F. When the charge had been molten for 15 minutes, the remainder of the yttrium and any other reactive solutes in

the particular alloy were added from the charging tray after raising the power setting to break the slag cover on the top of the melt. Each melt was then stirred by rapid cycling between power settings of 12 and 20 KW, held for an additional 4 to 5 minutes, and cast with power on.

Charges were cast into copper molds fit with 2-1/8" diameter CaO-stabilized ZrO_2 mold liners. These ceramic liners are necessary to prevent solidification cracks which occur in all but the most dilute Cr alloys upon casting directly into copper chill molds. If allowed to freeze in such molds with no hot-topping practiced, very extensive shrinkage occurs in cast Cr alloys. In order to prevent this severe pipe, the initial castings described here were arc-hot-topped by use of a retractable tungsten electrode mounted in the top of the furnace chamber, the lip of the mold liner having been notched to an appropriate depth to provide electrical contact between the melt and the copper mold. At a potential of 25 ± 5 volts, an arc current of 500 amps was employed for 30 to 45 seconds immediately after pouring and then was gradually reduced to about 50 amps before arc extinction. This procedure resulted in sound, crack-free ingots of approximately 3.5" height with very shallow shrinkage cavities. However, heats produced in the manner described above were badly contaminated by oxygen, with as much as 0.3% oxygen analyzed in one heat. Subsequent examination and revision of the melting technique revealed that the contamination resulted from a combination of several factors.

A large number of chromium alloys have been induction melted and cast in these laboratories, using similar techniques, as heats ranging in size from 10 to 100 pounds. Interstitial impurity levels in these earlier alloys were well below the limit of 300 ppm total which was specified for the present program. For example, the average oxygen and nitrogen contents of 15 heats of C-207 and directly related compositions were, respectively, 83 and 54 ppm.

In the present series of alloys the gas contents of the starting materials, ultimate vacuua and leak rates in the melting chamber, and purity of the inert gas introduced during melting were each equal or superior to those in prior work. Crucibles and mold liners were also of the same type employed successfully in the earlier heats. Although these factors did not appear to be involved in the drastic contamination experienced in initial melting, they were not ignored in the sequence of revised melts which were made to identify and correct the source(s) of oxygen pickup.

6.1.1 Revised Melting Techniques

Duplicate re-analysis of the gas contents of the lots of chromium and yttrium, which are the only two elements common to each of the contaminated heats, gave the following results:

Material	Gas Content (ppm)		
	O	N	H
Chromium Flake	49	86	1
Yttrium Sponge	730	10	25

Since the yttrium and other minor alloying elements shown previously in Table 14 were added in concentrations of less than 1 weight percent, the oxygen input from these sources amounts to only a few parts per million and cannot account for the observed contamination. Sampling of the purified argon showed a maximum oxygen content of about 5 ppm. In the furnace chamber with a volume of 95 cubic feet, the impurities in the argon could thus add less than 15 ppm oxygen to the 4-pound alloy charges.

A number of other factors connected with melting and casting practice were considered as potential sources of oxygen contamination. These are listed below:

1) The arc hot-topping of the ingots immediately after casting.

2) Intermediate-temperature bake out of the crucible and briquetted charge at 1300 ± 100°F under a vacuum of 10^{-4} to 10^{-3} torr.

3) Possibly excessive superheat during the stirring cycle after adding reactive solutes.

4) Contamination from the inert gas lines, which were blanked off during leak rate determinations.

5) Increased reaction of the melt with the Y_2O_3-stabilized ZrO_2 crucible due to the larger surface area-to-volume ratio in the smaller heats of this work, or to an inherent instability in the particular crucibles employed.

6) Reaction with the CaO-stabilized mold liner, which might be accelerated by arc hot topping.

7) Insufficient yttrium in the charge for complete deoxidation.

8) An undetected leak, or other source of oxygen, in the furnace chamber.

A series of melts was designed to separate the effects of each of the foregoing factors on the oxygen contents of the resultant ingots. Only carbon-free alloys were used in the sequence of heats to be described below, since those alloys in the contaminated series which contained carbon additions were partially deoxidized with residual oxygen levels of about 800 ppm. In the first group of revised heats, alloys which contained 0.3% Y in the briquetted charge were melted in the 50-pound furnace using crucibles and mold liners from the same lots employed in the contaminated series. The first four factors in the list above--arc hot topping, vacuum bake out, superheat, and the introduction of argon--were varied in this group. As in the contaminated alloys, samples for vacuum fusion analysis were taken from center locations at depths of 3/8 ± 1/8" from the surfaces. Specific variations in melting practice and gaseous impurity contents of the ingots are shown in Table 15.

It is clear from these data that the major portion of the oxygen contamination was caused by the intermediate-temperature (1200-1400°F) bake out of the crucible and briquetted charge which had been employed in all of the contaminated series. Elimination of this step resulted in a four- to five-fold decrease in the oxygen content. Neither the degree of superheat nor the introduction of argon appeared to influence the final oxygen level. Some indication of improvement was noted in the heat in which both the bake-out cycle and the arc hot-topping practice were dropped, but the combined interstitial contents in each of these heats were still 50 to 100% above acceptable limits.

Results to this point indicated that the remaining oxygen contamination was due to interaction with the crucibles and molds or with the furnace environment. In either case, the degree of contamination would be expected to be considerably greater in the 4-pound heats used here than in the larger heats of alloys melted in previous programs, most of which were prepared from charges of 12 to 15 pounds. The larger surface area-to-volume ratios in the smaller diameter crucibles and mold liners used here would magnify the effects of any reaction with the ZrO_2, and the lower volume of molten metal exposed to the furnace atmosphere of a given impurity level would also result in a greater impurity concentration in the ingot. On the other hand, oxygen pick up from either one or both of these possible sources might be reduced to acceptable levels by increasing the yttrium content in the initial charge to promote further deoxidation by slag formation. In order to separate these factors, a second group of alloys were melted and cast in the 50-pound furnace used in all induction melting work to this point and in a smaller lab furnace (NRC Model 2551) with a maximum capacity of 15 pounds and a chamber volume of 10 cubic feet. No intermediate-temperature bake out was used and the ingots were not arc hot topped. Yttrium contents in the briquetted charges were varied from 0.3 to 0.5%, and heats were cast into copper molds with and without the CaO stabilized ZrO_2 mold liners. In addition to vacuum fusion analysis for gas contents, the approximate yttrium and zirconium levels of each heat were determined by comparing in X-ray emission the respective intensities of $K\alpha$ lines with those from similar chromium alloys of known yttrium and zirconium

contents. Since none of the alloys contained any intentional zirconium addition, its concentration in the ingot is indicative of the degree of interaction with ZrO_2 crucibles and/or liners. Average results from cast samples taken at depths of 3/8 ± 1/8" from top and bottom surfaces of ingots in this series are presented in Table 16. With the one exception noted, individual analyses varied from the averages by no more than ± 20%.

Although elimination of the arc hot-topping step and increasing the yttrium content of the charges resulted in a further reduction in the oxygen level of heats melted in the larger furnace, the results were still unsatisfactory. Some interaction with the stabilized ZrO_2 crucibles has occurred in each melting facility, but the important factor appears to be the furnace environment itself. All the alloys melted in the 15-pound furnace, which has a chamber volume nearly 10 times smaller than that of the 50-pound furnace, have combined interstitial impurity contents well below the limit of 300 ppm. This smaller furnace was used exclusively in replacing the alloys which were contaminated in the initial series of melts, and in all the rest of the work described in this report.

Finally, the data in Table 15 indicate that the retained yttrium contents more nearly approach the intended values with initial charge additions of 0.4%. This concentration was employed in the alloys melted and processed to replace those which were contaminated by the earlier melting practice, and in all subsequent alloys in which a residual yttrium level was desired.

In the latter phases of the work after the beneficial effects of lanthanum on oxidation and nitridation behavior had been established on arc-melted buttons, as described in Sections 5.6 through 5.8, it was found to be impossible to retain sufficient amounts of this element in larger induction-melted heats. Additions of La as high as 1.8%, with two-thirds of the total in the briquetted charge and the remaining third added shortly before casting, resulted in residual La contents below 0.06%. Analysis of the crucible and skull at the liquid interface line revealed a high La content (greater than 5%) and analysis of the slag entrapped in the tundish showed a high concentration of Zr (0.3 to 0.6%). These results indicated that the inability to increase the retained La content is associated with its high reactivity with the ZrO_2 crucible. There was also violent surface reaction in the melt when the elemental La was changed. At this point the series of alloys with combined additions of La plus Y, described earlier in Section 5.9, was prepared and evaluated. Since the results were in general favorable, the remaining alloys in Phases C and D were prepared with such combined additions of nitridation-inhibiting elements. In order to better control the addition of La, the heats were first deoxidized by 0.4 weight percent Y in the briquetted charge, adding a small additional amount of Y (0.1 to 0.15%) with the reactive dispersion-forming solutes, and finally adding La to the melt 30 to 45 seconds before pouring. As a means of further reducing the surface reaction, the La was encased in a Mo envelope such that the density of the composite exceeded that of the molten alloy. The La was thus immersed in the melt rather than suspended on the surface.

Each of the 4-pound heats cast directly into copper molds with no ceramic liners contained solidification cracks. Those cast into ZrO_2 mold liners and allowed to freeze without external hot topping were free of these cracks, but had shrinkage cavities which extended 2 inches or more below the surfaces. In order to produce sound ingots of sufficient size for this program, it was therefore necessary to increase the charge weight to 7 pounds, extend the depth of the mold accordingly, and discard the portion of the ingot which contains the pipe. Briquetted charges containing 0.4% Y were melted under conditions described previously, except, of course, that neither intermediate temperature bake-out treatments nor arc hot-topping techniques were employed. The heats were cast through ZrO_2 tundishes into copper molds provided with ZrO_2 liners, the upper 3" of which is of 1" wall thickness to delay freezing in the hot top.

6.1.2 Structure and Analysis of Castings

Microstructural characteristics which are representative of the three general levels of purity produced in similar alloys by variations in the melting practice are illustrated in Figure 19. The grossly contaminated alloys in the initial series all contain numerous, rather massive oxide particles such as those shown for the CI-6 composition in Figure 19A. Elimination of the intermediate temperature bake-out cycle reduced the oxygen content to about 500 ± 100 ppm, but this concentration is still considerably above the solubility limit, as shown by the example in Figure 19B. Structures of the low-oxygen alloys are dependent on the residual yttrium content. Alloy CI-7A, with a retained yttrium level of approximately .10%, is free of oxide particles and shows only isolated evidence of an intergranular phase. The CI-5B alloy, which contains nearly twice as much yttrium, is structurally similar to CI-7A in that oxide particles are virtually absent, but the grain-boundary phase is much more pronounced. Electron microprobe traces across grain boundaries of cast and etched samples showed a significant but variable decrease in both chromium (5 to 15%) and molybdenum (2 to 5%) compared to their concentrations in the matrix, but there was only very slight increase in yttrium intensity. Scans of the entire spectrum of wave lengths emitted from such intergranular regions were conducted on the premise that this phase could be based on some low melting metallic impurity, but only chromium, molybdenum, and yttrium were detected. Since it was considered possible that this intergranular phase is yttrium-rich but that it was rapidly attacked by the light etching employed in sample preparation, experiments were repeated both in the unetched condition and after short-time air exposure of the specimens to convert any yttrium in this phase to the oxide and thereby retain its distribution. Microprobe traces in each condition showed very high (> 50%) concentrations of Y in triple points such as that on the right side of the photomicrograph in Figure 19D.

Nominal compositions of all the alloys of Phases A, C, and D are presented in Table 17, which also includes analyzed gas, yttrium, lanthanum, and zirconium contents. In alloys which contain no intentional zirconium addition, the latter analysis is indicative of the degree of reaction of the melt with the stabilized ZrO_2 crucibles and mold liners. In general, pickup of only a few hundred ppm Zr occurred. Gaseous impurities are well below the limit of 300 ppm established for this program. Revisions in the melting and casting practice described above effectively eliminated the drastic contamination experienced in the first series of heats of these alloys. Yttrium or yttrium plus lanthanum retention is generally within the intended range, but in a few instances very low residual levels were recorded. This behavior, which parallels earlier experience[9,10], reflects the high reactivity with impurities such as oxygen and is associated with differences in slag formation from heat to heat.

Cast microstructures of several alloys are shown in Figure 20. The composition of the "Kromic" acid etchant is as follows:

"Kromic" Acid Electrolytic Etchant

H_2O_2	100 ml
KOH	50 ml
H_3PO_4	40 ml
$K_3Fe(CN)_6$	50 g
$H_2C_2O_4$	20 g
$K_4Fe(CN)_6 \cdot 3H_2O$	5 g

Used at 8 ± 3 volts at a current density of 2 to 3 amps/cm^2.

The CI-1 alloy is representative of the Cr-Y and Cr-M-Y series where M is a non-reactive substitutional solute such as Mo or W. In such alloys isolated intergranular particles, presumably Y-rich by analog to alloy CI-5B discussed above, are observed and there is some intergranular pitting, as shown in Figure 20A. The Cr-4Re-.1Y alloy in Figure 20B exhibits in addition a semi-continuous grain-boundary phase in some areas. Since this Re concentration is far below the solubility limit and the residual Y content is quite low, it is possible that this phase is a complex oxide rich in Re. The suggestion of eutectic freezing at the triple point shown would tend to support this possibility.

Alloys with the standard ZTC (Zr-Ti-C) addition have the appearance illustrated in Figure 20C. An intergranular carbide network, which previous work[4,8,10] has shown to be rich in ZrC, is formed upon solidification. A

much finer carbide dispersion, rich in TiC, precipitates throughout the matrix during cooling. Alloys which contain as the carbide-stabilizing addition only Zr and/or Hf, each of which has rather restricted solubility in chromium, exhibit the same type of intergranular network but form only a few finely dispersed carbides in the as-cast condition, as shown in Figure 20D.

Carbide-containing alloys that have more highly soluble[19,24] stabilizing additions such as Ti, Cb, or Ta have much less pronounced intergranular networks and also form a more general intragranular distribution of fine carbides, as shown in Figures 20E and 20F. It will be shown in following sections that the strengths of such alloys are considerably higher than those which contain only ZrC or HfC additions.

6.2 Processing

After grit blasting to remove remnants of the ZrO_2 mold liner, each of the ingots was cropped by power hacksaw at the junction with the hot top. Prior to extrusion the ingots were encased in protective cans with an OD of 2.06". The dilute alloys, those which contained no major substitutional solutes, were canned in mild steel and the remainder in molybdenum. They were machined from as-cast diameters of 2.2 ± .1" to billet diameters of 1.9 ± .05", the exact dimensions being governed by the ID of the can. Lids were welded to the cans by the tungsten arc process in a vacuum-purged chamber back-filled with high purity helium, then the cans were evacuated and sealed by electron beam welding.

All of the alloys were extruded from 2.13" diameter containers through 0.75" diameter dies. A summary of the extrusion data is presented in Table 18. Heating was performed in an induction unit under a protective atmosphere of argon. The canned billets were soaked for 10 minutes at temperature, then transferred to the container of a 1250 ton hydraulic press (Lowey Hydropress) with handling times of 10 to 15 seconds. Lubricants were powdered glass plus a mixture of necroline and graphite. The tool steel dies were flame sprayed with ZrO_2 to reduce wash and extend their useful lives. Solid graphite back-up block were inserted behind the billets to reduce the extent of the extrusion defects in the trailing ends. Inspection of the extruded stock was performed by radiographic and fluorescent penetrant techniques. Other than minor nose bursts and the typical trailing end defects, no internal flaws were detected, except as noted.

Processing to final dimensions was accomplished by swaging. The general procedure in swaging to 0.25" diameter involved careful inspection of individual 3" lengths of extrusion by macroetching, fluorescent-dye penetrant, and in some

cases, metallographic techniques to ensure sound starting material. Initial swaging of the billets, with the protective jacket intact, was performed at temperatures ranging from 150 to 250°F below the extrusion temperature, the smaller temperature reductions being used for the more complex alloys. Heating was done in molybdenum-wound tube furnaces under a protective atmosphere of flowing hydrogen. The billets were first soaked at the highest temperature to be employed in swaging for 10 to 15 minutes to provide some relief of residual stresses from extrusion and sectioning. After the first reduction by swaging, subsequent heating between passes was limited to 3 to 5 minutes and any cracks which were observed during working were cropped while the material was still hot, using a high speed cut-off wheel. The bar stock was reduced to approximately .47" diameter under these conditions, then straightened in long stroke dies, and given a short stress relief at the swaging temperature.

Finish swaging to 0.25" was conducted at 1900°F for Cr-Y and related alloys, at 2050 ± 50°F for the dilute carbide- or boride-containing alloys, and wherever possible at 2200 ± 50°F for the more complex compositions. Some sections of the latter, because of extensive cracking at 2250°F, had to be finish swaged at somewhat higher temperatures but all alloys were worked to final dimensions below 2400°F.

6.2.1 Structure and Hardness

Microstructures of typical compositions in the final wrought condition are shown in Figure 21. The Cr-.10Y alloy CI-1 shows a considerable amount of polygonization and some evidence of recrystallization after swaging at 1900°F. The high-purity Cr-35Re alloy in Figure 21B is completely warm worked, with no sub-boundaries evident after final working at 2200°F.

As was the case in the cast condition, there is some non-uniformity in the distribution of the finer carbides in the as-worked Cr-.05Y-ZTC alloy pictured in Figure 21C. It should be pointed out in this respect that one-hour annealing at 2000 to 2200°F causes additional precipitation of fine carbides in the regions between the bands of particles in the swaged structure such that a more uniform dispersion is obtained. The Cr-.05Y-HZC alloy CI-21, which in the cast condition shows only a coarse intergranular carbide network, exhibits a uniform but rather widely spaced dispersion of finer carbides after working at 2000°F, as indicated in Figure 21D. Further aging at 2100 ± 100°F is also effective in this alloy in promoting a still finer dispersion but, at least in optical microscopy, the interparticle spacing appears to be too great for most effective dispersion strengthening.

The finest carbide dispersions in the wrought alloys are observed in systems in which the carbide-stabilizing element has a greater solubility in Cr than either Zr or Hf. Examples of such compositions, which include Ti-, Cb-, and Ta-rich reactive metal additions, are shown in Figures 21E and 21F.

A summary of the effect of processing on the microhardness of the alloys is shown in Table 19. Note that in the carbide-containing Cr-4Mo alloys, the greatest hardening from the cast to the swaged condition occurs in those alloys with the higher concentrations of those reactive metals which promote formation of fine carbides. Most of the alloys with major substitutional solute concentrations at or below 4 atomic percent and which contained no dispersion or had dispersions of relatively simple carbides were worked to 0.25" diameter without undue problems. However, some of the more highly alloyed compositions could not be worked by conventional techniques. In general, alloys with cast or extruded hardnesses above about 330 DPH fell into this category. Such alloys that could not be swaged directly were impact extruded from 0.75" to 0.375" diameter at 2450°F prior to further swaging attempts. The compositions that were so worked are designated in Table 19. Where a final swaging temperature is listed for the impact extruded alloys, a limited number of mechanical test specimens were successfully produced. Those that could not be swaged to final dimensions in spite of the intermediate processing step have no entry under swaging temperature in the tabulation.

Table 19 also includes an approximation of the temperature required for 50% recrystallization in one hour. The values shown are based on metallographic observations after vacuum annealing at intervals of 100°F. Other than the Cr-35Re alloy, the highest recrystallization temperatures were obtained in alloys with Cb-rich carbides. The only alloy of the entire series which retained a worked structure after one-hour annealing at 2400°F was the CI-36 composition containing a CbC dispersion.

6.2.2 Chemical Analysis

In order to detect any gross inhomogeneity as well as any contamination during processing, chemical analyses were conducted on wrought samples of alloys which represented each of the five general types under study, taking specimens which corresponded to positions near the top, center, and bottom of the original castings. Results are presented in Table 20. The concentration of Mo is uniformly 0.2 to 0.3% lower than the intended level of 7.1 weight percent, but there appears to be no significant change of Mo or any other addition from top to bottom of the ingot. Other than the slight trace of Co in one of the CI-1 and one of the CI-30 sections, and a trace of Ca in the bottom section of CI-4, no impurities other than those listed were detected. The residual level of Y is also rather uniform from section to section, although the level in CI-20 is much below the intended range. Comparison of the gas analyses shown in Table 20 with those presented in Table 17 for the as-cast condition indicates that little if any contamination occurred during the processing sequence employed here.

Carbon analyses were obtained on wrought samples of all alloys to which intentional carbon additions were made. At the nominal level of 0.4 atom percent (approximately 0.09 weight percent) duplicate analyses of the entire series varied only between 0.082 and 0.094 weight percent, with an average of 0.089%. The actual and intended carbon levels are thus essentially the same.

6.3 Response to Heat Treatment

Swaged sections of at least one representative alloy from each of the five general types under study were vacuum annealed for one hour at temperatures in the range 1400 to 3000°F using increments of 200°F, except in the recrystallization range where increments of 100°F were employed. Results of these treatments in terms of the microhardness and recrystallization behavior are presented in Figure 22. The recrystallization temperature of the Cr-Y alloy, approximately 1900°F for 50% recrystallization in one hour, is increased by about 50°F by the addition of 4 atomic percent Mo and by an additional 50 to 100°F by the (Zr,Ti)C dispersion. The concentrated Cr-Re solid solution has a considerably higher hardness and the recrystallization temperature, as defined here, is about 2300°F.

Each of the carbide-containing alloys exhibits a hardening peak at 2000 ± 200°F. As shown in Figure 22, this peak occurs in one-hour aging at about 1800°F in the Cr-Y-ZTC alloy and is increased to 2000°F by the addition of 4Mo. The effects of exposure in this temperature range on the microstructure are pictured in Figure 23. The Cr-Y-4Mo alloy with the (Hf,Zr)C addition was selected for illustrative purposes, since its as-swaged structure is virtually free of fine particles and the precipitation of carbides upon aging is more evident. Stability of the fine carbide dispersion in this particular alloy is rather low, with almost complete dissolution occurring in one hour at 2400°F. Complex carbides containing Ti, Cb, or Ta resist dissolution or agglomeration to somewhat higher temperatures.

Electron micrographs of selected alloys are shown in Figure 24. Standard replication techniques were employed, using negative collodion-carbon replicas shadowed at 40° to 60° with germanium. The first three collodion films were discarded prior to making the final replica by vapor deposition of carbon and dissolving the collodion. The alloys with dispersions of CbC and TaC have, after one-hour aging at 2000°F, a mean particle size of 500 to 700A with an interparticle spacing which varies between less than 1 and approximately 5 microns. More of the areas observed exhibit a reasonably uniform distribution with spacings near the former value, as shown by the example in Figure 24A, but there are regions in which the particles are rather widely spaced and arranged in a banded distribution. Such areas are also evident in the light micrograph in Figure 21F. This structure possibly reflects microsegregation in the castings and may be partly responsible for the greater difficulty experienced in working alloys which contain Cb or Ta. Steps to improve homogeneity, such as extended high-temperature annealing prior to final working, will be considered in the continuation of this work. At any rate, considerably more effective dispersions are obtained in alloys with Cb or Ta as the principal carbide-stabilizing addition than with alloys which employ only Zr and/or Hf, as illustrated in Figure 24D.

Identification of dispersed phases was performed in several instances by X-ray diffraction of residues electrolytically extracted in 10% H_2SO_4-C_2H_5OH, using General Electric XRD-5 equipment with nickel-filter copper radiation to record Debye-Scherrer film patterns. Results from selected alloys are presented in Table 21. The carbides in the alloys which contain only one element from Group IV-A or V-A as the dispersion-stabilizing addition appear to be relatively pure phases, since their lattice constants are rather close to the accepted values for cubic monocarbides. They should probably more properly be referred to as "carbo-oxynitrides" since the cubic monoxides and nitrides exhibit complete mutual solubility with the carbides. A carbonitride, with very nearly equiatomic concentrations of carbon and nitrogen, apparently is formed in the CI-58 alloy. In the alloys with CbC and TaC as the major phases, a few very weak diffraction lines near the strongest d spacings of Y_2O_3 were observed. Since neither yttrium nor oxygen contents are particularly high in either of these alloys (both being somewhat higher in the HfC alloy CI-35 for example) no reason for the appearance of Y_2O_3 only in these two is readily apparent. Trace amounts of the oxide could well be present in all compositions, but in too small amount to be detected by Debye-Scherrer techniques.

The data also indicate that the solubility of Hf in Cr is quite low. Although most of the Hf in alloys CI-35 and CI-37 must be tied up as the Hf-rich carbide, each alloy contains a detectable amount of the $HfCr_2$ phase of the Laves type. A similar phase was not found in the alloy with atomic concentrations of 0.6% Zr and 0.4% C, although earlier work[5] show it to be present at about 1.5 atomic percent Zr.

In addition to the hardness and microstructural response, an exploratory investigation of the effects of selected heat treatments on the low-temperature tensile behavior of representative alloys was also conducted. Tests were made at a nominal strain rate of .03 per minute using a .120" diameter specimen with a 0.5" gauge length provided with generous fillet radii. Prior to testing, specimens were electropolished in a 10% perchloric - 90% acetic acid bath maintained at or below 50°F. In general, an annealing temperature below the one hour recrystallization temperature (1800°F), one at or near the aging peak for carbide-containing alloys (2000°F), and one above the recrystallization temperature (2400°F) were included in this portion of the study. The results are summarized in Table 22. It should be noted that the ductility of each of the dilute alloys with carbide additions is superior to that of the Cr-Y binary. The compositions with (Zr,Ti)C or (Hf,Zr)C dispersions are rather ductile at room temperature and exhibit measurable plastic flow at -50°F in both the wrought and fully recrystallized conditions. Their strengths are also considerably higher than that of CI-1. These simultaneous improvements in strength and ductility are a result of interaction of the carbide particles during working and/or annealing at 2000 ± 200°F with both residual interstitial

impurities and with the dislocation array. It is also possible, as suggested by Hahn and Rosenfield[18] that such particles are sources of mobile dislocations and thus help to prevent large stress concentrations which result in intergranular crack initiation in single-phase chromium alloys.

Addition of 4 atomic percent Mo raises the ductile-brittle transition temperature (DBTT) by at least 200°F. The Cr-Y-4Mo ternary appears to be slightly more ductile than corresponding alloys with carbides in this tabulation, but the difference, if real, is not great. Strengths of the compositions with carbide dispersions are at least 10 to 15% higher than their carbon-free counterpart at these lower temperatures, and show an even higher advantage at elevated temperatures, as will be shown in the following sections.

The best balance of strength and ductility was generally observed after a one-hour anneal at 2000°F. This temperature was selected for treatment of the rest of the alloys of this series for initial screening of mechanical properties.

6.4 Tensile Properties

6.4.1 Stress-Relieved Condition

Screening tests conducted to date have been made on specimens annealed for one hour at 2000°F and at 2400°F. Data after the low-temperature heat treatment are presented in this section. Low-temperature testing procedures were described previously. Elevated-temperature tests were made on ground button-head specimens with an overall gauge length of 1.1" and a diameter of .160". In each temperature range, an Instron machine was employed at a nominal strain rate of .03 per minute. Tests at 1900°F and above were made in vacuum at pressures of 10^{-5} torr or below.

Ultimate tensile strengths and low-temperature reduction of area values from representative alloys are plotted as a function of temperature in Figures 25 and 26, respectively. The Cr-Y binary has quite low strength over the entire temperature range of interest. Addition of the (Zr,Ti)C dispersion results in an increase of at least 60% in these strengths at the higher temperatures, but the absolute values are still rather low. A concentration of 4 atomic percent Mo doubles the low-temperature strength of Cr-Y and raises its strength by a factor of 3 to 4 at 1900 to 2400°F. The increment due to the ZTC dispersion appears to be about the same in either a Cr-Y or a Cr-Mo-Y base. The CA-2 alloy (Cr-35Re) has considerably higher strength at 1900°F, but at 2400°F, where the alloy is completely recrystallized prior to test, the strengthening by the concentrated Re addition is not much greater than that afforded by 4 atomic percent Mo.

Based on the criterion of 5% reduction of area defining the transition from brittle to ductile behavior, the DBTT values of Cr-Y, Cr-Y(Zr,Ti)C and Cr-Y-(Zr, Ti)B alloys are near or below room temperature, and that of the Cr-4Mo-Y composition about 300°F. Low-temperature tests on the particular Cr-4Mo-ZTC alloy shown in Figure 26 indicate that the carbide dispersion raises the DBTT of the Cr-4Mo base by about 150°F, but as will be shown below, other carbides have much less drastic effect. The Cr-35Re alloy is, of course, quite ductile well below room temperature.

All of the tensile results obtained after one-hour annealing at 2000°F are presented in Appendix A. Elevated-temperature tensile strengths of the strongest compositions of each type are compared to the C-207 alloy developed in this laboratory[9,10] in Figure 27. C-207 has the composition Cr-2.25W-.1Y- 4Zr-.2Ti-.4C in atomic percent. In the condition shown in the comparison, this alloy has a tensile DBTT of 350 to 400°F. Data are plotted in Figure 27 as scatter bands on an expanded temperature scale in order to better illustrate the differences between types of alloys.

The 1900 and 2400°F strengths of 81,000 and 30,100 psi measured in the Cr-6W-.1Y alloy (CI-8) represent the highest strengths for a solid-solution Cr alloy known to the writer. It will be noted in Appendix A that W is a considerably more effective strengthener than Mo on the basis of atomic concentration. However, this Cr-6W alloy and other ternary compositions with 6 to 8 atomic percent W and/or Mo are among those which could not be swaged directly from the extruded condition. Even the alloy with 4 atomic percent W was quite difficult to work and its DBTT is significantly higher than at the level of 4% Mo. The few tensile tests reported here and in the following section represent the only useful bar stock which was obtained from such alloys, and most of it was worked only by impact extrusion prior to final swaging. It is clear that major solute concentrations of W or Mo are very effective with respect to strength, but their adverse effect on workability and low-temperature ductility limits their practical application to rather low levels. Since W is more favorable in its strength characteristics and Mo in its workability and ductility behavior, additions of these two solutes at individual or combined levels of 4 to 6 atomic percent were made to alloys containing selected carbide dispersions in the extension of the work into later phases, in Alloys CI-44 through CI-49. Only those with W plus Mo at 4 atomic percent could be worked using conventional procedures. Thus, in order to reach strengths above about 50,000 psi at 1900°F, one of the supplemental means of strengthening must be employed.

All the dilute alloys with carbon added exhibit strength increases over the base and those shown in Figure 27 (CI-19 through -21 and CI-50 and -51) all are ductile well below room temperature, with DBTT values of 0 ± 25°F. The boron-containing alloys CI-22 through -24 are considerably stronger, particularly at 1900 to 2100°F, but their DBTT rises to the range 150 ± 100°F. Carbide-containing Cr-4Mo alloys all show elevated-temperature strength increases over the solid solution. The increase is least in the alloys containing Zr at levels above 0.4 atomic percent, and in the "standard" ZTC alloy at the higher Y concentration (CI-30). This latter result parallels earlier observations that Y has a weakening effect at higher temperatures, particularly in alloys with dispersed carbides[9,10].

The best balance of properties was observed in the Cr-4Mo or Cr-2W-2Mo alloys which contain Cb-rich or Ta-rich carbides, or in one case a carbonitride. Elevated-temperature strengths of such alloys (CI-36, -41, -42, -43, -46, -47, -58) are shown in the scatter band of Figure 27. These alloys not only have strength advantages of 25 to 50% over that of C-207, but several of them exhibit tensile DBTT values in the same range of 350 to 400°F.

Several alloys with complex borides or combinations of carbides and borides were prepared in the later phases of the work, but some of them could not be worked successfully even using the expedient of impact extrusion prior to swaging. One such alloy which yielded a limited amount of bar stock (CI-56) has attractive high-temperature properties, with tensile strengths slightly above the highest scatter band in Figure 27, but its DBTT is above 600°F. The Cr-20V-5W alloy CI-52 which is the only composition with a W content above 4 atomic percent that was successfully worked in this program, also shows rather high tensile strengths. However, as will be described in following sections, the air oxidation behavior is extremely poor and creep-rupture properties are inferior to Cr-4Mo alloys with CbC, TaC, or TiC dispersions. This alloy also has a tensile DBTT of about 550°F.

6.4.2 Recrystallized Condition

Tensile properties in the recrystallized condition are recorded in Appendix B. Except as noted, a vacuum anneal of one hour at 2400°F was employed. In order to facilitate comparisons between alloys and between structural conditions, some of the critical properties of the entire series are presented in Table 23. It will be noted by comparison of the complete data in Appendices A and B that at a test temperature of 2400°F there is very little difference between the strengths of the recrystallized specimens and those which were stress relieved prior to testing. Most of the latter are recrystallized during heating in the 2400°F tests. In Table 23, the average tensile strengths at this temperature are recorded. The tabulation also shows the strengths of the stress-relieved and recrystallized specimens at 1900°F, which is well below the recrystallization range in all but the most dilute alloys, and presents the approximate DBTT in each structural condition. These DBTT values are estimated by interpolation of ductility versus temperature data in the appendices to a reduction of area value of 5%. Very few duplicate tests were made because of material limitations. The DBTT values should therefore be considered as approximations only. In those alloys that yielded insufficient amounts of bar stock to conduct screening tests in both the wrought and recrystallized conditions, emphasis was placed on the former structure. The wrought conditions of most alloys show considerably higher strengths in the temperature range of 1900 to 2100°F where chromium has its highest potential, and the low-temperature properties are generally superior in the wrought structure.

The effects of recrystallization on the mechanical behavior appear to be markedly dependent upon the type of alloy. In most of the single-phase alloys containing major substitutional solutes at or above 4 atomic percent, recrystallization lowers the wrought tensile strength at 1900°F by 15 to 30% and, in general, raises the DBTT over that of the wrought structure by 50 to 200°F. Many of the alloys with dispersed phases, on the other hand, exhibit much less drastic losses of elevated-temperature strength upon annealing at 2400°F, and some show slight increases. In several such alloys the DBTT either changes insignificantly upon recrystallization or in some instances (CI-24, -30, -40, -60, -61 of the alloys for which data in both structures are available) shows a pronounced decrease from that measured on wrought specimens. Although it is realized that these observations are open to some question, both because of the rather arbitrary definition of the DBTT and the limited number of tests per alloy conducted in this screening investigation to locate the transitions, it appears to be significant that 4 of the 5 alloys which show a reduction in DBTT upon annealing at 2400°F contain Ta or Cb as the major dispersion stabilizing addition. Several other such alloys (Ci-36, -41, -42, -43, -47) retain their elevated-temperature strength after recrystallization, have reasonably low DBTT values in the wrought condition, and so far as data are available, show little adverse change in low-temperature properties after recrystallization.

In addition to retaining or improving the wrought DBTT, alloys with Cb-rich or Ta-rich dispersed phases show considerably higher values of flow stress at low temperatures after recrystallization. It should be mentioned in this regard that the annealing temperatures employed in several of these alloys were close to the recrystallization temperatures presented earlier in Table 19. Although optical microscopy indicated that the samples were in fact recrystallized, it is possible that some effects of warm working remained. It has been shown by a number of workers (for a review see Reference 28) that only a very small amount of cold work or a relatively low density of mobile dislocations, greatly affects the low-temperature flow and fracture of chromium. As recently shown by Ryan[8], fine carbides greatly retard recrystallization in chromium, primarily by interaction with a non-cellular dislocation array produced in warm working and thus may result in a sufficiently high mobile dislocation density after annealing at 2400 to 2500°F. Even if this is not the case and the structure if fully recrystallized, the arguments of Hahn and Rosenfield[18] predict that fine dispersions should enhance ductility both through making cleavage more difficult by limiting dislocation pile up and through acting as sources of mobile dislocations in a source-poor structure. Whatever the mechanism(s) involved, it is clear that fine dispersions are quite effective in raising the strength of chromium alloys at least through 2100°F without any markedly adverse, and in some cases with a beneficial, effect on ductility. Cb-rich or Ta-rich dispersions appear to yield the best balance of tensile properties.

With respect to the (Zr,Ti)C dispersion in the Cr-4Mo-.05Y base, there is no evidence that improved properties are obtained by changes in the atomic ratio of the concentration of reactive metals to that of carbon (CI-31 and CI-32) or in the volume fraction of the carbide phase (CI-38 and CI-39) compared to the 0.4Zr-0.2Ti-0.4C in CI-29. In fact, higher levels of Zr appear to be detrimental both to 1900°F strength in the recrystallized specimens and to the DBTT in each structural condition. Similar observations have been made in earlier work in this laboratory[3] and by Wilms and Rea[6] in their exploration of dilute alloys in the Cr-Ta-Zr-C-B system. Atomic concentrations of the Group IV-A and/or Group V-A metals at 0.6 percent and of the interstitials at 0.4 percent were therefore maintained in most of the alloys in the later phases of the work (CI-40 through CI-61).

Alloys that contain particles of secondary phases had smooth stress-strain curves at low temperatures in both structural conditions tested. The stress-strain curves recorded in tests at 400 to 800°F on recrystallized specimens of some of the Cr-Y alloys with ternary additions (CI-4 through CI-17) show rather sharp breaks or inflections in the curves at departure from linearity, but no drops in load were observed. As shown by the data in the appendices, Cr-35Re was the only alloy which exhibited distinct upper and lower yield points in the recrystallized condition, as did high-purity Cr in both the recovered and recrystallized structures. Ductility of the Cr-35Re alloy is outstanding, with substantial elongation and reduction of area values measured at temperatures as low as -200°F. Flow stresses at low temperatures are also quite high. However, elevated-temperature strengths of Cr-35Re (65 weight percent Re) are inferior to those that result from much lower concentrations of W or Mo. In most aerospace applications it is not the absolute value of strength that is of prime importance, but the strength-to-density ratio. Since the density of Re is very high, the latter property is compared to those obtained in more dilute Cr-W, Cr-Mo, and carbide-containing alloys in the following tabulation:

Alloy	Nominal Composition (Atomic %)	Density, ρ (lb/in^3)	Temp °F	UTS (ksi)	UTS/ρ (in.)
CI-4	Cr-4Mo-.1Y	.274	1900	46.4	169,000
			2400	17.2	63,800
CI-5	Cr-6Mo-.1Y	.277	1900	(61.0)	(220,000)
			2400	24.0	87,000
CI-7	Cr-4W-.1Y	.292	1900	63.6	218,000
			2400	23.8	82,000
CI-8	Cr-6W-.1Y	.303	1900	81.0	267,000
			2400	30.1	99,000
CI-33	Cr-4Mo-.05Y-TiC	.272	1900	59.0	217,000
			2400	22.3	82,000

CI-36	Cr-4Mo-0.05Y-CbC	0.275	1900 2400	65.7 20.4	239,000 74,000
CI-47	Cr-2W-2Mo-0.15 (La + Y)-TaC	0.286	1900 2400	70.3 22.1	246,000 77,000
CA-2	Cr-35Re	0.463	1900 2400	69.7 22.1	150,000 48,000
*	Cr-35Re-Carbide	0.463	1900 2400	(99.0) (27.2)	(214,000) (59,000)

*Cr-35Re with strength increments due to most effective carbides added to actual strengths.

The highest incremental strengthening due to carbide additions in the present series, about 19,300 psi from CbC and TaC at 1900°F and about 5,100 psi from TiC at 2400°F, were added to the measured data from the binary Cr-35Re in order to estimate the potential of a carbide dispersion in the ductile Cr-Re alloy. It is evident from the tabulation that strength-to-density ratios would still lie well below those achieved with much more dilute concentrations of W or Mo.

One final observation concerning mechanical properties of Cr-Re alloys should be made. The addition of 4 atomic percent Re to a Cr-Y base (CI-16) resulted in rather low strengths at elevated temperatures, and a DBTT of 450 to 500°F, between the values exhibited by Cr-4Mo and Cr-4W alloys. However, addition of (Ta,Hf)C to the Cr-4Re alloy (CI-48) resulted in a DBTT near room temperature, although the strength is still rather low at 1900 and 2400°F. The same addition of (Ta,HF)C to Cr-4W or to Cr-2W-2Mo (CI-45 and CI-46) raises the elevated-temperature strength by a greater degree, but DBTT values of the latter alloys are 650 to 700°F. Reasons for the large ductility improvement in the Cr-4Re-(Ta,Hf)C alloy are at present unknown; and, unless the strength can be increased, they may be of little practical significance. It may well be possible, however, that strengthening additions of W or Mo can be made to such carbide-containing Cr-4Re alloys without completely overriding the ductility effect.

6.5 Creep-Rupture Properties

Creep-rupture tests were conducted on selected alloys at 2100 and 2400°F with emphasis on the lower temperature. Tests were made on 0.160"-diameter button-head specimens with a gauge length of 1.1" in capsules which were evacuated to at least 5×10^{-4} torr and, after purging, were back-filled with

purified helium at a slight positive pressure of about 800 torr. Loss of pressure during testing was negligible. Constant loads, using a load-train assembly made from a Mo-0.5% Ti alloy, were applied by the dead-weight technique at a lever ratio of 10:1. Strain-time relationships were recorded on multi-channel Gilmore units using the signals from linear variable differential transformers mounted externally in axial alignment with the specimens. Initial tests on each alloy at 2100°F were made at a stress corresponding to approximately 35% of the tensile strength at that temperature. Stresses in subsequent tests were raised or lowered by 2,000 or 2,500 psi depending on the rupture life in the first test.

Results obtained on recrystallized specimens are presented in Table 24A. Note that at 2400°F very rapid secondary creep rates are observed even at stresses as low as 3,500 psi. At 2100°F, however, all of the carbide-strengthened Cr-4Mo alloys exhibit 100-hour rupture strengths above 10,000 psi and have creep rates which are lower than those at 2400°F by more than an order of magnitude. A few of the alloys that have recrystallization temperatures among the highest measured in the series were also tested for comparison in the stress-relieved condition. These data are shown in Table 24B. Rupture lives at common stresses are increased by factors of 2 to 3 in the wrought and recovered structure, and creep rates decrease by a somewhat greater margin, with respect to those in recrystallized specimens. The best creep-rupture properties are observed in the alloy with a CbC dispersion, followed rather closely by those with dispersions of TaC and TiC. Gas analyses were made on portions of the gauge lengths from several of the longer-time specimens after testing to check the cleanliness of the testing environment. With one exception, oxygen and nitrogen contents increased by less than 50 ppm. In the stress-relieved CI-41 specimen, a pickup of 42 ppm nitrogen and 120 ppm oxygen was indicated.

Rupture data from several of the alloys are shown on a Larson-Miller plot in Figure 28. Values of 15, 20, and 25 were used for the constant C in the Larson-Miller parameter $P = T\ (C + \log t)$, where T is the test temperature in °Rankine and t the rupture time in hours. The data were best fit by the value C = 20, although a number of tests at common stresses as a function of temperature would be required to establish the pertinent value of C, which is directly related to the activation energy for creep. Included for comparison on this plot are data reported by Pugh[29] for unalloyed Cr and the average rupture curve for the C-207 alloy developed in this laboratory[9,10]. The tensile strengths of the present alloys are plotted at a rupture time of .05 hour on these curves, to give some indication of the degree of strength retention in time-dependent loading. Although these points appear to fit extrapolations of the rupture data rather well when plotted in this manner, the dashed portions of the curves should, of course, not be used as other than estimates of rupture behavior under other time and temperature conditions.

The substitutional solution of 4 atomic percent Mo raises the 100-hour strength of unalloyed Cr at 2100°F from less than 2000 to about 9000 psi. Addition of 0.4Zr-0.2Ti-0.4C, which results in the formation of a rather coarse dispersion of (Zr,Ti)C plus finer TiC, as shown previously, results in a further increase of 2500 to 3500 psi in the 100-hour strength at this temperature. The CbC dispersion, which is considerably finer, shows much greater strengthening in creep rupture at 2100°F. In fact, the strength increment associated with atomic concentrations of 0.6 Cb and 0.4 C is about the same as that due to addition of 4 atomic percent (7.1 weight percent) Mo. The 100-hour rupture strength of 16,500 to 17,000 psi exhibited by this alloy in the wrought and recovered condition at 2100°F represents an increase of about 100°F over C-207, and 500 to 600° over unalloyed Cr. This same advantage is maintained to at least 2400°F, but strengths at the latter temperature are far too low for practical application.

The curves in Figure 28 and the data in Table 24A also serve to illustrate the essential equivalence of W and Mo as solution-strengthening additions to Cr at 2100°F on the basis of weight percentages of these solutes. Rupture points appear to fall on the same curves for CI-29, which has 7.1 weight percent Mo and for C-207, which has 7.5 weight percent W, added to a Cr-Y-ZTC base. At higher temperatures, tensile results indicate that W is superior, as discussed previously. Since dispersion strengthening by carbides does not appear to be operative at 2500°F and possibly becomes ineffective at temperatures nearer 2200°F, it is unfortunate that both workability and low temperature ductility considerations limit the addition of refractory solutes other than Re to rather low levels. However, the combination of solution strengthening by about 4 atomic percent Mo or W plus dispersion strengthening by the more effective carbides results in chromium alloys with creep-rupture strength advantages of at least 200°F over the best available nickel-base superalloys. It should be pointed out that the properties reported here were measured in more or less standard wrought conditions. It has been shown that the size and distribution of dispersed phases, and hence mechanical properties, are strongly dependent upon processing history in similar alloys[3,5,8,9]. Further improvements of the present alloys are therefore probable through application of suitable thermal and mechanical treatments.

6.6 Air Oxidation Behavior

Specimens for oxidation tests were taken from swaged bar stock corresponding to locations near the center of the original ingots. They were centerless ground to about 0.2" diameter to completely remove the protective cladding, electropolished to remove a further 1 to 2 mils from the surfaces, but into lengths of approximately 0.5", and then stress relieved for one hour in vacuum at a temperature at least 100°F below the recrystallization temperature. Uninterrupted exposures were made in static air for 100 hours at 1500 and

2100°F and for 25 hours at 2400°F. Hevi-Duty laboratory furnaces, Model 7145 for the 1500°F tests and Model G-494 for the tests at higher temperatures, were used throughout the program. The specimens were held in small ZrO_2 crucibles. Porcelain lids were placed over the crucibles immediately upon their removal from the furnace to prevent the possible loss of any oxide that spalled during cooling. After measuring weight changes, the samples were mounted for metallographic examination. In addition to microstructural characterization of the degree of subsurface reaction, microhardness traverses were made at intervals of 0.5 to 1 mil using a diamond pyramid indentor at a 100-gram load.

A summary of the oxidation results is presented in Table 25. Several different types of internal reaction with gaseous contaminants, primarily nitrogen, were observed as indicated in the tabulation. Examples of each are illustrated in Figure 29. A number of the alloys, particularly the carbide containing compositions after testing at 2400°F, showed deep intergranular nitridation beneath thick surface nitride layers and the matrix was hardened to an even greater depth. In fact only one alloy in the entire series, the dilute Cr-Y-Th-Hf (CI-3), exhibited neither nitride formation nor significant subsurface hardening at each of the three temperatures included in the study. All of the other alloys showed some sort of detrimental subsurface reaction after exposure to at least one of the test conditions.

Close study of the data in Table 25 indicates that no completely consistent generalities can be made concerning the air oxidation behavior of these alloys. This is perhaps to be expected since the reaction of Cr with oxygen and nitrogen is a complex process. The weight-change data reflect not only weight gain due to oxidation of the alloy to form Cr_2O_3, but weight loss due to oxidation of Cr_2O_3 to the volatile oxide CrO_3 at higher temperatures[30,31]. They also reflect the degree of adherence of the surface oxide, as discussed previously, which in turn controls the rate of nitrogen absorption by the underlying alloy. Not only are there competing reactions involved in air oxidation of Cr, but a number of factors have been intentionally varied in this series of rather complex alloys. It is not unlikely that a comparable number, for example differences in trace impurities and degree of recovery in annealing prior to testing (which could affect interstitial diffusion rates and thus contamination in tests at the lower temperatures), have varied in an uncontrolled manner. Nevertheless, certain trends are apparent in the data and should be noted here.

In the Cr-Y alloys with additions of Mo or W, a residual Y content of about .12% appears to be sufficient to prevent severe nitridation in 100 hours at 2100°F, but a higher level of at least 0.19% is required at 2400°F. Even at this Y level there is some surface hardening in the CI-5 alloy, but not in CI-7.

Of the alloys containing dispersed phases, those stabilized by Hf or Zr are resistant to nitridation at 2100°F even with Y contents as low as 0.02% (for example CI-21, CI-23, CI-34, and CI-37). Several of the alloys containing HfC (CI-35, CI-49, CI-50, CI-51) exhibit no nitride after the 2400°F exposure when rare-earth contents are in the range 0.09 to 0.18%. It would appear from comparison of these data with those obtained in Alloys CI-27, which has only Hf and Zr addition and no C, or with CI-23, which contains (Hf, Zr)B, that the presence of relatively large and widely spaced Hf-rich carbide particles has a beneficial effect on contamination resistance at 2400°F. As discussed previously in Section 5, this behavior is thought to be related to the scavenging effect of such carbides in which O and N have a high solubility. The size and interparticle spacing are sufficiently large that the HfC particles are not rapidly saturated by the gaseous contaminants, provided that an adherent oxide is maintained. Although the rare-earth-type additions appear to be the primary factor in the control of oxide adherence, it may be possible that Hf(and Zr) assist in the promotion of protective scales. This could result either from increased plasticity of the oxide due to their dissolution in Cr_2O_3, thereby increasing the critical thickness at which spalling occurs, or in the case of coarse carbides formed by these additions, from these particles serving to "anchor" the Cr_2O_3, as suggested by the micrographs in Figure 11.

All of the alloys containing (Zr,Ti)C dispersions form continuous nitride layers and are hardened to considerable depths during air exposure at 2400°F and, with the exception of the carbon-free alloy CI-26, are hardened to a much lower depth at 1500°F. Oxidation behavior of these alloys at 2100°F, however, is rather erratic and does not correlate well with residual Y concentration. The CI-30 alloy, in which the Y content of 0.15% is the highest of the Cr-4Mo-(Zr,Ti)C series, shows the lowest weight gain and the least hardening. The other Cr-Y-ZTC alloys at 0, 4, and 6 atomic percent Mo show little dependence of 2100°F air oxidation characteristics on retained Y levels in the range 0.02 to 0.09%. Weight gains range from less than 1.0 to nearly 10 mg/cm^2. Three of the ten alloys of this type form continuous nitride layers at 2100°F. The others are all hardened, but by less than 100 DPH. Formation of nitride layers beneath the surface oxide invariably increases the hardness to at least 900 DPH and usually to greater than 1200 DPH, while much less severe hardening is associated with nitrogen dissolution or interaction with dispersed phases. Although some of the (Zr,Ti)C alloys with residual Y levels of 0.05% and below exhibit low weight gains and mild hardening of the latter type at 2100°F, it would appear that Y concentrations of at least 0.1% Y are required to reproducibly provide adequate 100-hour oxidation resistance in such compositions at 2100°F.

Each alloy with a Ti content above 0.2% exhibited intergranular oxidation at 2100°F as noted in Table 25 and illustrated in Figure 29E. This behavior, however, cannot account for the somewhat erratic results encountered in the (Zr,Ti)C alloys discussed above, since one such alloy (CI-31) did not form a continuous nitride layer whereas one with a low Ti content (CI-32) suffered fairly extensive nitridation.

In alloys which contain Cb or Ta as the major dispersion-stabilizing addition, Y at the levels employed in this series is not effective in providing resistance to rapid attack during air oxidation at either 2100 or 2400°F. Earlier results indicated that still higher concentrations are equally ineffective, as discussed in Section 5.4. Based on the results on arc-melted buttons presented in Sections 5.6 through 5.9, combined additions of Y and La were made to several such alloys with Ta or Cb in the later stages of the induction-melted series. Some of these also contained Zr or Hf in order to determine whether the beneficial effects of these elements could be retained in more complex compositions. The data recorded in Table 25 demonstrate that, provided the residual Y and La content is above about 0.12%, alloys containing Cb-rich or Ta-rich secondary phases have relatively low weight gains and are only moderately hardened in 100-hour air exposures at 2100°F. This represents considerable improvement over similar alloys with Y alone. However, each alloy of this type shows rapid scaling and formation of extensive nitride layers in shorter exposures at 2400°F, even at rare-earth concentrations above 0.2%. Since the quite low strengths at 2400°F appear to limit the potential usefulness of carbide-strengthened Cr alloys to lower temperatures, the oxidation behavior at 2100°F is probably of greater practical significance.

The oxidation behavior of the Cr-Re alloys is also worthy of note. At a concentration of 35 atomic percent Re, which is near the terminal solubility in Cr, oxidation at each test temperature results in precipitation of sigma phase in the matrix beneath the Cr_2O_3 scale. This results from depletion of the Cr content in this region, since Cr oxidized by outward cation diffusion through the scale. Although no nitrides are observed after air exposures over the temperature range investigated here, this formation of sigma phase is in itself highly embrittling. The Cr-4Re alloys, both the ternary composition CI-16 and CI-48 with a (Ta,Hf)C dispersion, are also rather resistant to nitridation and, at least through the exposure times included in this study, show no evidence of sigma formation.

7. EFFECTS OF THERMOMECHANICAL HISTORY ON THE PROPERTIES OF SELECTED ALLOYS

7.1 Thermomechanical Processing

Based on the earlier observation that concentrations of about 4 atomic % Mo appeared to result in the best balance of properties, a series of such alloys containing the most effective Group IV and V solutes with and without boron additions were prepared and evaluated to provide comparison with alloys with Carbon compositions and comparative tensile properties are shown in Table 26. Stress-rupture behavior is presented in Table 27 for some of these alloys, in addition to further results from earlier alloys not shown in Table 24.

The alloys with B, particularly those containing Cb or Ta, appeared promising but processing was rather difficult. The following tabulation compares critical mechanical behavior of the several systems that were considered for a somewhat more detailed evaluation of processing effects.

Comparative Properties of Alloys Considered for Processing Study			
Alloy	DBTT (°F)	UTS (ksi) at:	Approximate 100-Hr. Rupture Strength at 2100F (ksi)
Cr-4Mo-CbC	350	600°F 111.0 1000°F 65.7 2100°F 54.5 2400°F 21.8	17.0
Cr-4Mo-TaC	450	600°F 102.2 1900°F 61.5 2100°F 50.2 2400°F 21.5	15.5
Cr-4Mo-Cb	400	600°F 98.0 1900°F 65.0 2100°F -- 2400°F 22.1	12.5
Cr-4Mo-Ta	350	600°F 106.8 1900°F 60.0 2100°F 41.2 2400°F 21.3	(10.0)
Cr-4Mo-CbB	600*	600°F 118.5 1900°F 75.6 2100°F 48.7 2400°F 21.6	17.5*
Cr-4Mo-TaB	500	600°F 127.0 1900°F 70.3 2100°F -- 2400°F 20.9	(13.0)

* After creep-aging at 1900°F, the values of DBTT and 2100°F/100-hour rupture strength are approximately 400°F and 22,500 psi, respectively.

X-ray diffraction analyses were completed on phases electrolytically extracted from several of the B-containing alloys. In each case, the major phase is the hexagonal diboride MB_2. With one exception, in which ZrB_2 with lattice parameters very near the accepted values for that phase (a = 3.18 Å, c = 3.53 Å in the alloy vs. ASTM index values of a_o = 3.169 Å, c_o = 3.530 Å) was observed, these phases appear to be solutions of at least two diborides. Some evidence of partial transformation to cubic monoborides was noted after aging at 2000°F. Electron microscopy of such alloys shows a dual distribution of particle sizes, most of them being quite large (greater than 1_{μ} in diameter) with a very fine dispersion (less than 500 Å diameter) appearing in a somewhat banded distribution.

Although several attempts were made to hot and/or warm work heats containing borides, most of the thermomechanical study was confined to the alloys shown in Tables 28 and 29. Screening work was confined to examination of the effects of variations in the working schedule on the DBTT and on tensile behavior at 2100°F.

Solution annealing of the ingots prior to extrusion resulted in considerably improved workability during subsequent swaging. From the data presented in Tables 28 and 29, it would also appear that prior annealing of the castings is effective with respect to mechanical properties and, further, that such treatments applied at intermediate stages of final processing also result in somewhat higher strengths at elevated temperatures. Effects on DBTT are also positive.

7.2 Effects of Prestrain

Experiments to determine the effects of prestraining at low temperatures in the ductile region on subsequent ductile-brittle transition behavior were initiated on recrystallized samples of the dispersion-strengthened CI-58 alloys. A Cr-4Mo composition with a Db(C,N) dispersion was chosen for this study since the matrix in this case contains interstitially dissolved carbon and nitrogen in equilibrium with the reactive solute Cb. The transition temperature of this alloy in the virgin recrystallized condition was established at 600°F, with yield and ultimate strengths of 51,000 and 82,000 psi, respectively, at this temperature. Several other recrystallized specimens with gauge lengths of 1.10" were prestrained approximately 3% (2.78 to 3.11%) at 700°F, then the central 0.5" lengths were ground and electropolished to ensure that plastic flow in the following test sequence would take place in the prestrained section and not in unstrained shoulder radii. The test sequence began at 600°F and continued downward in decrements of 100°F until fracture occurred at a strain of less than 3%.

The virgin CBTT of approximately 600°F was not appreciably altered by 3% prestrain at 700°F. This behavior may have been at least partly due to a relatively high strain-hardening exponent, n, defined by the relationship $\bar{\sigma} = k\,\bar{\epsilon}^{n}$ where $\bar{\sigma}$ and $\bar{\epsilon}$ are the true stress and true strain, respectively. An average value of n = 0.21 was measured in prestraining at 700°F, during which the nominal flow stress increased from 52,000 psi at a strain of 0.2% to 76,000 psi at 3% elongation. Upon subsequent restraining at 600°F, duplicate samples fractured at less than 1% elongation at stresses of 78,300 and 81,400 psi and at room temperature a third sample failed at 85,000 psi without macroscopic plastic flow. These experiments were then repeated after prestraining at 1200°F, where the freshly formed dislocations may be more mobile than those generated at 700°F, with little effect on properties at lower temperatures. However, extremely pronounced serrated flow was observed at 1200°F. Further tensile testing in the temperature range of 1000 to 1400°F confirms that this phenomenon exists over that entire range and is associated with negative strain-rate sensitivity (a decreasing flow stress with increasing strain rate, as discussed for other types of materials by Wilcox and Rosenfield. Although it is not presently known over how many orders of magnitude of strain rate that this behavior persists, it could possibly lead to improved workability in any future exploitation of Cr alloys.

The first alloys rupture tested at 1900°F, those without dispersions or with relatively ineffective dispersions, had given rather low results, with lives that indicated that the 100-hour rupture strengths were less than 40% of the yield strengths at this temperature as shown in Tables 24 and 27. This fraction is significantly lower than that observed in the C-207 alloy developed prior to this contract, in which the 100-hour rupture strength was on the order of 50% of the yield strength at 1800 and 1900°F. Tests were therefore initiated on one of the alloys in the present series that has a reasonably fine dispersion, the Cr-4Mo-Y-Cb (C,N) alloy CI-58. The first test, conducted in the stress-relieved condition, gave a rupture life of 29.3 hours at 25,000 psi (40% YS) - - a result comparable to those from weaker alloys at similar fractions of their yield strengths. Since the finest dispersions have been observed after small amounts of strain at 1900 to 2100°F, it was decided to precreep a second specimen of this alloy at lower stresses at 1900°F, then to observe the behavior as the stress was increased to higher values. This specimen was initially loaded at 12,000 psi, then after establishing reasonably linear creep, the stress was raised in increments of 1000 psi to 2000 psi to a final level of 28,000 psi. Under these conditions, a total creep exposure of about 380 hours was imposed, with 160 hours at 28,000 psi, and over 200 hours at stresses above the earlier 30-hour rupture strength. This behavior suggests strain-enhanced precipitation or interaction with the dislocation array.

A similar treatment was applied to both the CI-33 and CI-70 alloys, with the results shown in the following tabulation:

Effects of Creep-Aging* at 1900°F and 2100°F Step-Loaded as Shown		
Alloy	Stress (ksi)	Life (hrs.)
CI-58	11.0	138.10
		33.0 @ σ = 13.0 to 23.0 ksi
(1900°F)	24.0	22.0
	26.0	23.6
	28.0	160.05 (no failure)
CI-33	8.5	15.9
	20.0	26.7
(1900°F)	27.5	15.0 (37.6% elongation)
CI-70	12.5	22.0
	15.0	85.5
(2100°F)	17.5	25.1
	20.0	82.6
	22.5	94.7 Total Time 310 hours
* All prestrain, including that in CI-70, applied at 1900°F		

In this instance, the same prestrain at 1900°F was quite effective in promoting low-temperature ductility. After such treatment of three samples, the apparent DBTT was decreased from 600 to about 400°F based on 5% reduction of area. Although intermediate-temperature strain is of little benefit, the present approach could have merit.

7.3 Properties at High Strain Rates

As an indication of the risk involved in sudden stressing of Cr alloys at low temperatures, brittle fracture data were generated at temperatures well below the DBTT. In alloys (CI-61 and CI-72) with a DBTT of about 500°F, extrapolation of yield and ultimate strengths from temperatures of 400 to 600°F indicates expected fracture strengths of 69,000 psi and 110,000 psi, respectively, near 0°F in the "ductilized" condition (ground + stress relieved + electropolished). In order to exaggerate the effects, all of the present tests were made without electropolishing, and some specimens were tested both without stress relief (S.R.) and after 24 hours air oxidation at 2100°F. Strain rates ranging from 1.0 to 2000% per minute were employed. Representative results, with the data normalized to the strength of the latter alloy, are summarized as follows:

Fracture Strength of Chromium Alloys**				
Condition	Test T (°F)	Strain Rate (%/min.)*	Fracture Stress (ksi)	Elong. (%)
Stress Relieved and Electropolished	-100	2.0	(110.0)	(0.0)
	75	2.0	(110.0)	(0.0)
	75	20.0	113.2	0.0
	75	200.0	102.1	0.0
	75	2000.0	46.7	0.0
	400	2.0	107.0	3.4
	600	2.0	118.5	5.3
As Ground	-100	2.0	57.0	0.0
	-100	20.0	55.2	0.0
	-100	200.0	23.8	0.0
	-100	2000.0	1.7	0.0
	75	2.0	105.1	0.0
	75	200.0	29.7	0.0
	75	2000.0	7.5	0.0
	800	20.0	103.0	7.0
	800	200.0	81.5	4.9
	800	2000.0	34.3	0.0
Ground + Air Oxidized 2100°F/24 hrs.	75	2.0	47.6	0.0
	75	200.0	10.6	0.0
	75	2000.0	2.9	0.0
	800	200.0	118.2	4.4

* In the elastic region, strain rates can be related to stress application rates. Since $E = 40 \times 10^6$ psi,

2000%/min. = 13,000,000 psi per second

200%/min. = 1,300,000 psi per second, etc.

** All data were normalized to the strength of CI-72.

It is clear that "prewarming" of components will be quite effective in preventing fracture at extremely low stresses, but even at stressing rates of over 10^6 psi per second, proper control of the residual stresses appears to be equally effective.

Micro-Izod impact tests were also conducted on several selected alloys. Specimens of 0.225" overall diameter, with center sections ground on a radius of 1.375" to a minimum diameter of 0.150" at mid-length, were employed in this work. In the original study of titanium alloys using this type of specimen

(ASTM Special Publication No. 204) it was found that impact energies measured in inch-pounds by this technique are essentially equal to values from standard charpy tests in foot-pounds. It is not known that the same relationship would hold for these chromium alloys, but the ratio should probably be near this value based on the respective cross-sectional areas of the specimens. Results are shown in Table 30. The values of tensile DBTT measured earlier in the same thermomechanical conditions are presented for comparison.

In general, impact transition temperatures are 250 to 400F above values measured in slow-strain-rate tensile tests. The one exception is the single-phase alloy containing 35 atomic percent Re, which was quite ductile in impact at -200F. This behavior represents large improvement over results measured several years ago at Battelle, where a similar Cr-Re alloy containing small amounts of sigma phase was brittle in notch impact well above room temperature in both the wrought and recrystallized conditions.

Based on the excellent impact properties reported here for Cr-35Re, micro-Izod tests were conducted on two alloys with much lower Re concentrations. Results from tests in the swaged and stress-relieved condition are tabulated below, with Cr-35Re for comparison:

Alloy	Composition (At %)	Test Temp. (°F)	Impact Energy (In-Lb)
CI-16	Cr-4Re-0.1Y	200	0.5
		600	3.4
CI-48	Cr-4Re-0.3Ta-0.3Hf-0.4C	200	3.1
		600	43.2*
CA-2	Cr-35Re	-200	43.9*
		-100	43.2*
		75	43.0*
		75	128.6*
		75	183.4*

* Did not fracture

The latter alloy was ductile in slow strain rate tensile testing at room temperature. Unlike the high purity arc melted Cr-35Re composition, which retained its very low DBTT even in impact, Cr alloys with low Re levels parallel all other Cr alloys studied in that they suffer an increase of several hundred degrees Fahrenheit in their transition behavior upon increasing the strain rate by orders of magnitude. The extremely ductile behavior appears to be confined to alloys containing sigma-forming solutes at concentrations near the solubility limit.

8. DUCTILITY OF A SELECTED DILUTE ALLOY

Work on the final phase of the contract was confined to the rather low-strength but nitridation resistant alloy Cr-0.1Y-0.05Hf-0.03Th, designated CI-203. The reasons for continued interest in this alloy are that, under normal strain rates and with reasonably smooth surfaces, it is ductile in tension at room temperature and it retains a relatively low DBTT after extended air oxidation at elevated temperatures. However, it has been shown in other Cr alloys that sudden stressing at temperatures below the DBTT can lead to fracture at stresses of less than 10% of the expected yield strength as the strain rate increases, as shown in section 7.3. This behavior is particularly pronounced in the case of specimens containing surface stress concentrations imposed by machining or by nitridation. Since such fragility would be highly detrimental in use of the Cr-Y-Hf-Th alloy in applications such as cladding, its low temperature properties as a function of strain rate and surface condition were examined. The salient results are summarized below:

Condition	Test (°F)	Strain Rate (%/min.)	Fracture Stress (ksi)	Approx. DBTT
As Ground	-100	2.0	30.6	150 ± 100F
	75	2.0	46.2	
	200	2.0	53.2	
	75	200.0	22.4	
	200	200.0	29.8	
	75	2,000.0	21.2	
	200	2,000.0	26.4	
	400	2,000.0	41.6	500 ± 100F
	600	2,000.0	54.0	
Ground + S.R.	-100	2.0	42.7	
	75	2.0	50.9	
	75	20.0	49.2	
	75	200.0	45.5	
	75	2,000.0	30.2	
	200	2,000.0	46.1	300 ± 100F
	400	2,000.0	53.0	
Ductilized*	-100	2.0	(52.0)	
	75	2.0	52.0	50F
	75	20.0	57.2	< 75F
	75	2,000.0	39.1	
	200	2,000.0	49.6	300 ± 100F
	400	2,000.0	54.5	
	500	2.0	35.0	82.0% RA
	1000	2.0	40.9	87.1% RA
	1500	2.0	31.4	95.0% RA

* Ground + stress relieved (S.R.) + electropolished

9. CONCLUSIONS

1. Complex chromium alloys were successfully induction melted, cast, extruded, and swaged to 0.25" bar stock. Interstitial impurity contents were maintained below 200 ppm total by revised consolidation techniques. Single-phase alloys with additions of 4 atomic percent Mo or W were processed without undue difficulty, but major solute concentrations of 6 and 8 atomic percent made necessary an intermediate working operation (impact extrusion) in order to produce even a limited supply of bar stock, as did complex dispersions based on combinations of carbides, borides, and silicides even at major solute concentrations of 4 atomic percent.

2. Several dilute carbide-containing and boride-containing alloys exhibited considerable ductility at room temperature and measurable plastic flow at 0°F and below in both the wrought and fully recrystallized conditions. Depending on the nature of the dispersion, some such alloys combined this low-temperature ductility with tensile strengths as high as 35,000 to 40,000 psi at 1900°F. Addition of 4 atomic percent Mo to the dispersed-carbide alloys increased the tensile strength at 1900°F to the range 60,000 to 70,000 psi but raised the CBTT to at least 300 to 400°F. Of the carbide-strengthened Cr-4Mo alloys, the best combinations of properties were obtained by CbC or TaC dispersions. A Cr-4Mo-0.6Cb-0.4C alloy had 100-hour rupture strengths above 15,000 psi at 2100°F in both the wrought and recrystallized conditions, and a tensile DBTT of 350 to 400°F. Poor creep-rupture behavior was observed in all alloys tested at 2400°F.

3. The highest strengths were observed in Cr-6W and Cr-4W (Ta,Hf) alloys, both of which had tensile strengths above 80,000 and 30,000 psi at 1900 and 2400°F, respectively. The tensile CBTT, however, was 700°F or above. W is definitely superior to Mo with respect to strengthening, particularly at 2400°F, but has a more adverse effect on workability and low-temperature ductility. Dilute Re additions were relatively ineffective in elevated-temperature strengthening, but room-temperature ductility was measured in a Cr-4Re-(Ta,Hf)C alloy.

4. Resistance to oxidation and nitridation was shown to be attractive in Cr-Y or Cr-Mo-Y alloys with Hf-rich or Zr-rich carbides at temperatures through 2400F. The binary Cr-35Re alloy had excellent air oxidation resistance, although sigma phase was formed beneath the scale due to Cr depletion during oxidation. Dilute Cr-Re-Y alloys showed promising air oxidation behavior at Re levels as low as 4 to 8 atomic percent.

5. Cr-Y or more complex alloys with CbC, TaC, and TiC additions had finely dispersed carbides and exhibited attractive strength characteristics. The oxidation-nitridation resistance of such alloys, however, was markedly inferior to those with HfC or ZrC dispersions. Their reliable use will require a more effective means of preventing nitrogen embrittlement than that afforded by Y.

6. Additions of La or of La plus Y were shown to be quite effective in preventing nitridation in complex alloys containing carbides as well as in simple Cr-La and Cr-Mo-La compositions. Somewhat higher concentrations of La were required in order to promote nitridation resistance in alloys with CbC or TaC dispersions than in alloys with Zr-rich carbides, and were effective only through 2100F in the former. Because of low solubility in Cr, some evidence of a rather low eutectic temperature, and a high reactivity with ZrO_2 crucibles, problems in consolidating La alloys were encountered, but its beneficial effect on air oxidation behavior is pronounced.

7. No attractive compositions were identified in the Cr-Cb-Si system or its binary components. Cr-Si-Y alloys were rather brittle and the poor air oxidation resistance of Cr-Cb-Y alloys was still evident after addition of Si.

8. Substitution of Co for much of the Re in ductile Cr-35Re alloys resulted in cold workability in single-phase alloys in the cast condition. These Cr-Re-Co compositions, however, were subject to profuse sigma precipitation and consequent embrittlement upon aging at 1600 to 1800F due to a rapid decrease in the Co solvus with decreasing temperature. Such alloys, therefore, do not appear to be practical, and low-Re alloys that showed some tensile ductility at room temperature were rather poor in impact.

9. Solution annealing of the precipitation-strengthened alloy systems studied here, both of the ingots and as an intermediate step in hot/warm working, is beneficial to both strength and ductility. Creep aging, in which samples were strained a very small amount using quite low stresses at 1900F, was beneficial to stress-rupture strength and to a lesser extent improved the DBTT.

10. Several rather dilute alloys exhibited rather attractive behavior at high strain rates, with some of them retaining about 50% of their low-strain-rate fracture strengths even at elastic loading rates above 10^6 psi per second.

10. ACKNOWLEDGEMENTS

The author is indebted to a number of his colleagues, particularly to C. S. Wukusick who collaborated in the earlier phases of this work and has continued to contribute valuable suggestions and discussions, and to W. H. Chang who has provided guidance throughout the program. Appreciation is also extended to J. F. Collins and W. E. Baxter who directed portions of the consolidation and processing work in General Electric's Nuclear Materials and Propulsion Operation and to F. E. Walker, R. J. Burgdorf, and W. F. Gill who assisted in various phases of the experimental work.

A special expression of thanks is made to J. R. Kittle, who not only was of invaluable help in the overall laboratory studies, but who ably conducted the program during the author's rather protracted illness in the earlier phases of the work, and to K. L. Metzgar, who provided excellent assistance during the latter portion of the study.

TABLE 1

TENSILE PROPERTIES OF WROUGHT CHROMIUM ALLOYS

Composition (Atomic %)						2000°F Tensile Properties			DBTT (°F)[b]	
Ti	Zr	Hf	Y	C	Cr	UTS (ksi)	0.2% Offset (ksi)	Elong. (%)	4T Bend*	Tensile**
--	--	--	.16	--	Bal.	9.4	7.7	18.0	50	75-100
2.8	.3	--	a	2.3	"	22.4	17.7	59.0	--	> 600
2.6	.2	--	a	1.4	"	18.4	13.8	48.0	--	> 400
1.3	.1	--	.04	.8	"	19.9	15.8	28.8	350	--
.2	.4	--	a	.4	"	24.5	19.1	24.0	-50	-30
.2	.1	.3	a	.4	"	24.7	20.3	27.0	< 50	--
.2	.2	.2	a	.5	"	26.9	24.7	24.6	100	150

a) Yttrium added to each alloy; less than .01% retained.

b) Ductile-brittle transition temperature, based on:

* 105° bends in .060" strip at ram speed of .05 ipm. Annealed 2000°F.

** 5% elongation in .160" diameter bars at strain rate of .01 per minute. Stress-relieved at 1800°F.

TABLE 2 SUMMARY OF SMALL HEATS, PHASE B

	System	Reason	Approximate Number
(1)	Cr-W-V	Increase solubility of W	10
(2)	Cr-Re(Ru)-Co	Inexpensive Re analog	20
(3)	Cr-Y-(Re,Ru,Co)	Oxidation resistance at low concentration	6 to 9
(4)	Cr-(Y)-(C)-Group IV & V Metals	Reactive solute interactions	50 to 60
(5)	Cr-Y-Si-(Cb)	Intermetallic dispersions	15
(6)	"Standard" matrix + (La,Ce,Be, etc.)	Alternate nitridation inhibitors	15
(7)	"Standard" ZTC + (6)	Carbide interaction with best from (6)	15 to 20
(8)	"Standard" matrix + best (4) + best (7)	Optimum minor solutes in S.S. matrix	25

TABLE 3

Cr-W-V ALLOY COMPOSITIONS AND METALLOGRAPHIC DATA

Alloy Composition (At. %)*		2900°F, 2 Hrs.		+ 1800°F, 200 Hrs.	
W	V	DPH	Structure	DPH	Structure
4.9	--	313	Single Phase	329	Single Phase
7.8	--	321	"	321	"
10.0	--	417	"	429	2 - Phase
5.1	5.1	358	"	337	Single Phase
4.8	9.6	358	"	346	2 - Phase
7.3	4.7	387	"	405	Single Phase
7.8	10.4	444	"	418	2 - Phase
7.6	15.5	417	"	438	"
10.1	10.1	453	"	459	"
10.3	15.6	458	"	479	"
10.1	20.3	448	"	482	"

* Calculated from charge weights and weignt changes during melting.

TABLE 4

COMPOSITIONS AND METALLOGRAPHIC OBSERVATIONS IN
Cr-Re-Co AND Cr-Ru-Co ALLOYS

Composition (At. %)			Metallographic Observations			
			2750°F, 2 Hrs.		+ 1650°F, 100 Hrs.	
Co	Re	Ru	Structure	DPH *	Structure	DPH *
5.7	30.2	-	2 - Phase	477	2 - Phase	487
2.5	25.6	-	Single Phase	365	Single Phase	371
4.9	24.8	-	" "	439	Slight Ppt.	439
5.2	20.4	-	" "	465	" "	435
7.5	18.9	-	" "	524	" "	515
5.1	15.3	-	" "	453	Single Phase	430
10.4	14.2	-	" "	564	Slight Ppt.	571
5.6	10.9	-	" "	465	Single Phase	462
11.5	11.0	-	" "	580	Slight Ppt.	591
17.2	11.0	-	" "	625	Approx. 50% Sigma	804
23.1	11.1	-	" "	670	Approx. 80% Sigma	957
5.2	6.7	-	" "	448	Single Phase	443
10.5	6.7	-	" "	570	Slight Ppt.	584
4.8	8.4	-	" "	442	Single Phase	434
9.7	8.5	-	" "	531	Approx. 10% Sigma	504
14.5	8.5	-	" "	580	Approx. 40% Sigma	674
4.5	5.5	-	" "	420	Single Phase	426
9.5	-	4.5	" "	524	Slight Ppt.	514

* Diamond Pyramid Hardness, 1 Kg Load.

TABLE 5

OXIDATION DATA FROM Cr-Y ALLOYS
WITH Re, Ru, AND Co ADDITIONS

Nominal Composition (At. %)	Wt. Change Data (mg/cm^2)[a]				
		2100°F, 100 Hrs.		2400°F, 24 Hrs.	
	1500°F, 100 Hrs.	Total	Net	Total	Net
4Re, 0.1Y	0.84	3.63	3.59	4.3	3.8
4Re, 0.5Y	0.87	3.87	3.83	2.05	1.63
8Re, 0.1Y	1.61	6.22	6.06	11.1	9.8
8Re, 0.5Y	0.76	0.87	0.79	1.2	0.53
4Ru, 0.1Y	0.60	4.02	3.26	2.17	-14.5
4Ru, 0.5Y	1.15	4.97	4.73	6.67	1.21
4Co, 0.1Y	0.65	1.17	-3.56	0.84	-15.0
4Co, 0.5Y	1.07	5.28	4.75	8.15	2.2

[a]Net weight change denotes the total weight gain less the weight of the loose oxide.

TABLE 6

EFFECTS OF SOLUTES FROM GROUPS IV-A AND V-A
ON THE AIR OXIDATION OF Cr-Y-C ALLOYS

Nominal Composition (At. %)	100-Hour Weight Gain (mg/cm^2) at 2100°F[a]					
	M = Ti	Zr	Hf	V	Cb	Ta
Cr-.5M	18.9	13.3	16.1	-	22.3	19.3
Cr-.5M-.1Y	2.7	1.4	2.8	12.8	12.2	14.2
Cr-.5M-.2Y	2.3	2.5	1.9	13.1	11.3	11.4
Cr-.5M-.4C	14.2	4.6	8.2	-	20.8	17.8
Cr-.5M-.4C-.1Y	4.6	3.0	5.7	3.0	18.1	12.9
Cr-.5M-.4C-.2Y	4.8	2.9	4.0	1.8	10.0	13.3
Cr-1M-.4C	11.9	3.7	6.6	10.2	33.1	-
Cr-1M-.4C-.1Y	2.5	3.0	2.3	8.4	24.5	13.9
Cr-1M-.4C-.2Y	2.3	2.2	3.4	2.3	12.5	-

[a]The 100-hour weight gains of unalloyed Cr and Cr-.1Y are 12.7 and 2.0 mg/cm^2, respectively, at 2100°F.

TABLE 7

LOW-TEMPERATURE BEND PROPERTIES OF SELECTED CARBIDE-STRENGTHENED CHROMIUM ALLOYS AND EFFECTS OF AIR OXIDATION

Nominal Composition (At. %)	Rolled + Annealed			1500°F-100 Hr.-Air		2100°F-100 Hr.-Air	
	DPH (kg/mm^2)[a]	DBTT (°F)[b]	400°F σ_D (ksi)[c]	DBTT (°F)	800°F σ_D (ksi)	DBTT (°F)	800°F σ_D (ksi)
Cr-.1Y	138	-50	18.1	< 75	11.4	100	14.2
Cr-1Ti-.4C	216	200	79.0	800	74.3	> 800	47.7
Cr-1Ti-.4C-.1Y	217	200	72.1	500	65.5	600	49.4
Cr-1Zr-.4C	161	75	48.6	400	41.7	800	37.4
Cr-1Zr-.4C-.1Y	152	0	47.1	200	58.8	300	35.7
Cr-1Zr-.4C-.2Y	156	75	55.3	400	41.0	200	27.5
Cr-1Hf-.4C-.1Y	172	150	42.4	200	59.7	400	25.8
Cr-1Hf-.4C-.2Y	160	100	50.4	-	-	200	31.5
Cr-1V-.4C	140	75	19.0	-	-	> 800	15.0
Cr-1V-.4C-.1Y	142	-50	17.3	200	24.7	> 800	26.1
Cr-1V-.4C-.2Y	149	100	28.5	-	-	Broke in handling	
Cr-1Cb-.4C	215	300	74.1	> 800	69.5	Broke in handling	
Cr-1Cb-.4C-.1Y	199	200	77.2	800	80.1	> 800	68.6
Cr-1Ta-.4C-.1Y	224	300	82.9	-	-	> 800	70.5

a) Diamond pyramid hardness, 100 gram load.

b) Ductile-brittle transition temperature based on 15° deflection in 4T bend tests at a ram speed of .05 ipm.

c) σ_D denotes fiber stress at deviation from linearity on load-time curves at indicated temperatures.

TABLE 8

HARDNESS AND OXIDATION BEHAVIOR OF ALLOYS IN THE Cr-Y-Cb-Si SYSTEM

Alloy (At. %)			Cast DPH (kg/mm^2)	SA DPH* (kg/mm^2)	Aged DPH (kg/mm^2)		100-Hr. Air Oxidation At 2100°F**	
Y	Cb	Si			1800°F/25 hr.	2200°F/5 hr.	Wt. Change (mg/cm^2)	Nitride (Mils)
0.1	-	-	101	-	-	-	2.0	0
0.1	0.5	-	170	145	165	160	17.4	1.5
0.1	1.0	-	219	190	198	207	29.1	2.5
0.1	1.5	-	262	231	251	274	44.4	7.5
-	1.5	-	371	322	322	279	- 71.4	13.5
0.1	3.0	-	363	327	322	287	72.5	15.0
0.1	4.5	-	405	350	356	405	117.0	17.0
0.1	-	1.0	131	221	137	145	5.3	1.0
0.1	-	2.0	160	243	162	160	10.0	0.7
-	-	4.0	247	283	251	227	17.3	2.0
0.1	-	4.0	240	311	243	236	12.1	1.5
0.1	1.5	1.0	296	279	254	240	40.0	6.0
0.1	3.0	2.0	383	327	311	296	46.2	16.0
0.1	4.5	4.0	441	383	344	397	53.5	12.0

*Solution annealed at 2600°F, one hour
All Diamond Pyramid Hardnesses at 2.5 kg load

**Oxidation tests conducted on samples forged 60-70% at 2300°F

TABLE 9.

EFFECT OF SELECTED REACTIVE METALS ON THE AIR OXIDATION OF Cr-4Mo ALLOYS

Nominal Composition (At. %)	Weight Change Data (mg/cm^2)[a]				
	1500°F-100 Hrs.	2100°F-100 Hrs.		2400°F-24 Hrs.	
		Total	Net	Total	Net
4Mo	0.83	12.1	7.93	1.32	-15.6
4Mo-0.1Y	0.87	3.27	3.27	4.6	0.15
4Mo-0.5Y	1.52	2.80	2.76	6.2	5.7
4Mo-0.1Ce	0.95	2.38	2.26	6.55	- 0.8
4Mo-0.5Ce	0.84	1.63	1.63	6.4	5.0
4Mo-0.1La	0.76	-0.38	-0.38	1.86	- 0.95
4Mo-0.5La	0.69	0.8	0.72	2.2	1.71
4Mo-0.1Th	1.38	8.2	7.3	14.0	5.1
4Mo-0.5Th	1.72	5.0	5.0	10.25	2.7
4Mo-0.1Pr	0.87	1.03	1.03	5.3	1.63
4Mo-0.5Pr	0.72	0.95	0.76	3.4	- 0.1
4Mo-0.1Be	0.76	8.2	7.0	1.63	-11.8
4Mo-0.5Be	0.72	5.5	3.8	- .57	- 5.75
4Mo-0.1MM[b]	0.87	2.64	2.53	5.65	2.64
4Mo-0.5MM	0.20	1.68	1.56	4.5	3.5

[a] Net weight change denotes total gain less the weight of loose oxide.

[b] Mischmetal: 50% Ce + 50% (La, Nd and Pr)

TABLE 10.

METALLOGRAPHIC OBSERVATIONS OF AIR-OXIDATION EFFECTS
IN ALLOYS WITH ALTERNATE NITRIDATION INHIBITORS

Nominal Composition (At. %)	1500°F-100 Hrs.[a]	2100°F-100 Hrs.		2400°F-24 Hrs.	
	DPH[b]	DPH[b]	REMARKS[c]	DPH[b]	REMARKS[c]
4Mo	280	296	GBN + layer	298	Extensive nitride
4Mo-0.1Y	282	305	GBN + needles	305	GBN
4Mo-0.5Y	271	286	Needles	285	Needles
4Mo-0.1Ce	271	298	GBN + needles	294	GBN
4Mo-0.5Ce	262	292	Needles	291	GBN
4Mo-0.1La	255	270	GBN + needles	295	GBN + needles
4Mo-0.5La	249	239	No nitride	260	No nitride
4Mo-0.1Th	-	-	GBN	-	GBN + layer
4Mo-0.5Th	-	-	GBN	-	Extensive nitride
4Mo-0.1Pr	256	275	Needles	275	GBN
4Mo-0.5Pr	277	270	No nitride	278	No nitride
4Mo-0.1Be	-	-	GBN + layer	-	Extensive GBN
4Mo-0.5Be	-	-	GBN	-	Extensive GBN
4Mo-0.1MM	265	295	GBN	278	GBN
4Mo-0.5MM	267	295	No nitride	309	Small amt. GBN

[a] No nitrides observed in any of the alloys after 1500°F air exposure.

[b] Diamond Pyramid Hardness - 100 gm load. Average matrix hardness does not include grain boundary nitrides.

[c] GBN denotes grain boundary nitride.

TABLE 11 AIR OXIDATION OF DISPERSED-CARBIDE ALLOYS WITH La, Pr, AND MM

Nominal Comp.[a] (At. %)	Temp. (°F)	Weight Gain (mg/cm²) Total	Net	DPH, 1Kg Edge	Core	Comments[b]
Cr-ZTC	1500	0.31	0.31	283	249	
	2100	2.5	-3.2	1332	252	Thick surface nitrides
	2400	7.5	-6.7	1226	202	at 2100° and 2400°F.
Cr-ZTC-.2La	1500	0.30	0.30	251	200	
	2100	0.20	0.20	247	178	Little or no nitriding.
	2400	0.40	-0.6	225	179	
Cr-ZTC-.5La	1500	0.26	0.26	270	206	
	2100	0.75	0.75	227	212	No nitriding at any T.
	2400	0.70	0.70	230	199	
Cr-ZTC-.2Pr	1500	0.27	0.27	281	224	
	2100	0.86	0.86	276	254	Small am't. intergranular
	2400	1.3	0.80	233	179	nitride at 2100° and 2400°F.
Cr-ZTC-.5Pr	1500	0.48	0.48	322	239	
	2100	1.5	1.5	247	196	No nitriding.
	2400	1.9	1.9	227	170	
Cr-ZTC-.2MM	1500	0.39	0.39	278	241	
	2100	1.5	1.5	254	178	Some IG nitride at 2100°F,
	2400	1.9	1.9	251	186	thin layer at 2400°F.
Cr-ZTC-.5MM	1500	0.67	0.67	281	236	
	2100	1.2	1.2	264	199	Small am't IG nitride.
	2400	2.0	2.0	221	192	
Cr-CbC-.2La	1500	0.54	0.54	297	297	
	2100	7.1	4.3	630	189	Extensive nitriding.
	2400	67.0 [c]	-20.0	1560	1452	
Cr-CbC-.5La	1500	0.04	0.04	258	236	
	2100	0	0	247	221	Little or no nitriding.
	2400	0.9	0.5	260	192	
Cr-CbC-.2Pr	1500	0.22	0.22	251	251	
	2100	5.2	5.2	268	230	Extensive nitriding.
	2400	6.7	-23.0	1750	199	
Cr-CbC-.2MM	1500	0.92	0.92	281	289	
	2100	3.1	1.9	1081	192	Extensive nitriding.
	2400	71.5 [c]	-29.2	1505	292	
Cr-TiC-.2La	1500	0.78	0.78	281	233	Little or no nitride;
	2100	6.7	6.7	258	198	thick irregular oxide
	2400	3.6	3.2	251	184	with internal stringers.
Cr-.2La	1500	0.10	0.10	196	198	
	2100	0.98	0.98	183	189	No nitriding or incipient
	2400	1.3	1.3	197	160	melting.
Cr-.5La	1500	0.26	0.26	160	201	
	2100	0.03	0.03	138	150	No nitriding, but incipient
	2400	4.5	-1.7	143	137	melting at 2100° and 2400°F.

a) ZTC = .4Zr-.2Ti-.4C
CbC = .6Cb-.4C
MM = mischmetal

b) No nitriding at 1500°F in any alloy.

c) Specimen badly cracked.

TABLE 12

COMPOSITIONS OF COMPLEX Cr-Mo-MC-La ALLOYS AND METALLOGRAPHIC OBSERVATIONS AFTER OXIDATION

Alloy Compositions* (Atomic %)	Oxidized 24 Hrs. @ 2400°F (As Cast)			Oxidized 100 Hrs. @ 2100°F (As Swaged)		
	Total Wt. Change mg/cm^2	Net Wt. Change mg/cm^2	Remarks	Hardness DPH, 100 Gm. Center	Hardness DPH, 100 Gm. Edge (.001")	Remarks
0.4Zr-0.2Ti-0.4C-0.3La	2.8	-1.9	Little or no nitride	316	290	No nitride
0.6Ti-0.4C-0.3La	11.5	-24.2	Little or no nitride	340	364	Little or no nitride
0.6Zr-0.4C-0.3La	3.2	1.5	Nitride needles	340	358	Little or no nitride
0.6Cb-0.4C-0.3La	20.4	-9.75	Intergranular nitride + needles	358	364	Slight nitride (irregular)
0.6Cb-0.4C-0.4La	30.2	-54.5	Extensive nitride	333	393	Small amount internal nitride
0.6Ta-0.4C-0.3La	34.0	-30.1	Extensive nitride	327	346	Slight intergranular nitride
0.3Ta-0.3Hf-0.4C-0.3La	19.0	-52.0	Extensive nitride	322	295	Slight intergranular nitride
0.6Hf-0.4C-0.3La	5.1	-8.1	Little or no nitride	351	340	Little or no nitride

* All contain 4 atomic percent Mo.

TABLE 13

EFFECTS OF La AND Y ON THE 2100°F OXIDATION
OF CHROMIUM ALLOYS WITH TaC DISPERSIONS

Nominal Composition[a] (At. %)		2100°F - 100 Hour Wt. Gain (mg/cm^2)			
Y	La	Total	Net	Subsurface Condition[b]	Incipient Melting
-	-	18.8	- 5.8	Thick (.005") nitride layer	No
0.1	-	13.7	- 1.2	Thick (.003") nitride layer	No
-	0.1	15.4	6.9	Thick (.003") nitride layer	No
0.2	-	8.0	- 4.6	Irregular (.001-.003") nitride	No
-	0.2	4.4	2.9	Thin (.001") layer, IG nitride	Slight?
0.1	0.1	7.9	6.2	No layer, IG nitride	No
0.2	0.1	4.2	4.0	Slight IG nitride	No
0.1	0.2	6.7	6.4	Slight IG nitride	No?
0.2	0.2	10.2	8.9	No nitride; IG oxide	Slight
-	0.3	3.8	3.8	No nitride or oxide	Yes
0.3	0.1	7.2	6.8	IG oxide	No
0.1	0.3	4.8	4.6	No nitride or oxide	Yes
0.4	-	12.3	12.0	Heavy IG oxide	No
-	0.4	7.9	7.9	No nitride or oxide	Yes
0.3	0.3	7.0	7.0	No nitride; IG oxide	Yes

a - Base composition Cr-.6Ta-.4C

b - Refers to structure beneath any adherent surface oxide.

TABLE 14

ANALYSES OF RAW MATERIALS USED IN ALLOYS OF PHASES A TO D

Element	Purity	Form	Impurities (ppm) O	N	H	C	Fe	Ni	Al	Si	S	Other
Chromium	99.94%	H_2-reduced flake*	42	84	<8	58	75	25	10	70	75	-
Chromium	99.997%	Iodide crystal	7	1	.5	9	13	1	.3	10	-	2Ca
Yttrium	99.9%	Sponge	890	8	-	-	20	-	5	50	-	10Ca, 400RE[c]
Molybdenum	99.9%	Pellets	105	12	-	-	160	61	25	55	-	435W
Tungsten	99.95%	Granules	80	10	-	20	10	20	10	10	-	160Mo
Vanadium	99.9%	Granules	700	50	10	200	-	-	-	-	-	-
Rhenium[a]	99.7%	Powder	1900	150	-	40	Less than 100 ppm total metallics					
Cobalt	99.5%	Shot	140	-	5	100	1100	1700	340	60	60	90Cu
Zirconium[b]	99.8%	Crystal bar	250	20	90	150	20	15	40	50	-	0.9% Hf
Titanium	99.5%	Sheet	1050	130	30	290	800	-	300	-	-	500Sn
Hafnium[b]	99.9%	Crystal bar	160	15	-	70	200	-	15	25	-	1.6% Zr
Columbium	99.8%	EB melted	250	80	-	100	<100	-	-	<100	-	1000Ta
Tantalum	99.96%	Foil	35	40	5	10	15	5	5	5	-	25W, 20Cb
Boron	99.6%	Powder	300	-	-	100	160	-	-	-	-	-
Lanthanum		Ingot	300	10	-	-	10	1	1	50	-	200Ca, 500RE[c]

* Average of 5 lots used in program

[a] Oxygen content reduced to less than 100 ppm by H_2 treatment at 2550°F.

[b] Purity refers to combined Zr and Hf contents.

[c] Rare earth impurities, principally Yt, Ho, Ce, Pr, Nd

TABLE 15

REVISED HEATS MELTED IN 50-POUND FURNACE

Alloy	Melting Variables	Gas Content (ppm)		
		O	N	H
CI-25A	1300°F bakeout, no arc hot-topping.	2230	58	7
CI-26A	Outgassed at room temperature. Arc hot-topped.	482	65	5
CI-27A	Outgassed at room temperature. Entire heating cycle under argon. Superheat reduced 50%. Arc hot-topped.	587	64	7
CI-5A	Outgassed at room temperature. Entire heating cycle under vacuum. Superheat reduced 50%. Arc hot-topped.	522	90	3
CI-8A	Outgassed at room temperature. Heating cycle under vacuum. No arc hot-topping.	390	85	6

TABLE 16.

EFFECTS OF FURNACE AND CASTING VARIABLES ON CHROMIUM ALLOY PURITY

Alloy	Heat Size (Lb)	Mold	Furnace	Yttrium in Briquette (Wt %)	Gas Content (ppm)			Approx. Analysis (Wt %)[a]	
					O	N	H	Y	Zr
CI-8A	4	ZrO_2	50-Pound	0.3	390	85	6	<.06	.08
CI-6A	4	Cu	50-Pound	0.5	329	45	8	.14	.06
CI-6B	7	ZrO_2	50-Pound	0.5	170[b]	58	8	.17	.06
CI-4A	4	ZrO_2	15-Pound	0.3	37	133	7	<.06	<.04
CI-5B	4	Cu	15-Pound	0.5	34	72	6	.19	.09
CI-7A	7	ZrO_2	15-Pound	0.4	29	69	11	.10	.05
CI-9A	7	ZrO_2	15-Pound	0.4	22	76	7	.15	.07

[a]From semi-quantitative x-ray emission.

[b]Triplicate analyses yielded values of 62, 315, and 132 ppm oxygen.

TABLE 17

COMPOSITIONS OF EXPERIMENTAL CHROMIUM ALLOYS

Alloy Designation	Nominal Composition (Atomic %)	Gas Content (ppm)			Approx. Analysis[a] (Wt. %)	
		N	O	H	Y	Zr
CI-1	Cr-.1Y	77	120	10	.13	.07
CI-2	Cr-.2Y	104	69	13	.25	.07
CI-3	Cr-.1Y-.05Hf-.03Th	92	25	11	.13	.08
CI-4	Cr-4Mo-.1Y	133	37	8	.15	.06
CI-5	Cr-6Mo-.1Y	72	35	6	.19	.10
CI-6	Cr-8Mo-.1Y	87	19	5	.13	.08
CI-7	Cr-4W-.1Y	89	28	13	.19	<.02
CI-8	Cr-6W-.1Y	89	29	7	.09	.16
CI-9	Cr-4Mo-2W-.1Y	76	22	8	.15	.07
CI-10	Cr-6Mo-2W-.1Y	99	29	6	.15	.07
*CI-11	Cr-4V-.1Y	-	-	-	-	-
*CI-12	Cr-10V-.1Y	-	-	-	-	-
*CI-13	Cr-20V-.1Y	-	-	-	-	-
CI-14	Cr-10V-4Mo-.1Y	86	60	7	.13	.06
CI-15	Cr-10V-4W-.1Y	87	58	7	.02	.08
CI-16	Cr-4Re-.1Y	99	60	5	<.02	<.02
CI-17	Cr-4Co-.1Y	61	41	7	.07	.06
CI-18	Cr-8Co-.1Y	67	86	10	.13	.04
CI-19	Cr-.05Y-.4Zr-.2Ti-.4C	81	38	5	<.02	>.40
CI-20	Cr-.1Y-.4Zr-.2Ti-.4C	72	24	6	.07	>.40
CI-21	Cr-.05Y-.3Hf-.3Zr-.4C	74	21	11	<.02	>.40
CI-22	Cr-.05Y-.4Zr-.2Ti-.4B	92	20	7	<.02	>.40
CI-23	Cr-.05Y-.3Hf-.3Zr-.4B	76	19	8	.08	>.40
CI-24	Cr-.05Y-.4Ta-.2Zr-.4B	88	23	8	.08	.25
*CI-25	Cr-4Mo-.05Y-4Zr-.2Ti	-	-	-	-	-
CI-26	Cr-4Mo-.1Y-.4Zr-.2Ti	97	34	12	.08	>.40
CI-27	Cr-4Mo-.1Y-.3Hf-.3Zr	89	18	17	.14	>.40
CI-28	Cr-4Mo-.1Y-.05Hf-.03Th	85	31	6	.03	<.02
CI-29	Cr-4Mo-.05Y-.4Zr-.2Ti-.4C	93	26	11	.05	>.40
CI-30	Cr-4Mo-.1Y-.4Zr-.2Ti-.4C	100	12	13	.15	>.40
CI-31	Cr-4Mo-.05Y-.5Zr-.25Ti-.4C	71	18	13	.05	>.40
CI-32	Cr-4Mo-.05Y-.3Zr-.15Ti-.4C	79	20	9	.09	.28
CI-33	Cr-4Mo-.05Y-.6Ti-.4C	68	16	12	.05	.06
CI-34	Cr-4Mo-.05Y-.6Zr-.4C	86	18	15	.03	>.40
CI-35	Cr-4Mo-.05Y-.6Hf-.4C	13	52	8	.09	.03
CI-36	Cr-4Mo-.05Y-.6Cb-.4C	80	77	5	.05	.06
CI-37	Cr-4Mo-.05Y-.3Hf-.3Zr-.4C	55	43	12	<.02	>.40
CI-38	Cr-4Mo-.05Y-.6Zr-.3Ti-.6C	86	70	16	.05	1.09
CI-39	Cr-4Mo-.05Y-.2Zr-.1Ti-.2C	91	13	12	.07	.42
CI-40	Cr-4Mo-.05Y-.4Ta-.2Zr-.4C	63	13	12	.05	.51
CI-41	Cr-4Mo-.05Y-.6Ta-.4C	53	36	2	.07	.06
CI-42	Cr-4Mo-.05Y-.4Cb-.2Zr-.4C	46	19	3	.07	.31

TABLE 17 (CONCL'D)

Alloy Designation	Nominal Composition (Atomic %)	Gas Content (ppm)			Approx. Analysis[a] (Wt. %)	
		N	O	H	Y	La
CI-43	Cr-4Mo-.4Cb-.2Zr-.4C-.2La	89	134	5	-	<.03
CI-44	Cr-6Mo-.4Zr-.2Ti-.4C-.05Y	63	13	12	.05	-
CI-45	Cr-4W-.3Ta-.3Hf-.4C-.15(Y+La)	68	26	3	<.013	<.03
CI-46	Cr-2Mo-2W-.3Ta-.3Hf-.4C-.15(Y+La)	74	26	9	.051	.086
CI-47	Cr-2Mo-2W-.6Ta-.4C-.15(Y+La)	82	146	1	<.01	.06
CI-48	Cr-4Re-.3Ta-.3Hf-.4C-.15(Y+La)	36	37	6	.03	.05
CI-49	Cr-2Mo-2W-.6Hf-.4C-.15(Y+La)	53	9	11	.095	.089
CI-50	Cr-.6Hf-.4C-.15(Y+La)	80	32	7	.08	.05
CI-51	Cr-.6Hf-.03Th-.4C-.10Y	73	22	8	.13	-
CI-52	Cr-5W-20V-.15(Y+La)	87	84	8	.014	.059
CI-53	Cr-2W-2.5Cb-1.5Si-.15(Y+La)	88	43	4	.10	.06
CI-54	Cr-4Mo-.6Ta-.4Hf-.8C-.15(Y+La)	50	41	6	.09	.11
CI-55	Cr-4Mo-.4Ta-.2Hf-.4B-.15(Y+La)	45	23	7	.09	.09
CI-56	Cr-4Mo-.3Ta-.3Hf-.2C-.2B-.15(Y+La)	46	16	6	.06	.08
CI-57	Cr-4Mo-.8Hf-.2B-.2C-.2Si-.15(Y+La)	34	26	5	.04	.08
CI-58	Cr-4Mo-.6Cb-.2C-.2N-.15(Y+La)	318	39	5	.07	.10
CI-59	Cr-4Mo-.8Cb-.2C-.2N-.2B-.15(Y+La)	366	92	5	.04	.08
CI-60	Cr-4Mo-.3Ta-.3Ti-.4C-.15(Y+La)	24	64	6	.058	.15
CI-61	Cr-4Mo-.3Cb-.3Ti-.4C-.15(Y+La)	37	121	8	.041	.08
CA-1	Unalloyed Cr (extruded)	10	17	2	-	-
CA-2	Cr-35Re	<10	48	3	-	-

[a]From quantitative x-ray emission.

*Dropped from program, not melted.

TABLE 18

EXTRUSION DATA - CHROMIUM ALLOYS REDUCED FROM 2-1/8" TO 3/4" DIAMETER

Alloy	Extrusion Temp (°F)	Glass* Lubricant	Extrusion Force (Tons) Upset	Average	Speed (in/sec)
CI-1	2000	7052	150	150	3
CI-2	2000	7052	175	175	2
CI-3	2000	7052	150	130	2.5
CI-4	2700	7740	225	190	2.5
CI-5	2700	7740	250	200	2.5
CI-6	2750	7052	250	250	2.5
CI-7	2750	7740	200	200	2.5
CI-8	2750	7740	200	180	3
CI-9	2750	7740	200	180	3
CI-10	2750	7740	260	225	2
CI-14	2700	7740	225	175	2.5
CI-15	2700	1720	210	210	2.5
CI-16	2750	7052	200	200	4
CI-17	2500	7052	175	160	2.5
CI-18	2500	7052	175	160	2.5
CI-19	2200	7052	175	175	2.5
CI-20	2200	7052	150	125	3
CI-21	2200	7052	135	100	2.5
CI-22	2200	9774	225	200	5
CI-23	2200	8378	175	175	2.5
CI-24	2200	7052	Stalled (temp. too low)		-
CI-24	2400	0010	200	200 (re-run)	4.5
CI-26	2700	7740	235	200	2
CI-27	2750	7052	200	200	2
CI-28	2750	7052	175	175	3
CI-29	2700	7052	200	200	2.5
CI-30	2750	7052	200	200	2
CI-31	2750	7052	175	175	2.5
CI-32	2750	7052	200	200	3
CI-33	2750	7052	225	225	-
CI-34	2750	7052	180	180	3.5
CI-35	2700	7740	235	200	2
CI-36	2750	7052	200	200	4
CI-37	2700	7740	250	220	-
CI-38	2750	7052	200	200	3
CI-39	2750	7052	175	175	2
CI-40	2750	7052	175	175	4
CI-41	2750	7052	225	225	2.5
CI-42	2750	7052	225	225	2.5
CI-43	2750	7052	260	260	-

TABLE 18 (CONCL'D)

Alloy	Extrusion Temp (°F)	Glass* Lubricant	Extrusion Force (Tons) Upset	Average	Speed (in/sec)
CI-44	2750	7052	Record Not Available		-
CI-45	2750	7052	280	Stall	2.5
CI-46	2750	7052	210	160	3.5
CI-47	2750	7052	240	220-Stall	2
CI-48	2750	7052	190	170	4.5
CI-49	2750	7052	210	200-225	2.5
CI-50	2200	7052	150	150	3
CI-51	2200	7052	135	125	3
CI-52	2750	7052	220	210	2.5
CI-53	2750	7052	220	180-240	1.5
CI-54	2750	7052	175	140	3
CI-55	2750	7052	240	220	2.5
CI-56	2750	7052	240	200	2
CI-57	2750	7052	230	200	2.5
CI-58	2750	7052	230	210	2.5
CI-59	2750	7052	275	250	-
CI-60	2750	7052	214	189	4
CI-61	2750	7052	325	277	4

* Corning Designation

TABLE 19

EFFECT OF PROCESSING ON THE MICROHARDNESS AND RECRYSTALLIZATION OF CHROMIUM ALLOYS

Alloy	Nominal Composition (At. %)	Diamond Pyramid Hardness (kg/mm^2)[a] Cast	Extruded	Swaged	Swaging Temp. (°F)	RX Temp.[b] (°F)
CI-1	Cr-.1Y	101	156	177	1900	1900
CI-2	Cr-.2Y	111	165	172	1900	1950
CI-3	Cr-.1Y-.05Hf-.03Th	115	142	221	1900	1900
CI-4	Cr-4Mo-.1Y	251	268	325	2100	2000
CI-5	Cr-6Mo-.1Y *	330	306	332*	2250	2150
CI-6	Cr-8Mo-.1Y *	345	353	- *	-	-
CI-7	Cr-4W-.1Y	297	299	358	2250	2100
CI-8	Cr-6W-.1Y *	307	371	398*	2300	2200
CI-9	Cr-4Mo-2W-.1Y *	339	332	350*	2250	2200
CI-10	Cr-6Mo-2W-.1Y *	378	333	374*	2300	2300
CI-14	Cr-10V-4Mo-.1Y *	310	401	395*	2200	2250
CI-15	Cr-10V-4W-.1Y *	313	349	370*	2250	2300
CI-16	Cr-4Re-.1Y	183	240	274	2250	2100
CI-17	Cr-4Co-.1Y	330	336	353	2200	2000
CI-18	Cr-8Co-.1Y *	493	524	- *	-	-
CI-19	Cr-.05Y-.4Zr-.2Ti-.4C	137	166	191	2000	2000
CI-20	Cr-.1Y-.4Zr-.2Ti-.4C	128	136	188	2000	1950
CI-21	Cr-.05Y-.3Hf-.3Zr-.4C	134	146	175	2000	2050
CI-22	Cr-.05Y-.4Zr-.2Ti-.4B	122	157	190	2000	2000
CI-23	Cr-.05Y-.3Hf-.3Zr-.4B	116	150	206	2000	2100
CI-24	Cr-.05Y-.4Ta-.2Zr-.4B	158	198	206	2200	2050
CI-26	Cr-4Mo-.1Y-.4Zr-.2Ti	279	283	296	2200	2100
CI-27	Cr-4Mo-.1Y-.3Hf-.3Zr	241	296	302	2200	2100
CI-28	Cr-4Mo-.1Y-.05Hf-.03Th	283	268	276	2200	2050
CI-29	Cr-4Mo-.05Y-.4Zr-.2Ti-.4C	260	265	309	2200	2150
CI-30	Cr-4Mo-.1Y-.4Zr-.2Ti-.4C	274	280	293	2250	2100
CI-31	Cr-4Mo-.05Y-.5Zr-.25Ti-.4C	236	286	345	2200	2150
CI-32	Cr-4Mo-.05Y-.3Zr-.15Ti-.4C	261	289	283	2250	2100
CI-33	Cr-4Mo-.05Y-.6Ti-.4C	287	327	369	2200	2250
CI-34	Cr-4Mo-.05Y-.6Zr-.4C	266	311	311	2200	2100
CI-35	Cr-4Mo-.05Y-.6Hf-.4C	292	274	316	2200	2050
CI-36	Cr-4Mo-.05Y-.6Cb-.4C	274	322	376	2250	2450
CI-37	Cr-4Mo-.05Y-.3Hf-.3Zr-.4C	296	283	316	2200	2200
CI-38	Cr-4Mo-.05Y-.6Zr-3Ti-.6C	283	292	356	2250	2150
CI-39	Cr-4Mo-.05Y-.2Zr-.1Ti-.2C	287	274	306	2200	2050
CI-40	Cr-4Mo-.05Y-.4Ta-.2Zr-.4C	260	277	283	2250	2250
CI-41	Cr-4Mo-.05Y-.6Ta-.4C	280	333	363	2250	2350

TABLE 19 (CONCL'D)

Alloy	Nominal Composition (At. %)	Diamond Pyramid Hardness (kg/mm^2)[a] Cast	Extruded	Swaged	Swaging Temp (°F)	RX Temp[b] (°F)
CI-42	Cr-4Mo-.05Y-.4Cb-.2Zr-.4C	279	311	345	2300	2300
CI-43	Cr-4Mo-.2La-.4Cb-.2Zr-.4C	262	333	338	2350	2300
CI-44*	Cr-6Mo-.4Zr-.2Ti-.4C-.05Y	338	283	363*	2200	2200
CI-45*	Cr-4W-.3Ta-.3Hf-.4C-.15(Y+La)	294	322	375*	2250	2250
CI-46	Cr-2Mo-2W-.3Ta-.3Hf-.4C-.15(Y+La)	287	322	412	2150	2250
CI-47	Cr-2Mo-2W-.6Ta-.4C-.15(Y+La)	306	350	428	2150	2300
CI-48	Cr-4Re-.3Ta-.3Hf-.4C-.15(Y+La)	227	243	322	2150	2150
CI-49	Cr-2Mo-2W-.6Hf-.4C-.15(Y+La)	279	306	356	2100	2200
CI-50	Cr-.6Hf-.4C-.15(Y+La)	155	146	191	1900	2050
CI-51	Cr-.6Hf-.03Th-.4C-.10Y	142	143	193	1900	2050
CI-52	Cr-5W-20V-.15(Y+La)	382	397	420	2100	2300
CI-53*	Cr-2W-2.5Cb-1.5Si-.15(Y+La)	390	405	- *	-	
CI-54*	Cr-4Mo-.6Ta-.4Hf-.8C-.15(Y+La)	296	296	369*	2350	2300
CI-55*	Cr-4Mo-.4Ta-.2Hf-.4B-.15(Y+La)	296	306	- *	-	-
CI-56*	Cr-4Mo-.3Ta-.3Hf-.2C-.2B-.15(Y+La)	292	301	351*	2350	2300
CI-57*	Cr-4Mo-.8Hf-.2B-.2C-.2Si-.15(Y+La)	292	296	311*	2350	
CI-58	Cr-4Mo-.6Cb-.2C-.2N-.15(Y+La)	306	333	322	2150	2250
CI-59*	Cr-4Mo-.8Cb-.2C-.2N-.2B-.15(Y+La)	296	322	- *	-	-
CI-60	Cr-4Mo-.3Ta-.3Ti-.4C-.15(Y+La)	283	279	327	2200	2250
CI-61	Cr-4Mo-.3Cb-.3Ti-.4C-.15(Y+La)	283	283	383	2200	2300
CA-1	Unalloyed Cr	-	134	188	1400	1750
CA-2	Cr-35Re	330	-	437	2200	2300

[a] 2.5 kilogram load.

[b] Temperature for approximately 50% recrystallization in one-hour annealing.

* Impact extruded at 2450°F/Argon prior to final swaging trials.

TABLE 20

CHEMICAL ANALYSIS OF REPRESENTATIVE ALLOYS AS A FUNCTION OF POSITION IN INGOT

Alloy	Location	Analyzed Composition (Wt. %)*							
		Y	Mo	Zr	Ti	C	O	N	Other
CI-1	Top	.11	ND	.03	ND	.014	.0107	.0081	-
(Cr-.1Y)	Center	.13	ND	.04	ND	.013	.0113	.0072	Trace Co
	Bottom	.13	ND	.03	ND	.014	.0092	.0074	-
CI-4	Top	.14	6.80	.02	ND	.010	.0042	.0106	-
(Cr-4Mo-.1Y)	Center	.14	6.77	.02	ND	.014	.0034	.0083	-
	Bottom	.16	6.86	.04	ND	.012	.0038	.0091	Trace Ca
CI-20	Top	.05	ND	.68	.19	.085	.0038	.0064	-
(Cr-.1Y-ZTC)	Center	.05	ND	.66	.19	.083	.0024	.0080	-
	Bottom	.06	ND	.65	.19	.087	.0032	.0075	-
CI-30	Top	.14	6.73	.67	.22	.084	.0023	.0110	-
(Cr-4Mo-.1Y-ZTC)	Center	.15	6.85	.70	.21	.089	.0046	.0085	Trace Co
	Bottom	.11	6.81	.72	.22	.085	.0028	.0092	-
CI-36	Top	.06	7.05	.06	ND	.092	.0064	.0081	0.95 Cb
(Cr-4Mo-.05Y-CbC)	Bottom	.05	6.89	.04	ND	.088	.0072	.0070	0.97 Cb
CI-41	Top	.07	6.85	.05	ND	.088	.0042	.0061	1.80 Ta
(Cr-4Mo-.05Y-TaC)	Bottom	.08	6.93	.06	ND	.092	.0047	.0054	1.73 Ta
CA-2	Top	ND	ND	ND	ND	.003	.0052	.0013	64.4 Re
(Cr-35Re)	Center	ND	ND	ND	ND	.004	.0044	.0015	63.8 Re
	Bottom	ND	ND	ND	ND	.004	.0040	.0008	64.7 Re

* ND - Not detected.

Al, Fe, Ni, Si and S contents are all below 100 ppm in each section.

H analyses less than 10 ppm in each section.

TABLE 21

SUMMARY OF PHASE IDENTIFICATION DATA, WROUGHT CHROMIUM ALLOYS

AGED 1 HOUR AT 2000°F

Alloy	Nominal Composition (At. %)	Phases Present *	ASTM Standard
CI-29	Cr-4Mo-.05Y-.4Zr-.2Ti-.4C	(Zr,Ti)C (a_o = 4.682A) TiC (a_o = 4.322A)	ZrC = 4.696A TiC = 4.329A
CI-33	Cr-4Mo-.05Y-.6Ti-.4C	TiC (a_o = 4.323A)	TiC = 4.329A
CI-34	Cr-4Mo-.05Y-.6Zr-.4C	ZrC (a_o = 4.698A)	ZrC = 4.696A
CI-35	Cr-4Mo-.05Y-.6Hf-.4C	HfC (a_o = 4.644A) $HfCr_2$ (a_o = 7.190A)	HfC = 4.641A $HfCr_2$ = 7.15A
CI-36	Cr-4Mo-.05Y-.6Cb-.4C	CbC (a_o = 4.456A) (Y_2O_3)	CbC = 4.470A
CI-37	Cr-4Mo-.05Y-.3Hf-.3Zr-.4C	(Hf,Zr)C (a_o = 4.667A) (Hf,Zr)Cr_2 (a_o = 7.220A)	HfC = 4.641A, ZrC = 4.696A $HfCr_2$ = 7.15A, $ZrCr_2$ = 7.21A
CI-41	Cr-4Mo-.05Y-.6Ta-.4C	TaC (a_o = 4.446A) (Y_2O_3)	TaC = 4.456A
CI-58	Cr-4Mo-.15(La + Y)-.6Cb-.2C-.2N	Cb(C,N) (a_o = 4.420A)	CbC = 4.470A, CbN = 4.375A

* Where more than one phase is present, the first listed is the more abundant.

TABLE 22

EFFECTS OF POST-WORK ANNEALING ON
TENSILE BEHAVIOR OF REPRESENTATIVE CHROMIUM ALLOYS AT LOW TEMPERATURES

Alloy	Nominal Comp. (At. %)*	1-Hr. Anneal Temp °F	Tensile Properties At: -50°F UTS ksi	-50°F RA %	75°F UTS ksi	75°F RA %	200°F UTS ksi	200°F RA %	400°F UTS ksi	400°F RA %	600°F UTS ksi	600°F RA %
CI-1	.10Y	2000	-	-	38.8	1.5	45.4	78.3	-	-	-	-
		2400	-	-	32.7	0	43.9	69.8	-	-	-	-
CI-4	4Mo-.10Y	1800	-	-	-	-	86.1	1.6	94.0	26.9	-	-
		2000	-	-	-	-	78.3	1.7	90.6	29.9	-	-
		2400	-	-	-	-	-	-	72.5	3.4	75.2	53.5
CI-19	.05Y-ZTC	1800	-	-	-	-	72.0	61.1	58.0	71.6	-	-
		2000	-	-	59.4	8.2	64.1	61.6	54.9	73.0	-	-
		2400	72.5	0	59.2	11.7	-	-	-	-	-	-
CI-20	.10Y-ZTC	2000	71.9	0.5	57.6	24.6	-	-	-	-	-	-
		2400	48.8	1.7	58.3	24.8	-	-	-	-	-	-
CI-21	.05Y-HZC	1800	-	-	-	-	66.0	57.6	67.0	70.0	-	-
		2000	67.7	0.8	71.5	24.2	63.5	64.8	54.7	70.7	-	-
		2400	-	-	52.1	7.9	50.7	37.1	-	-	-	-
CI-30	4Mo-.10Y-ZTC	2000	-	-	-	-	-	-	68.6	1.8	77.3	4.3
		2400	-	-	-	-	-	-	70.2	3.9	73.5	6.8
CI-37	4Mo-.05Y-HZC	1800	-	-	-	-	-	-	95.8	1.6	99.5	48.8
		2000	-	-	-	-	-	-	104.0	5.7	104.5	48.0
		2400	-	-	-	-	-	-	77.4	3.9	73.0	5.5

* Balance Cr, ZTC = .4Zr-.2Ti-.4C, HZC = .3Hf-.3Zr-.4C

TABLE 23

COMPARISON OF SELECTED TENSILE PROPERTIES OF CHROMIUM ALLOYS IN THE STRESS-RELIEVED AND RECRYSTALLIZED CONDITIONS

Alloy	Nominal Composition (Atomic %)	Tensile Strength (ksi) at: 2400°F Avg.	1900°F S.R.	1900°F RX	Approx. DBTT (°F) S.R.	Approx. DBTT (°F) RX
CI-1	Cr-.1Y	5.2	12.4	11.5	100	125
CI-2	Cr-.2Y	4.2	9.3	9.6	100	50
CI-3	Cr-.1Y-.05Hf-.03Th	5.4	19.9	13.2	75	50
CI-4	Cr-4Mo-.1Y	17.2	46.4	38.9	300	450
CI-5	Cr-6Mo-.1Y	24.0	-	48.5	-	-
CI-7	Cr-4W-.1Y	23.8	63.6	49.6	600	700
CI-8	Cr-6W-.1Y	30.1	81.0	60.2	-	-
CI-9	Cr-4Mo-2W-.1Y	23.3	54.5	48.0	-	-
CI-10	Cr-6Mo-2W-.1Y	29.2	-	57.3	-	-
CI-14	Cr-10V-4Mo-.1Y	21.0	68.9	45.5	400	600
CI-15	Cr-10V-4W-.1Y	26.1	67.2	51.7	600	500
CI-16	Cr-4Re-.1Y	12.3	34.3	29.2	450	500
CI-17	Cr-4Co-.1Y	4.6	21.7	18.9	>600	>600
CI-19	Cr-.05Y-.4Zr-.2Ti-.4C	7.6	21.7	22.7	25	50
CI-20	Cr-.1Y-.4Zr-.2Ti-.4C	5.7	15.1	14.3	0	0
CI-21	Cr-.05Y-.3Hf-.3Zr-.4C	5.7	36.5	15.2	0	50
CI-22	Cr-.05Y-.4Zr-.2Ti-.4B	8.1	35.7	25.2	50	75
CI-23	Cr-.05Y-.3Hf-.3Zr-.4B	8.5	34.8	24.0	100	100
CI-24	Cr-.05Y-.4Ta-.2Zr-.4B	10.4	44.3	28.3	250	100
CI-26	Cr-4Mo-.1Y-.4Zr-.2Ti	19.1	54.9	47.7	600	700
CI-27	Cr-4Mo-.1Y-.3Hf-.3Zr	17.9	52.8	48.2	500	500
CI-28	Cr-4Mo-.1Y-.05Hf-.03Th	17.2	49.7	37.1	400	500
CI-29	Cr-4Mo-.05Y-.4Zr-.2Ti-.4C	20.0	56.4	45.7	450	550
CI-30	Cr-4Mo-.1Y-.4Zr-.2Ti-.4C	19.0	47.8	37.9	600	500
CI-31	Cr-4Mo-.05Y-.5Zr-.25Ti-.4C	19.3	46.7	45.3	600	600
CI-32	Cr-4Mo-.05Y-.3Zr-.15Ti-.4C	16.9	56.6	50.1	500	450
CI-33	Cr-4Mo-.05Y-.6Ti-.4C	22.3	59.0	49.4	>600	600
CI-34	Cr-4Mo-.05Y-.6Zr-.4C	20.5	45.5	45.3	500	600
CI-35	Cr-4Mo-.05Y-.6Hf-.4C	18.4	58.2	45.8	500	500
CI-36	Cr-4Mo-.05Y-.6Cb-.4C	20.4	65.7	61.0	350	400
CI-37	Cr-4Mo-.05Y-.3Hf-.3Zr-.4C	20.1	61.0	50.3	400	500
CI-38	Cr-4Mo-.05Y-.6Zr-3Ti-.6C	19.8	52.5	47.1	600	600
CI-39	Cr-4Mo-.05Y-.2Zr-.1Ti-.2C	19.8	50.3	49.4	500	500
CI-40	Cr-4Mo-.05Y-.4Ta-.2Zr-.4C	21.3	49.0	46.2	650	400
CI-41	Cr-4Mo-.05Y-.6Ta-.4C	19.6	61.5	61.9	450	450
CI-42	Cr-4Mo-.05Y-.4Cb-.2Zr-.4C	20.2	59.4	-	400	-

TABLE 23 (CONCL'D)

Alloy	Nominal Composition (Atomic %)	Tensile Strength (ksi) at: 2400°F Avg.	1900°F S.R.	1900°F RX	Approx. DBTT (°F) S.R.	Approx. DBTT (°F) RX
CI-43	Cr-4Mo-.2La-.4Cb-.2Zr-.4C	21.0	58.8	-	350	-
CI-44	Cr-6Mo-.4Zr-.2Ti-.4C-.05Y	27.0	64.8	-	700	-
CI-45	Cr-4W-.3Ta-.3Hf-.4C-.15(Y+La)	30.6	84.1	-	700	-
CI-46	Cr-2Mo-2W-.3Ta-.3Hf-.4C-.15(Y+La)	20.5	70.9	49.0	650	-
CI-47	Cr-2Mo-2W-.6Ta-.4C-.15(Y+La)	22.1	70.3	62.2	500	-
CI-48	Cr-4Re-.3Ta-.3Hf-.4C-.15(Y+La)	14.9	46.8	37.3	75	-
CI-49	Cr-2Mo-2W-.6Hf-.4C-.15(Y+La)	19.6	46.9	47.8	400	-
CI-50	Cr-.6Hf-.4C-.15(Y+La)	5.5	19.0	18.0	25	-
CI-51	Cr-.6Hf-.03Th-.4C-.10Y	5.0	18.6	17.5	-25	-
CI-52	Cr-5W-20V-.15(Y+La)	29.4	73.4	53.7	550	-
CI-54	Cr-4Mo-.6Ta-.4Hf-.8C-.15(Y+La)	20.7	68.2	-	700	-
CI-56	Cr-4Mo-.3Ta-.3Hf-.2C-.2B-.15(Y+La)	22.3	71.0	-	650	-
CI-57	Cr-4Mo-.8Hf-.2B-.2C-.2Si-.15(Y+La)	18.1	58.2	-	-	-
CI-58	Cr-4Mo-.6Cb-.2C-.2N-.15(Y+La)	20.8	67.8	54.0	550	-
CI-60	Cr-4Mo-.3Ta-.3Ti-.4C-.15(Y+La)	20.7	45.2	43.7	650	500
CI-61	Cr-4Mo-.3Cb-.3Ti-.4C-.15(Y+La)	19.4	42.6	46.8	500	400
CA-1	Unalloyed Cr	2.6	7.0	7.2	150	350
CA-2	Cr-35Re	22.1	69.7	53.6	<-200	<-100

TABLE 24

CREEP-RUPTURE PROPERTIES OF CHROMIUM ALLOYS

A. RECRYSTALLIZED-ANNEALED 1 HOUR AT 2400°F

Alloy	Nominal Comp. (At. %)	Test Temp (°F)	Stress (ksi)	MCR (%/hr)	Life (hours)	Elong. (%)
CI-4	4Mo-.1Y	2100	12.5	-	7.31	21.3
		2100	10.0	0.045	53.5	17.5
		2100	8.0	0.0073	231.4	12.3
		2400	5.0	-	7.0	16.0
		2400	3.5	0.24	31.7	11.6
CI-7	4W-.1Y	2100	15.0	0.073	20.6	30.4
		2100	12.5	0.038	67.2	28.8
		2100	10.0	0.0058	305.2	19.3
CI-9	4Mo-2W-.1Y	2100	12.5	0.047	41.7	12.0
		2100	10.0	0.011	184.6	8.6
CI-19	.05Y-.4Zr-.2Ti-.4C	2100	6.0	0.040	48.6	21.4
		2100	5.0	0.019	152.9	11.1
		2100	4.0	0.0061	>250	-
CI-21	.05Y-.3Hf-.3Zr-.4C	2100	6.0	-	14.6	38.5
		2100	4.0	0.032	73.0	23.0
CI-22	.05Y-.4Zr-.2Ti-.4B	2100	8.0	-	21.4	18.3
		2100	6.0	0.028	97.1	13.7
CI-26	4Mo-.1Y-.4Zr-.2Ti	2100	12.5	-	21.3	23.6
		2100	10.0	0.018	87.8	17.3
CI-27	4Mo-.1Y-.3Hf-.3Zr	2100	12.5	-	11.2	22.6
		2100	10.0	0.024	74.2	14.8
CI-29	4Mo-.05Y-.4Zr-.2Ti-.4C	2100	12.5	0.031	58.1	19.0
		2100	10.0	0.010	194.0	14.3
CI-33	4Mo-.05Y-.6Ti-.4C	2100	15.0	0.040	35.9	27.5
		2100	12.5	0.0092	210.6	20.7
		2400	6.5	-	15.9	88.0
		2400	4.5	0.28	35.4	77.0
		2400	4.0	0.22	59.4	57.0
CI-35	4Mo-.05Y-.6Hf-.4C	2100	12.5	-	9.70	12.4

TABLE 24 (CONCL'D)

Alloy	Nominal Comp. (At. %)	Test Temp (°F)	Stress (ksi)	MCR (%/hr)	Life (hours)	Elong. (%)
CI-36	4Mo-.05Y-.6Cb-.4C	2100	17.5	0.042	30.6	31.4
		2100	15.0	0.011	90.9	23.2
		2400	6.5	-	22.4	77.0
		2400	4.5	0.17	103.2	40.0
CI-37	4Mo-.05Y-.3Hf-.3Zr-.4C	2100	15.0	-	9.72	29.4
		2100	12.5	0.015	120.4	17.7
		2400	6.0	-	6.2	36.0
		2400	4.0	0.50	30.0	27.0
CI-41	4Mo-.05Y-.6Ta-.4C	2100	15.0	0.033	49.9	29.2
		2100	15.0	-	17.6	32.8
CI-52	5W-20V-.15(Y+La)	2100	15.0	-	10.4	7.7
		2400	5.0	-	8.2	7.0
CI-58	4Mo-6Cb-.2C-.2N-.15(Y+La)	2100	13.0	0.030	53.9	44.0
		2400	4.5	0.52	26.7	43.0

B. STRESS RELIEVED-ANNEALED 1 HOUR AT 2000°F

Alloy	Nominal Comp. (At. %)	Test Temp (°F)	Stress (KSI)	MCR (%/hr)	Life (hours)	Elong. (%)
CI-33	4Mo-.05Y-.6Ti-.4C	2100	15.0	0.011	80.1	32.1
CI-36	4Mo-.05Y-.6Cb-.4C	2100	17.5	0.013	62.2	38.4
		2100	15.0	0.0065	246.0	25.0
CI-37	4Mo-.05Y-.3Hf-.3Zr-.4C	2100	15.0	-	19.8	32.2
CI-41	4Mo-.05Y-.6Ta-.4C	2100	15.0	0.009	132.7	27.5
CI-58	4Mo-.6Cb-.2C-.2N-.15(Y+La)	2100	15.0	0.015	52.4	39.0

TABLE 25

SUMMARY OF AIR OXIDATION BEHAVIOR, WROUGHT CHROMIUM ALLOYS, ANNEALED 1 HOUR AT 2000°F

Alloy	Alloy Type	Retained Y + La (%)	Temp (°F)[a]	Total Wt. Change (mg/cm^2)	Nitride Layer (mils)[b]	Depth Hardened (mils)[c]	Hardness (DPH) Surf.	Hardness (DPH) Core
CI-1	Cr-Y	.13	1500	0.7	0	0	164	164
			2100	2.3	1-4	1-4	>1000	181
			2400	10.6	2.5	4	1500	156
CI-2	Cr-Y	.25	1500	0.3	0	0	172	159
			2100	1.8	0	0	201	186
			2400	25.1	1-2	2	1500	150
CI-3	Cr-Y-Th-Hf	.13+	1500	0.04	0	0	168	156
			2100	1.9	0	0	201	190
			2400	1.9	0	0-1	259	170
CI-4	Cr-4Mo-Y	.15	1500	2.0	0	0	346	333
			2100	0.06	0	0	311	305
			2400	7.7	3-4(P)	4-5	850	322
CI-5	Cr-6Mo-Y	.19	1500	0.5	0	2	434	393
			2100	11.1	0	0	395	380
			2400	-6.3	6(P)	6	425	358
CI-6*	Cr-8Mo-Y	.13	1500	0.3	0	3	470	403
			2100	1.9	2(IG)	4	920	420
			2400	43.9	6-8	8-10	1500	390
CI-7	Cr-4W-Y	.19	1500	0	0	0	349	333
			2100	4.7	0-4(P)	0	372	351
			2400	9.0	0-1(P)	0-1	336	342
CI-8	Cr-6W-Y	.09	1500	1.2	0	1	389	364
			2100	23.7	1.5(IG)	22	864	383
			2400	6.3	1-2	2	1200	420
CI-9	Cr-4Mo-2W-Y	.15	1500	0.09	0	4	427	368
			2100	7.6	0	4	503	340
			2400	36.9	2-3(P)	2-3	472	360

TABLE 25 (CONT'D)

Alloy	Alloy Type	Retained Y + La (%)	Temp (°F)[a]	Total Wt. Change (mg/cm^2)	Nitride Layer (mils)[b]	Depth Hardened (mils)[c]	Hardness (DPH) Surf.	Hardness (DPH) Core
CI-10	Cr-6W-2Mo-Y	.15	1500	0.7	0	0	426	426
			2100	7.4	0-1(P)	3	462[d]	386
			2400	8.2	3-4(P)	4	552	401
CI-14	Cr-10V-4Mo-Y	.13	1500	1.8	0	0	316	322
			2100	19.5	1-3(P)	7	493	364
			2400	55.7	8(P)	18	737	340
CI-15	Cr-10V-4W-Y	.02	1500	1.5	0	2	444	377
			2100	34.0	2(P)	10	486	379
			2400	68.2	6(P)	>50	492	471
CI-16	Cr-4Re-Y	.02	1500	0.4	0	0	268	254
			2100	5.3	2(IG)	6	1200	245
			2400	37.2	0	0	227	255
CI-17	Cr-4Co-Y	.07	1500	0.7	0	4	379	352
			2100	1.4	10(IG)	12	434	379
			2400	14.9	7(IG)	7	462	386
CI-18*	Cr-8Co-Y	.13	1500	0.3	0	0	481	471
			2100	8.3	0-1	0	537[d]	426
			2400	1.3	1-2(P)	2	575	537
CI-19	Cr-Y-(Zr,Ti)C	.02	1500	2.0	0	3	224	194
			2100	0.6	0-1	6-7	227[d]	166
			2400	37.2	14	23	1670	199
CI-20	Cr-Y-(Zr,Ti)C	.07	1500	1.9	0	5	526	193
			2100	0.2	0	3-4	217	163
			2400	15.3	5	8	1190	164
CI-21	Cr-Y-(Hf,Zr)C	.02	1500	0.3	0	0	189	184
			2100	0.4	0	0	175	166
			2400	18.5	12	14	1460	184
CI-22	Cr-Y-(Zr,Ti)B	.02	1500	0.05	0	0	194	186
			2100	9.4	1-2	4	1190	149
			2400	27.1	5-7	13	980	175

TABLE 25 (CONT'D)

Alloy	Alloy Type	Retained Y + La (%)	Temp (°F)[a]	Total Wt. Change (mg/cm²)	Nitride Layer (mils)[b]	Depth Hardened (mils)[c]	Hardness (DPH) Surf.	Hardness (DPH) Core
CI-23	Cr-Y-(Hf,Zr)B	.08	1500	0.6	0	0	192	182
			2100	25.4	0	2	217	152
			2400	37.1	9	15	893	182
CI-24	Cr-Y-(Ta,Zr)B	.08	1500	1.9	1-2(IG)	3	301	214
			2100	-13.8	1-2	20	1200	192
			2400	73.7	9-11	41	1220	184
CI-26	Cr-4Mo-Y-Zr,Ti	.08	1500	1.6	0	0	372	358
			2100	0	0	4	401	316
			2400	18.4	2(10 IG)	12	1073	386
CI-27	Cr-4Mo-Y-Hf,Zr	.14	1500	0.03	0	3	372	305
			2100	3.6	0	0	346	322
			2400	37.2	3(12 IG)	18	1106	327
CI-28	Cr-4Mo-Y,Th,Hf	.03+	1500	2.5	0	5	409	282
			2100	2.3	0	0	301	282
			2400	12.6	0	2	401	246
CI-29	Cr-4Mo-Y-(Zr,Ti)C	.05	1500	3.6	0	4	360	306
			2100	6.5	0-1	5	481[d]	311
			2400	30.8	3-4	>50	920	401
CI-30	Cr-4Mo-Y-(Zr,Ti)C	.15	1500	0.5	0	5	346	275
			2100	2.6	0	2	333	302
			2400	34.5	1-6 (IG)	35	800	313
CI-31	Cr-4Mo-Y-hi(Zr,Ti)C	.05	1500	0.3	0	10	492	295
			2100	5.6	0-1[e]	4	351[d]	304
			2400	38.1	3-10 (IG)	16	1050	316
CI-32	Cr-4Mo-Y-lo(Zr,Ti)C	.09	1500	0.4	0	8	462	316
			2100	9.7	0.5-1	6	1200	290
			2400	14.7	1-2	>50	1200	395
CI-33	Cr-4Mo-Y-TiC	.05	1500	1.1	0	5	480	355
			2100	7.3	2-3[e]	10	920	340
			2400	25.0	4	16	935	281

TABLE 25 (CONT'D)

Alloy	Alloy Type	Retained Y + La (%)	Temp (°F)[a]	Total Wt. Change (mg/cm^2)	Nitride Layer (mils)[b]	Depth Hardened (mils)[c]	Hardness (DPH) Surf.	Core
CI-34	Cr-4Mo-Y-ZrC	.03	1500	1.1	0	0	322	327
			2100	5.2	0	0-2	358	316
			2400	56.6	3(15 IG)	32	1407	268
CI-35	Cr-4Mo-Y-HfC	.09	1500	2.5	0	7	450	340
			2100	1.7	0	0-2	333	303
			2400	8.0	0	0	322	316
CI-36	Cr-4Mo-Y-CbC	.05	1500	2.5	0	8	331	295
			2100	16.1	4	15	1220	311
			2400	43.1	5-7	19	1700	327
CI-37	Cr-4Mo-Y-(Hf,Zr)C	.02	1500	0.3	0	2-3	401	372
			2100	1.4	0	0	322	305
			2400	20.0	2(12 IG)	33	717	340
CI-38	Cr-4Mo-Y-(Zr,Ti)-hiC	.05	1500	0.9	0	2	346	316
			2100	8.1	0-2 (IG)	2-6	379[d]	327
			2400	44.2	3 (8 IG)	12	1200	295
CI-39	Cr-4Mo-Y-(Zr,Ti)loC	.07	1500	0.08	0	10	503	305
			2100	5.0	0	4	426	335
			2400	33.4	4(12 IG)	30	1187	290
CI-40	Cr-4Mo-Y-(Ta,Zr)C	.05	1500	0.04	0	0	295	295
			2100	1.3	0-2 (IG)	5	430[d]	290
			2400	23.7	4 (8 IG)	13	1200	281
CI-41	Cr-4Mo-Y-TaC	.07	1500	0.4	0	6	352	317
			2100	13.6	0.5-2 (IG)	4	1050	327
			2400	35.6	3 (7 IG)	8	800	319
CI-42	Cr-4Mo-Y-(Cb,Zr)C	.07	1500	0.2	0	0	316	322
			2100	29.0	6	15	1580	316
			2400	51.4	4 (28 IG)	45	1350	316
CI-43	Cr-4Mo-La-(Cb,Zr)C	<.03	1500	0.9	0	2	346	318
			2100	16.9	3-5	13	950	298
			2400	52.2	2 (13 IG)	22	1048	333

TABLE 25 (CONT'D)

Alloy	Alloy Type	Retained Y + La (%)	Temp (°F)[a]	Total Wt. Change (mg/cm²)	Nitride Layer (mils)[b]	Depth Hardened (mils)[c]	Hardness (DPH) Surf.	Hardness (DPH) Core
CI-44	Cr-6Mo-Y-(Zr,Ti)C	.05	1500	0.2	0	3	434	343
			2100	2.7	0	0	379	358
			2400	32.4	7-12	40	1190	340
CI-45	Cr-4W-(La+Y)-(Ta,Hf)C	.04	1500	1.5	0	2	379	322
			2100	28.3	4.5	17	1575	389
			2400	90.0	24	40	1635	372
CI-46	Cr-2W-2Mo-(La+Y)-(Ta,Hf)C	.14	1500	0.2	0	0	380	386
			2100	3.8	0	3	409	372
			2400	68.5	>20 (IG)	>60	1700	1500
CI-47	Cr-2W-2Mo-(La+Y)-TaC	<.07	1500	0.2	0	2	426	379
			2100	18.1	1-2	45	1700	372
			2400	122.5	21 (IG)	32	1700	364
CI-48	Cr-4Re-(La+Y)-(Ta,Hf)C	.08	1500	0.2	0	2	346	311
			2100	1.8	0	5	346	295
			2400	24.2	0	4	340	276
CI-49	Cr-2W-2Mo-(La+Y)-HfC	.18	1500	0.1	0	2	386	346
			2100	1.1	0	7	418	327
			2400	8.8	0	0	264	340
CI-50	Cr-(La+Y)-HfC	.13	1500	0.5	0	2	248	198
			2100	1.4	0	0	196	184
			2400	15.5	0	6	426	194
CI-51	Cr-Y,Th-HfC	.13+	1500	1.9	0	0	197	182
			2100	13.9	0-3 (IG)	6	364[d]	189
			2400	4.4	0	3	272	160
CI-52	Cr-20V-5W-(La+Y)	.07	1500	0.7	0	3	492	434
			2100	131.0	4(P)	4	409	364
			2400	143.0	6(P)	8	590	386
CI-54	Cr-4Mo-(La+Y)-hi(Ta,Hf)C	.20	1500	0.2	0	0	340	352
			2100	14.6	0-1 (IG)	5	471[d]	358
			2400	82.6	3-10 (IG)	20	756	340

TABLE 25 (CONCL'D)

Alloy	Alloy Type	Retained Y + La (%)	Temp (°F)[a]	Total Wt. Change (mg/cm²)	Nitride Layer (mils)[b]	Depth Hardened (mils)[c]	Hardness (DPH) Surf.	Hardness (DPH) Core
CI-56	Cr-4Mo-(La+Y)-(Ta,Hf)C,B	.14	1500	2.4	0	0	305	351
			2100	11.2	0	5	409	358
			2400	25.6	8	45	1105	311
CI-57	Cr-4Mo-(La+Y)-Hf(C,B,Si)	.12	1500	2.5	0	0	358	336
			2100	1.1	0	5	372	322
			2400	39.1	0-2 (IG)	3	401[d]	351
CI-58	Cr-4Mo-(La+Y)-Cb(C,N)	.17	1500	0.5	0	3	492	409
			2100	4.7	0-1 (IG)	5	358[d]	305
			2400	36.5	1-3 (IG)	10	1190	300
CI-59*	Cr-4Mo-(La+Y)-Cb(C,N,B)	.12	1500	-	0	0	351	346
			2100	6.8	0.5	22	379[d]	305
			2400	51.4	20	32	1460	364
CI-60	Cr-4Mo-(La+Y)-(Ta,Ti)C	.21	1500	0.7	0	3	360	322
			2100	7.4	0[e]	1	340	316
			2400	65.3	6	11	946	316
CI-61	Cr-4Mo-(La+Y)-(Cb,Ti)C	.12	1500	0.5	0	6	342	305
			2100	6.3	0[e]	4	311	276
			2400	81.9	8	13	1048	316
CA-1	Unalloyed Cr	0	1500	3.1	0	0	132	132
			2100	6.9	2-3	3-4	1350	149
			2400	17.1	5	5	1200	154
CA-2	Cr-35Re	0	1500	0.4	0[f]	0	435	432
			2100	3.2	0-4 (IG)[f]	0	401	386
			2400	6.2	0[f]	0	351	348

* Tests made on extruded specimens. All others swaged.

[a] 100-hour air exposures at 1500° and 2100°F, 25 hours at 2400°F.

[b] Refers to thickness of surface nitride layer and/or:

P - Precipitation of Cr_2N within grains.
IG - Intergranular nitride.

[c] Depth of contaminated zone which exceeds the hardness of the core by greater than 25 points DPH, measured at 100 gram load.

[d] Hardness measured outside nitrided area.

[e] Intergranular oxide.

[f] Sigma phase formed in Cr-depleted zone beneath oxide.

TABLE 26

COMPARATIVE MECHANICAL PROPERTIES OF
SELECTED REACTIVE-SOLUTE ALLOYS

Designation	Solute	Avg. Tensile Strengths (ksi) 1900°F 2400F	Wrought	Rx	600F	DBTT (°F)
CI-62	0.6Ti	13.5	53.2	51.9	90.6	500
CI-63	0.6Zr	15.3	42.2	44.8	83.9	550
CI-64	0.6Hf	15.8	49.8	48.4	95.0	500
CI-65	0.6Cb	22.2	65.1	55.0	98.0	400
CI-66	0.6Ta	21.3	60.7	-	106.8	>600
CI-67	0.45Ti-0.3B	-	40.3	-	-	-
CI-70(77)	0.45Cb-0.3B	21.6	75.6	-	118.5	600
CI-71	0.45Ta-0.3B	-	70.3	-	127.0	>600
CI-72	0.3Ta-0.3Ti-0.3B	20.9	75.4	58.2	118.5	450

TABLE 27

ADDITIONAL RUPTURE PROPERTIES

A. Stress Rupture - Stress Relieved

Alloy	Nominal Composition	Test Temp. °F	Stress (ksi)	Life (hrs.)	Elong. (%)
CI-3	Hf-Th	1900	6.0	88.7	
CI-16	Re	1900	12.0	149.1	
CI-19	Zr-Ti-C	1900	8.0	0.1	
CI-22	Zr-Ti-B	1900	13.0	108.0	
CI-26	Mo-Zr-Ti	1900	17.5	32.2	9.6
CI-30	Mo-Zr-Ti-C	1900	17.0	28.2	6.9
CI-33	Mo-Ti-C	1900	22.5	38.9	
CI-37	Mo-Zr-Hf-C	1900	27.5	9.2	24.5
CI-37	Mo-Zr-Hf-C	1900	20.0	44.0	
CI-48	Re-Ta-Hf-C	1900	22.5	18.1	16.8
CI-58	Mo-Cb-N-C	1900	25.0	29.3	31.4
CI-22	Zr-Ti-B	2100	5.0	191.1	22.3
CI-47	Mo-W-Ta-C	2100	15.0	40.6	42.8
CI-65	Mo-Cb	2100	15.0	18.2	21.4
CI-66	Mo-Ta	2100	15.0	Broke on Loading	
CI-70	Mo-Cb-B	2100	15.0	283.0	
CI-71	Mo-Ta-B	2100	15.0	14.8	20.2
CI-72	Mo-Ti-Ta-B	2100	15.0	29.8	26.3
CI-72	Mo-Ti-Ta-B	2100	10.0	135.2	44.1

B. Creep Rupture - Recrystallized

CI-23	Zr-Hf-B	2100	8.0	45.5	22.0
CI-34	Mo-Zr-C	2100	15.0	17.4	23.9
CI-47	Mo-W-Ta-C	2100	15.0	25.6	31.4
CI-48	Re-Ta-Hf-C	2100	15.0	14.4	16.7
CI-65	Mo-Cb	2100	15.0	141.9	1.1
CI-66	Mo-Ta	2100	15.0	Broke on Loading	
CI-72	Mo-Ti-Ta-B	2100	15.0	33.9	35.0

TABLE 28

2100°F TENSILE PROPERTIES, PHASE TM ALLOYS

Alloy	Pre-Extrusion Condition[a]	Working Schedule[b]	2100°F Tensile Properties			
			UTS (ksi)	0.2% Offset (ksi)	Elong. (%)	RA (%)
CI-73(Cr-4Mo-CbC)	A	2	42.0	39.3	27.2	72.4
	A	4	-	-	-	-
	B	1	39.6	37.2	35.2	88.9
	B	2	45.4	44.4	33.3	90.5
	B	3	48.0	41.0	26.8	66.2
	B	4	54.5	52.2	22.7	85.2
	B	5	-	-	-	-
CI-74(Cr-4Mo-TaC)	A	1	40.1	34.4	38.8	85.0
	A	2	43.3	40.9	0.6	1.5
	B	1	-	-	-	-
	B	2	48.4	46.5	18.3	59.4
	B	4	50.2	48.2	22.9	83.8
CI-75(Cr-4Mo-Ta)	A	2	41.2	37.1	6.0	6.0
	B	1	32.0	23.8	27.4	80.0
	B	2	-	-	-	-
	B	3	34.4	33.8	17.9	48.5
	B	4	-	-	-	-

a) A = as-cast B = Cast plus solution annealed, 2800°F

b) Working schedules (swagging):

(1) 50% at 2500°F, finish at 2300°F

(2) 50% at 2500°F, finish at 2100°F

(3) 50% at 2500°F, finish at 1900°F

(4) 50% at 2500°F, anneal at 2800°F, finish at 2100°F

(5) 50% at 2500°F, anneal at 2800°F, finish at 1900°F

TABLE 29

LOW-TEMPERATURE TENSILE PROPERTIES, PHASE TM

Alloy	Pre-Extrusion Condition[a]	Working Schedule	800°F YS	DBTT(°F)
CI-73 (CbC)	A	2	83.8	400
	B	2	95.4	600
	B	3	101.0	450
	B	4	87.5	350
CI-74 (TaC)	A	1	76.2	800
	B	2	87.5	650
CI-75 (Ta)	B	1	52.0	600
	B	3	76.5	350

a) See Table 28 for definition of conditions and schedules

TABLE 30

IMPACT PROPERTIES OF SELECTED CHROMIUM ALLOYS

(Smooth Micro-Izod Specimens)

Alloy	Composition (at %) and Condition	Test Temp (°F)	Impact Energy (In-Lb)	Approx. DBTT (°F)
CA-1	Unalloyed Cr Finish swaged 1300°F Annealed 1600°F	400 500 600 700	1.2 1.9 37.3* 43.2*	550 ± 50 tensile (150)
CI-3	Cr-0.1Y-0.05Hf-0.03Th Finish swaged 1900°F Annealed 2000°F	73 200 250 300 400 600	1.7 2.4 1.7 43.1* 43.4* 43.6*	275 ± 25 tensile (50)
CI-26	Cr-4Mo-0.1Y-0.4Zr-0.2Ti Finish swaged 2200°F Annealed 2000°F	400 500 700 900 1100	4.3 2.6 10.6 13.6 44.4*	1000 ± 100 tensile (600)
CI-51	Cr-0.1Y-0.03Th-0.6Hf-0.4C Finish swaged 2100°F Annealed 2000°F	75 200 300 400 600	1.8 2.4 44.0* 43.1* 43.1*	250 ± 50 tensile (-25)
CI-64	Cr-4Mo-0.15 (Y+La)-0.6Hf Finish swaged 2150°F Annealed 2000°F	400 600 700 800	3.0 5.0 9.7 42.8*	750 ± 50 tensile (500)
CA-2	Cr-35Re Finish swaged 2200°F Annealed 2000°F	-200 -100 75 75[a] 75[a]	43.9* 43.2* 43.0* 128.6* 183.4*	< -200 tensile (< -200)

* Did not fracture

[a] 192 inch-pound tup energy. All others 48 inch-pounds.

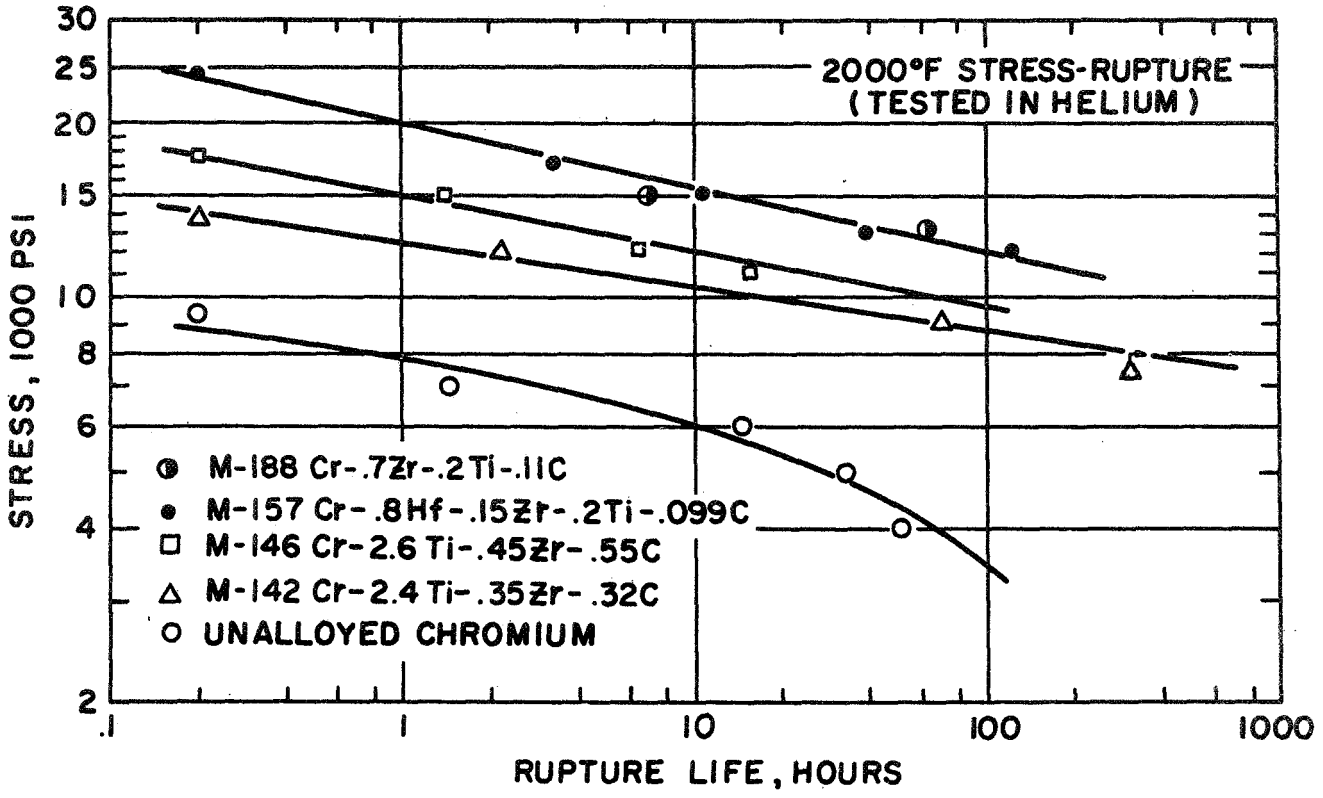

Figure 1. Stress-Rupture Properties of Wrought, Carbide-Strengthened Chromium Alloys. (Compositions in Weight Percent).

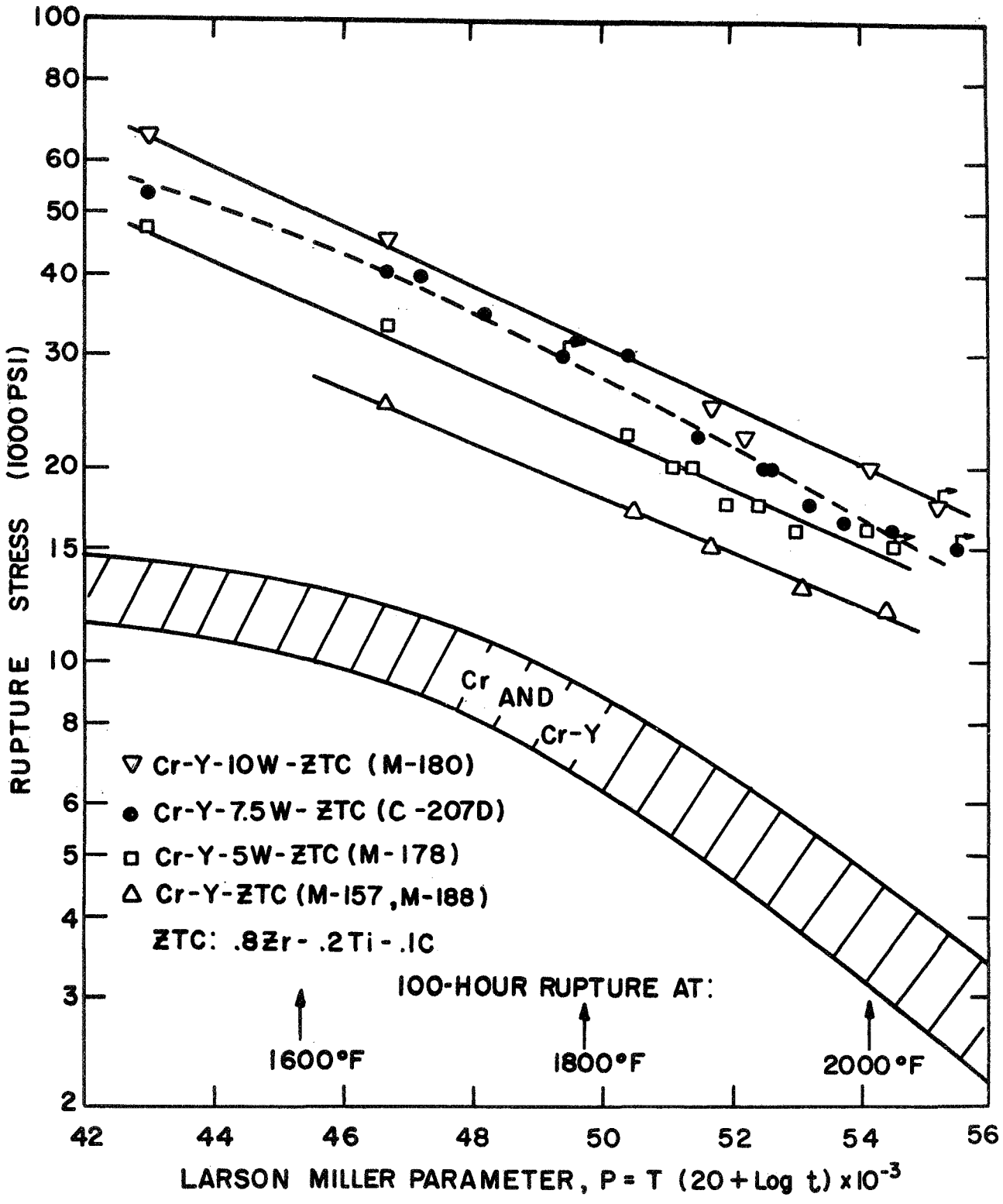

Figure 2. Stress-Rupture Properties of Wrought Chromium Alloys Tested in Helium Atmosphere. (Compositions in Weight Percent).

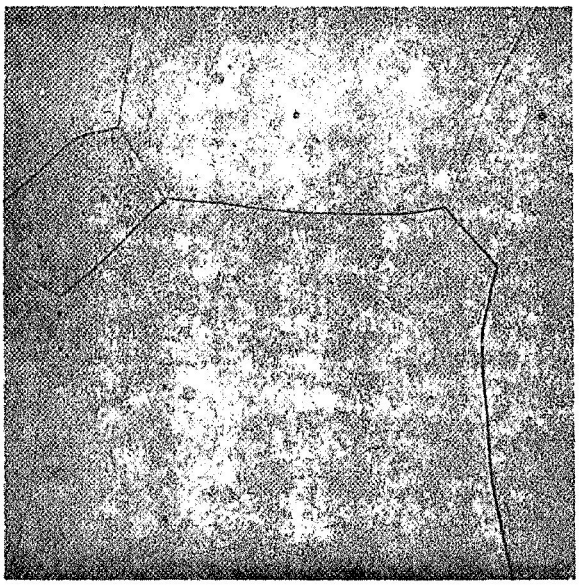

A. Cr-5.1W-5.1V 250X

B. Cr-4.8W-9.6V 250X

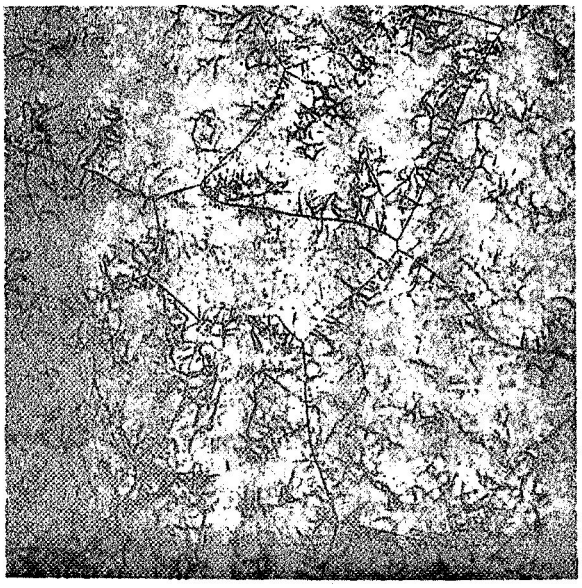

C. Cr-10.3W-15.6V 250X

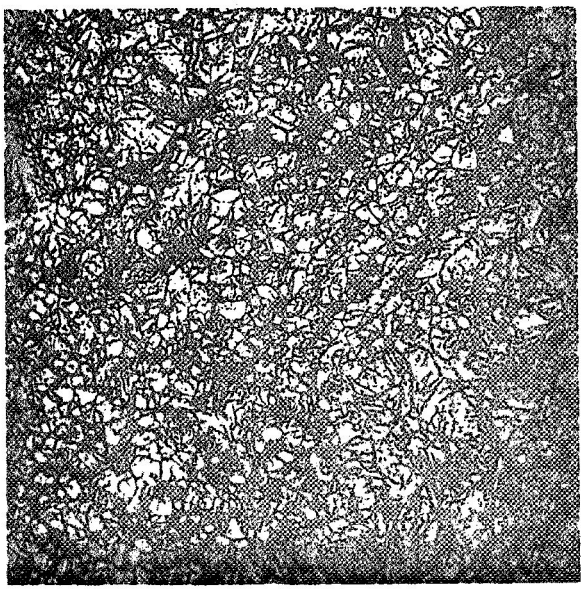

D. Cr-10.1W-20.3V 250X

Figure 3. Microstructures of Cr-W-V alloys aged 200 hours at 1800°F. Etched 10% oxalic acid.

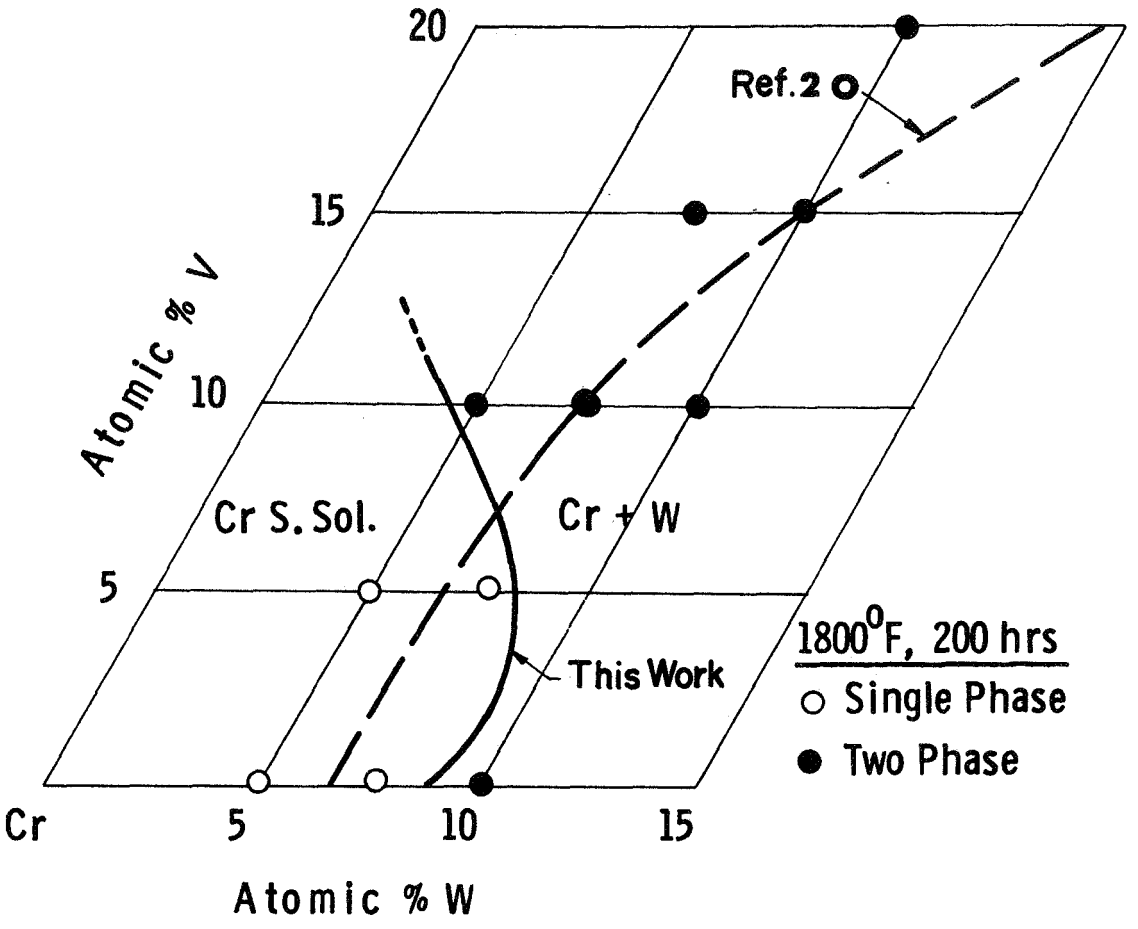

Figure 4. Cr-rich corner of the Cr-W-V equilibrium diagram at 1800°F, showing location of experimental alloys and extent of W solubility according to English[20].

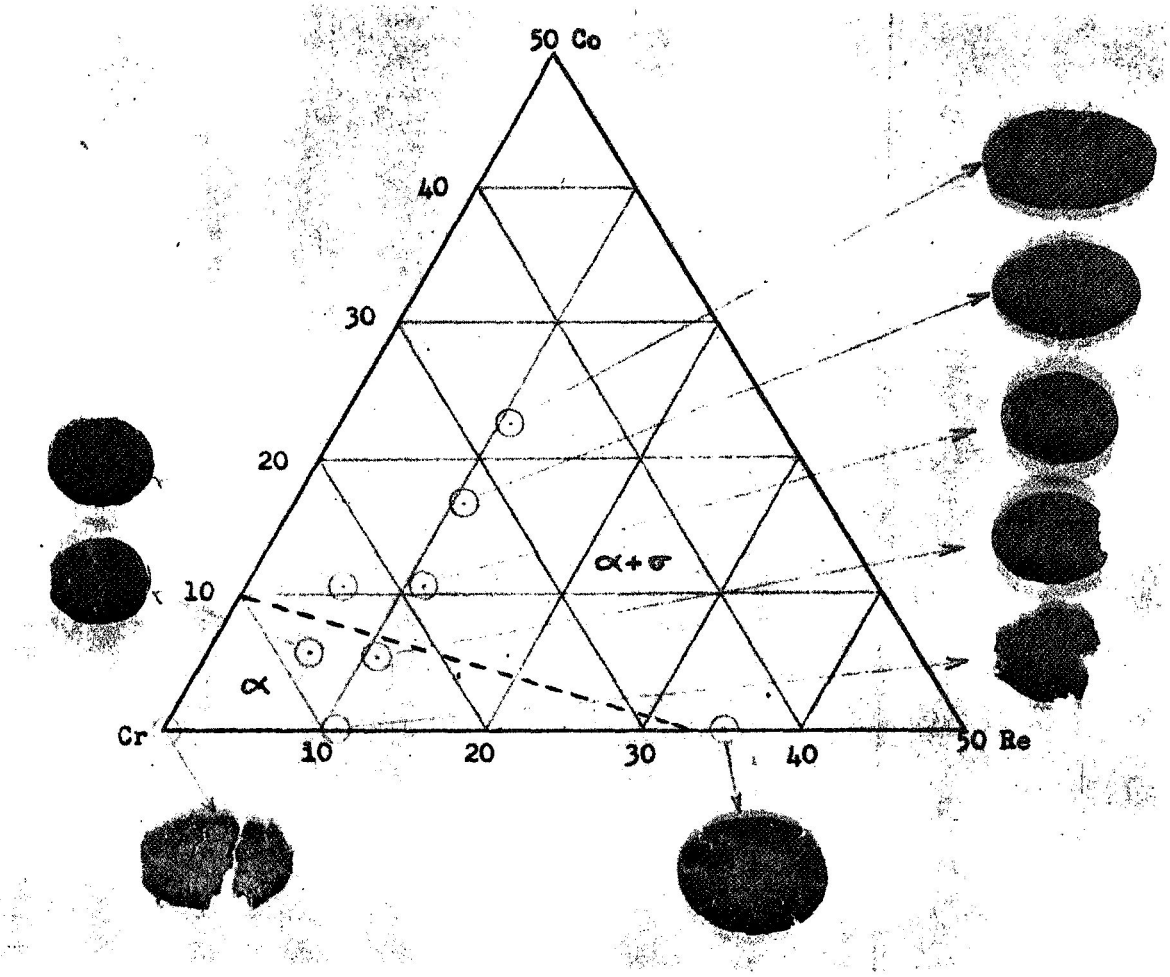

Figure 5. Cold workability of drop cast Cr-Re-Co alloys with compositions shown in atomic %. Tentative phase boundary at 1650°F.

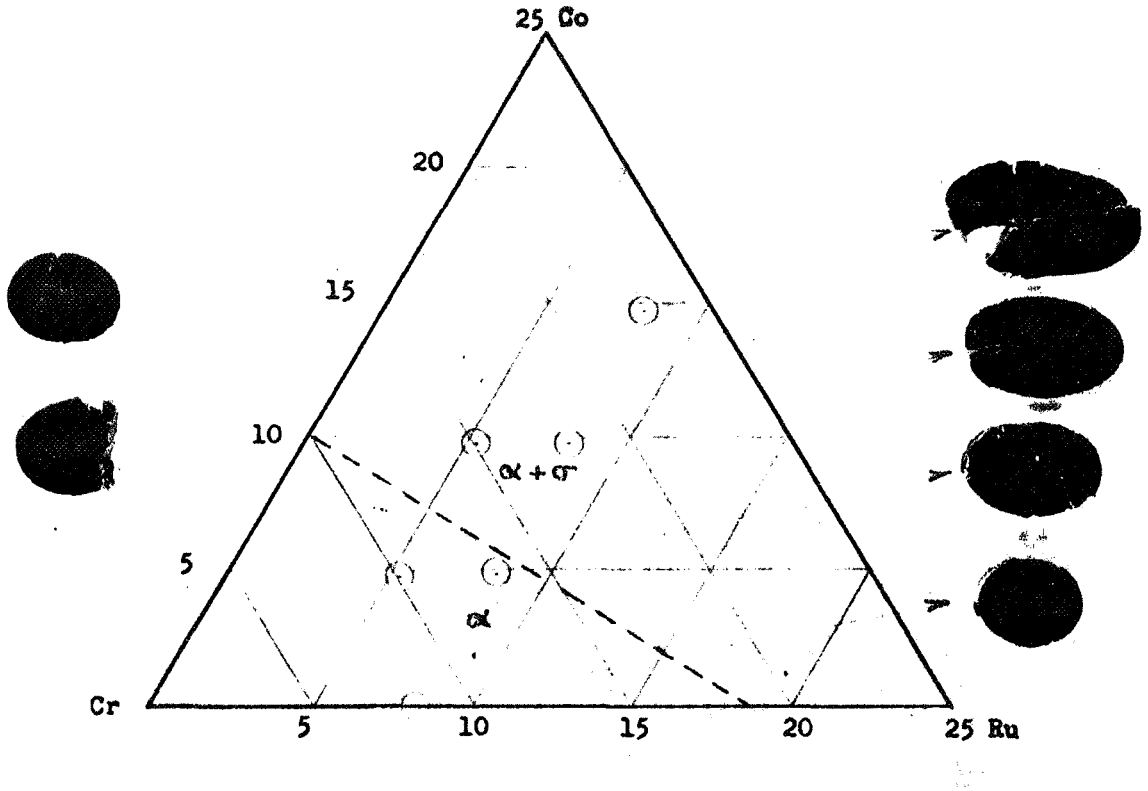

Figure 6. Cold workability of drop cast Cr-Ru-Co alloys with compositions shown in atomic %. Tentative phase boundary at 1650°F.

A. Cr-14.2Re-10.4Co

Grain-boundary sigma

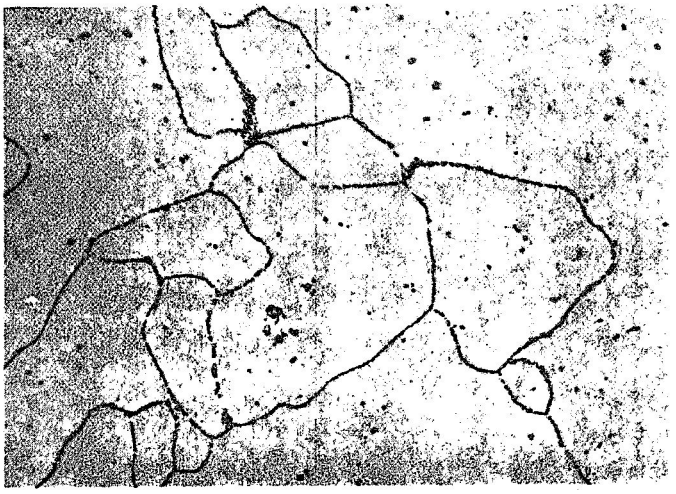

M9871 250X

B. Cr-11.0Re-17.2Co

Approximately 50% sigma

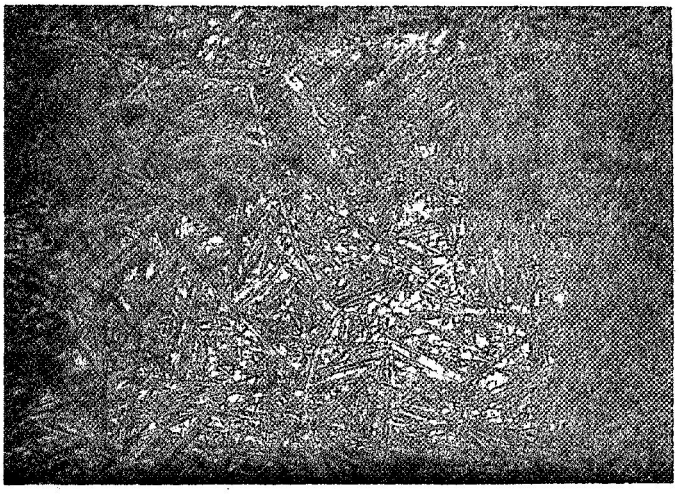

M7973 250X

C. Cr-11.0Re-23.1Co

Approximately 80% sigma

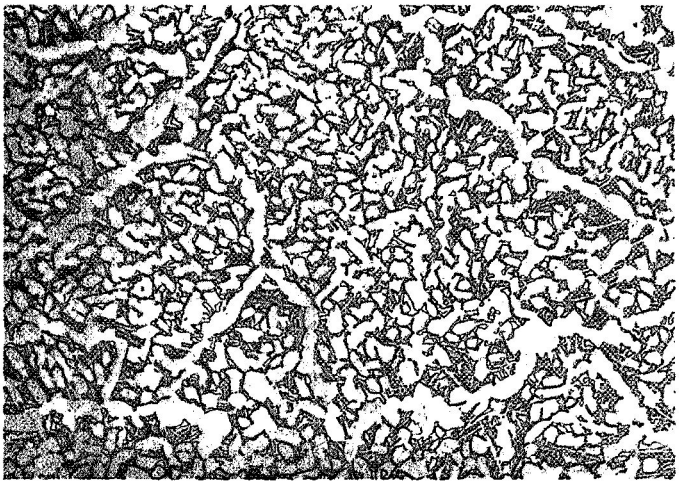

M7974 250X

Figure 7. Effect of 100-hour aging at 1650°F on the structure of Cr-Re-Co alloys at indicated atomic concentrations. Etched 10% oxalic acid.

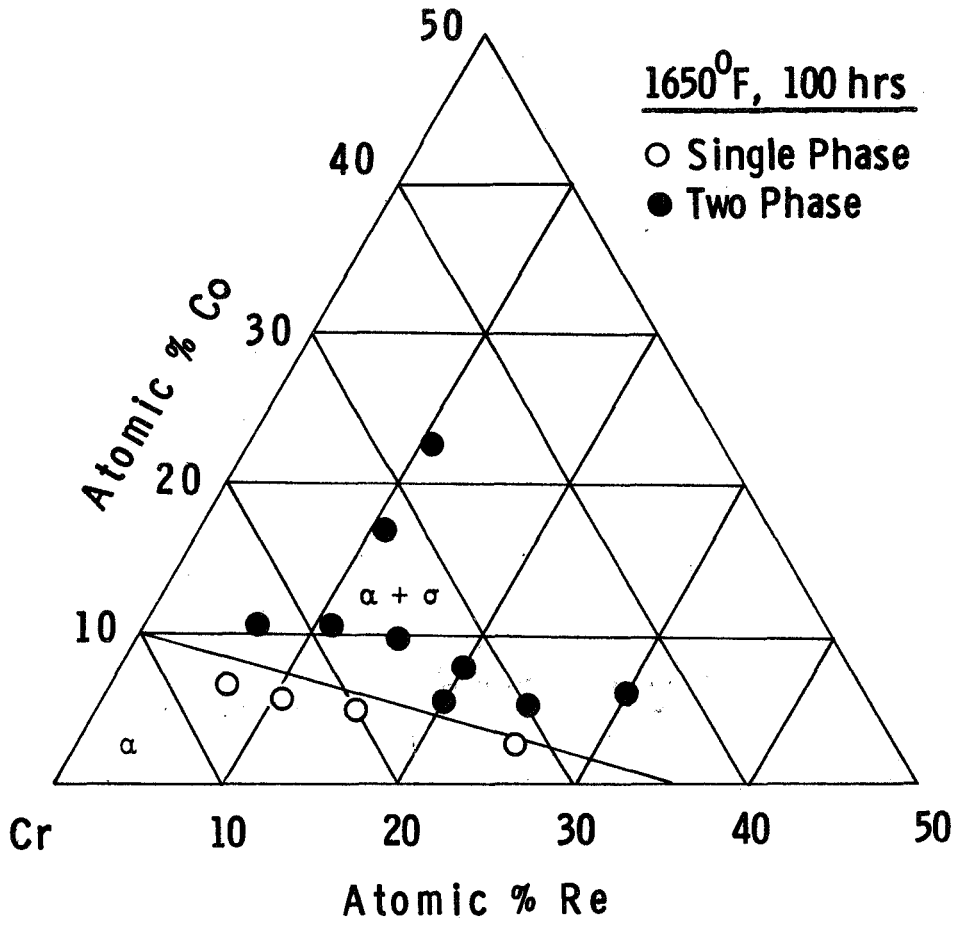

Figure 8. Cr-rich corner of the Cr-Re-Co equilibrium diagram at 1650°F, showing extent of chromium solid solutions.

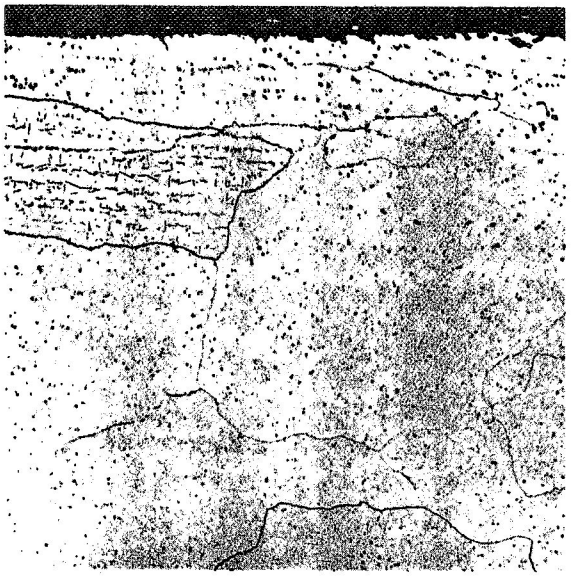

6377 100X

A. Cr-4Re-.1Y, 100 hours at 2100°F

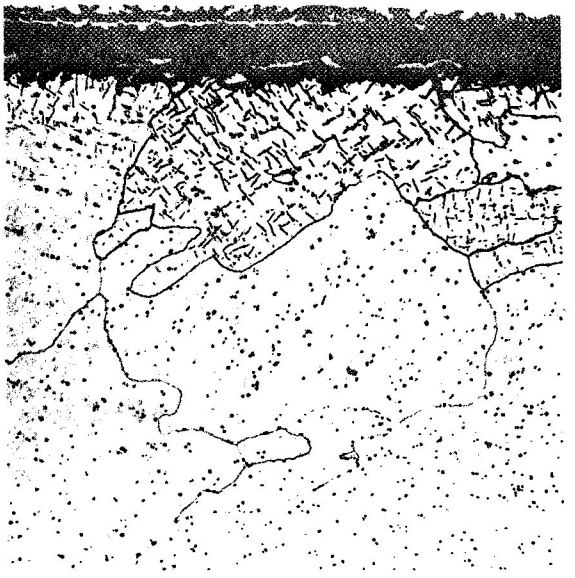

6378 100X

B. Cr-4Re-.1Y, 24 hours at 2400°F

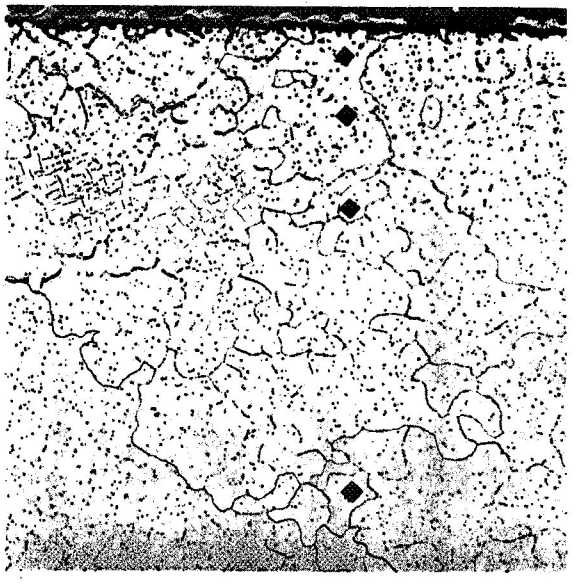

6379 100X

C. Cr-4Re-.5Y, 100 hours at 2100°F

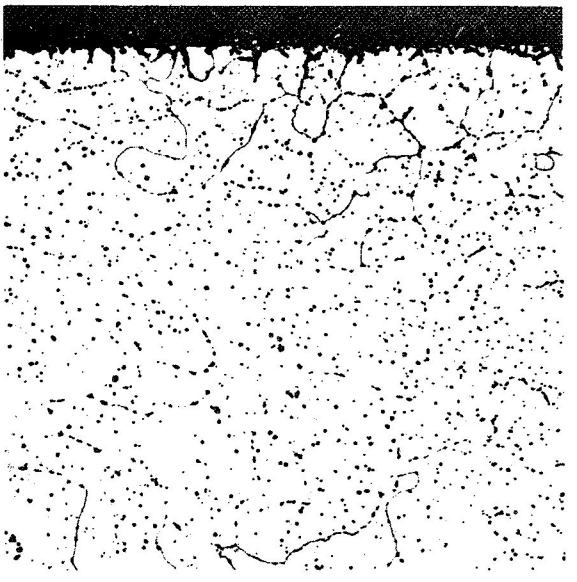

6380 100X

D. Cr-4Re-.5Y, 24 hours at 2400°F

Figure 9. Air oxidation effects on Cr-Re-Y alloys at indicated atomic concentrations. Etched 10% oxalic acid.

6381 100X

A. Cr-8Re-.5Y, 100 hours at 2100°F

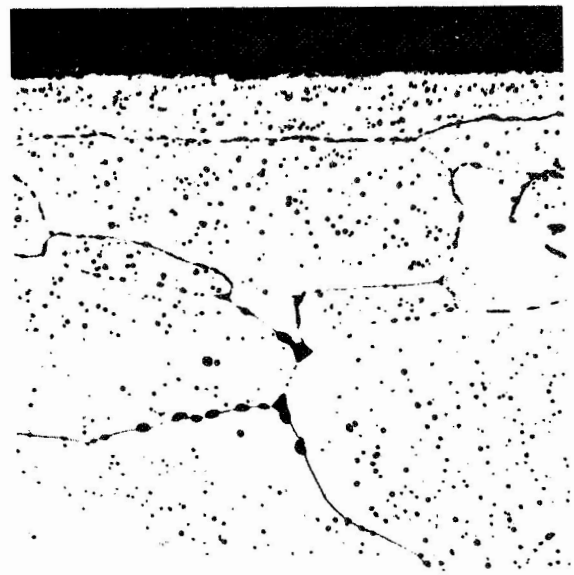

6382 100X

B. Cr-8Re-.5Y, 24 hours at 2400°F

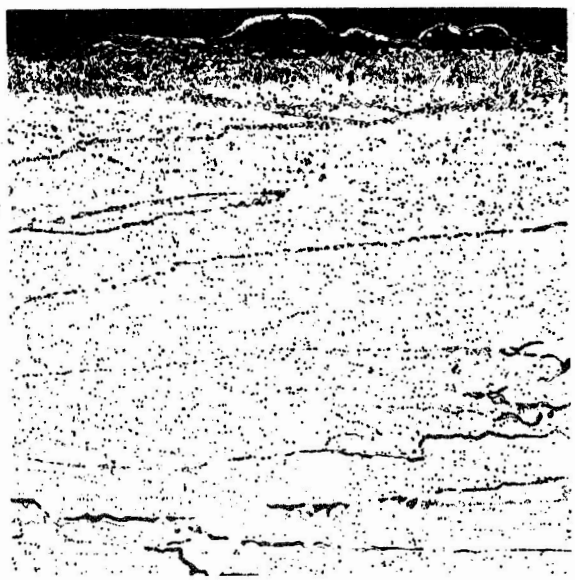

6383 100X

C. Cr-4Ru-.5Y, 24 hours at 2400°F

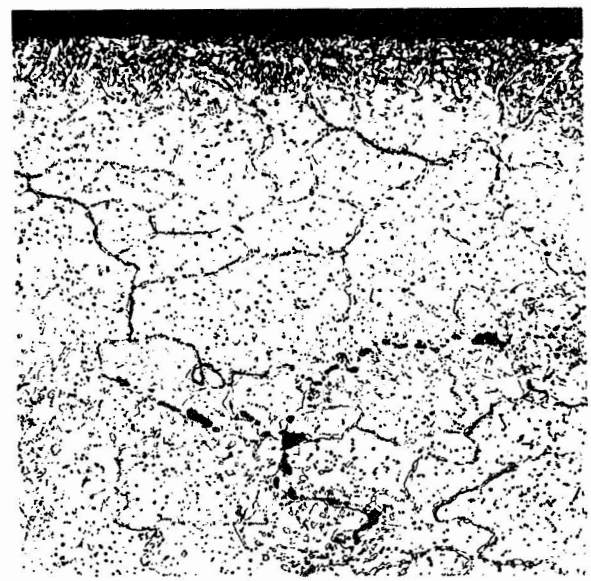

6384 100X

D. Cr-4Co-.5Y, 24 hours at 2400°F

Figure 10. Air oxidation of Cr-.5Y alloys with Re, Ru and Co additions (all atomic %). Etched 10% oxalic acid.

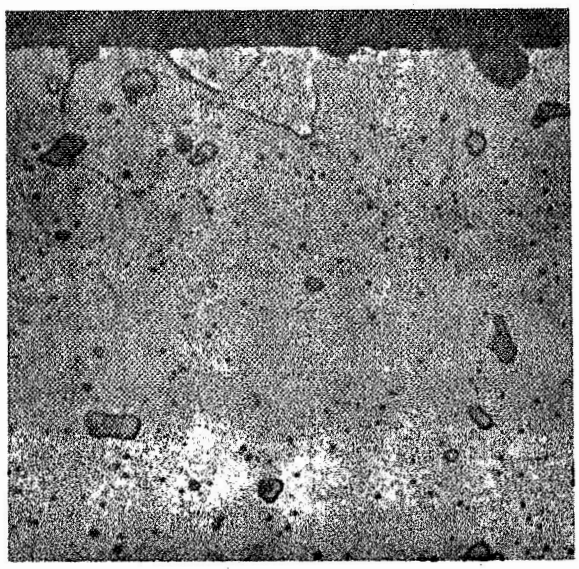

3871 1000X

A. Cr-1Zr-.4C-.1Y at 1500°F

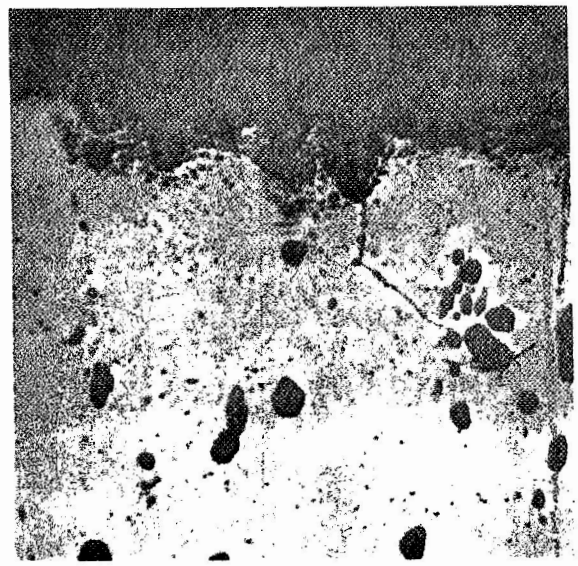

3698 1000X

B. Cr-1Zr-.4C-.1Y at 2100°F

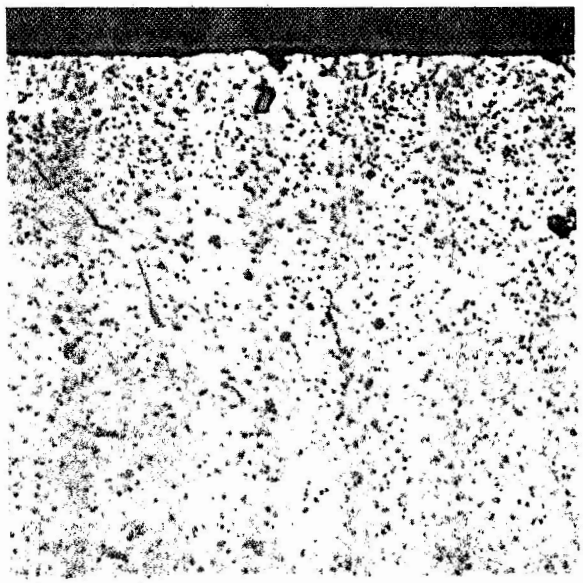

2546 1000X

C. Cr-1Cb.4C-.1Y at 1500°F

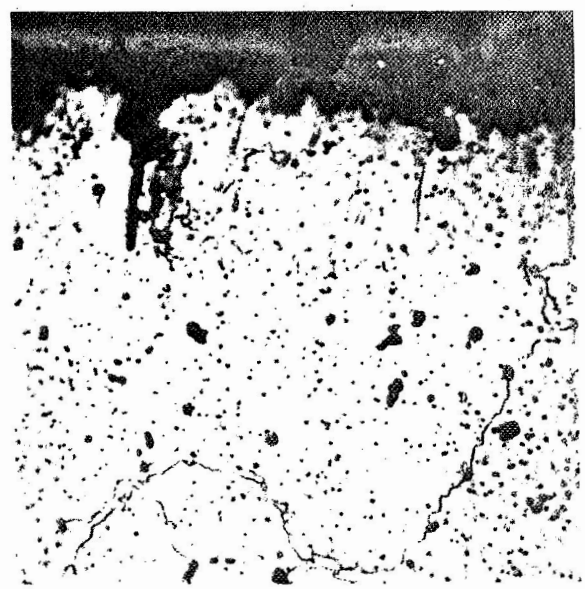

3838 1000X

D. Cr-1Cb-.4C-.1Y at 2100°F

Figure 11. Dilute Cr-Y alloys containing ZrC and CbC dispersions after 100-hour air oxidation at indicated temperatures. Nominal compositions in atomic %. Etched in Kromic acid.

A. Cr-3Cb-.1Y Aged 2200°F/5Hrs

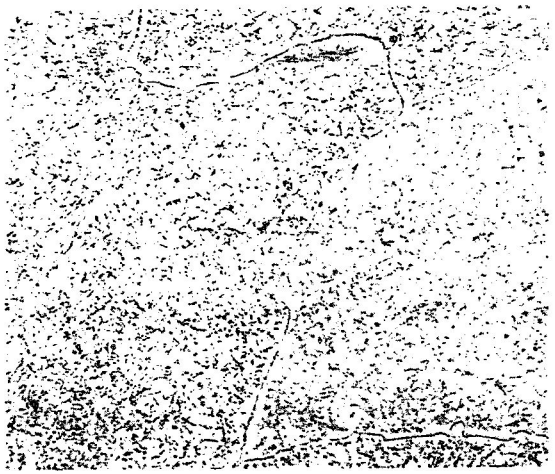

F1590 250X

C. Cr-2Si-.1Y Aged 2200°F/5Hrs

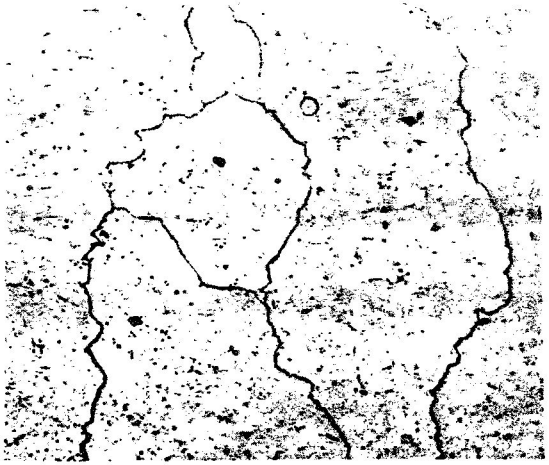

F1825 250X

E. Cr-3Cb-2Si-.1Y Aged 2200°F/5Hrs

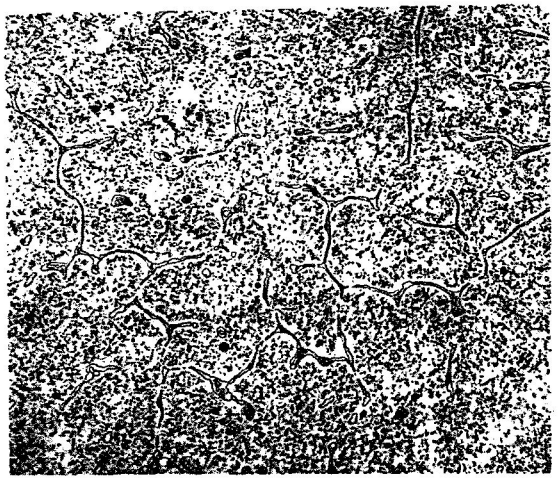

F1598 250X

B. Cr-3Cb-.1Y Oxidized 2100°F/100 Hours

F1821 100X

D. Cr-2Si-.1Y Oxidized 2100°F/ 100 Hours

F1823 250X

F. Cr-3Cb-2Si-.1Y Oxidized 2100°F/ 100 Hours

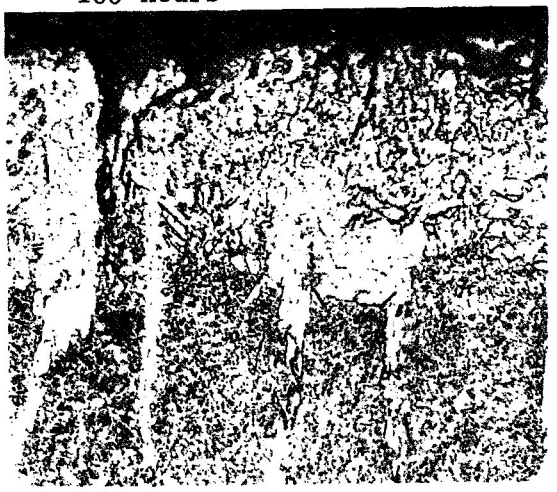

F1826 250X

Figure 12. Effects of aging and of oxidation on the structure of alloys in the Cr-Y-Cb-Si system. Etched Kromic acid.

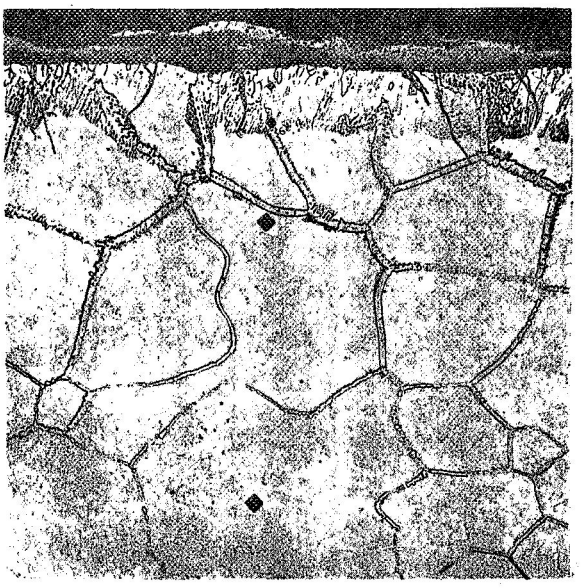

6366 100X

A. Cr-4Mo, 100 hours at 2100°F

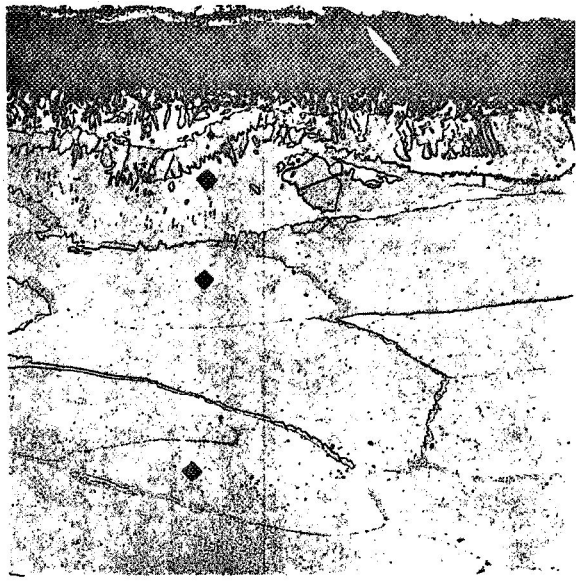

6367 100X

B. Cr-4Mo, 24 hours at 2400°F

6368 100X

C. Cr-4Mo-.1Y, 100 hours at 2100°F

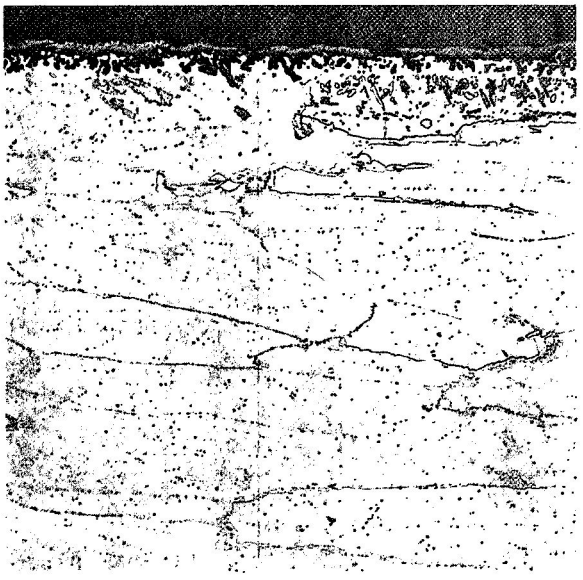

6369 100X

D. Cr-4Mo-.1Y, 24 hours at 2400°F

Figure 13. Effects of 0.1 a/o Y addition on the air oxidation of Cr-4Mo. Etched 10% oxalic acid.

6371 100X

A. Cr-4Mo-.5Y

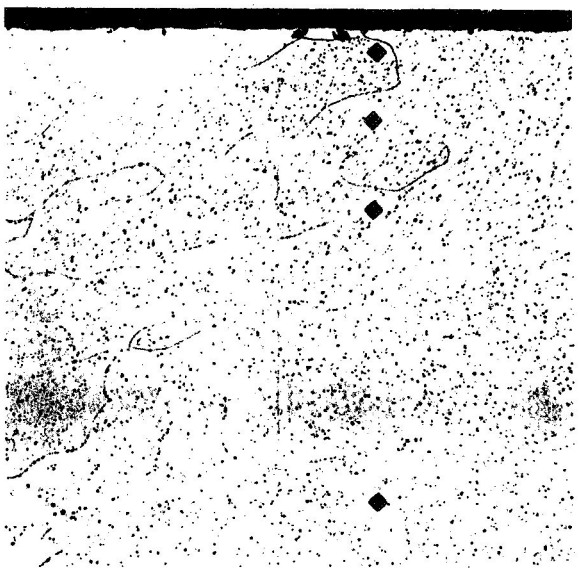

6373 100X

B. Cr-4Mo-.5La

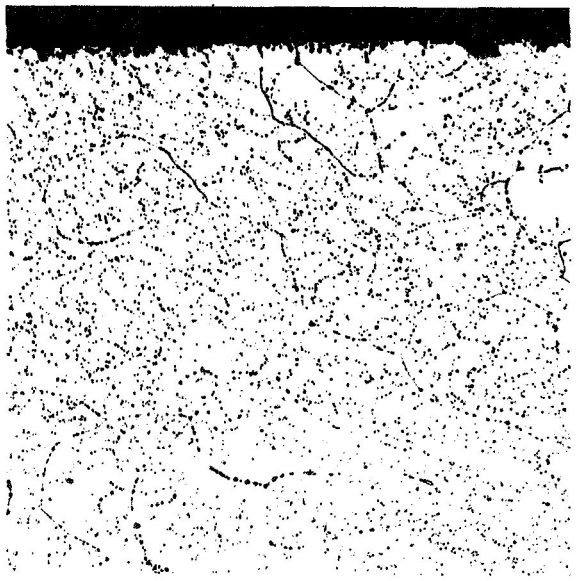

6375 100X

C. Cr-4Mo-.5Pr

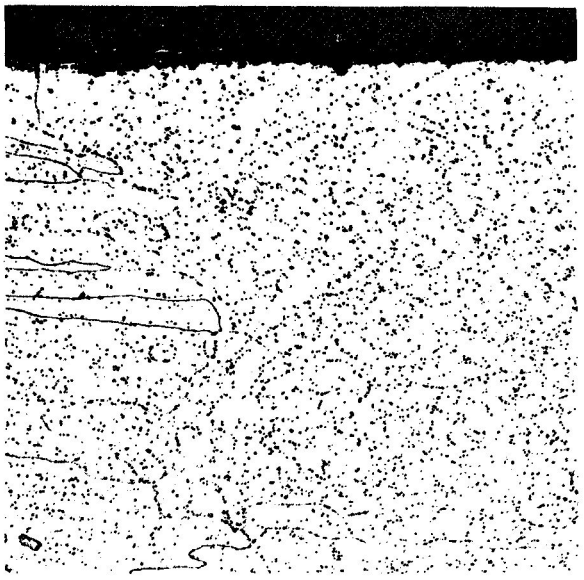

6376 100X

D. Cr-4Mo-.5 Mischmetal

Figure 14. Cr-4Mo alloys with 0.5 atomic % additions of Y, La, Pr and Mischmetal after 24-hour air oxidation at 2400°F. Etched 10% oxalic acid.

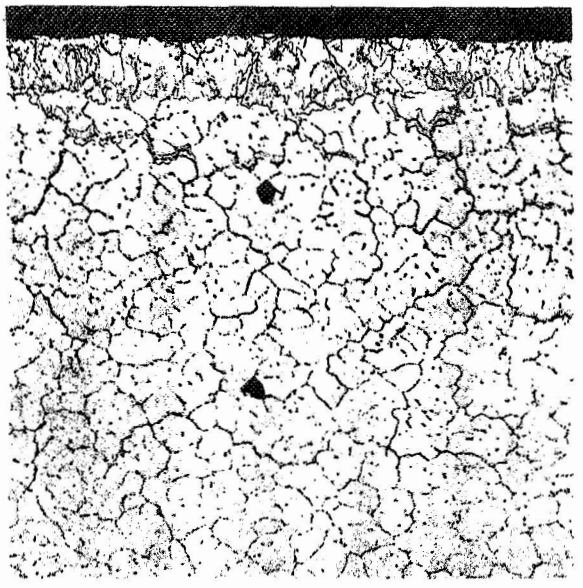

6917 100X

A. Cr-ZTC 100Hrs at 2100°F

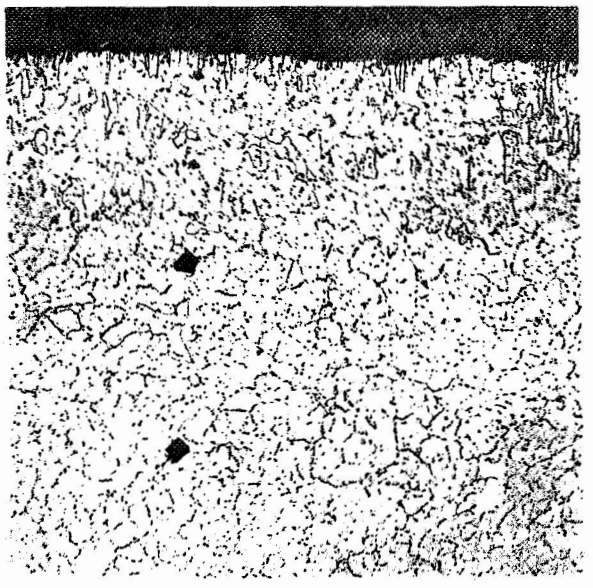

6916 100X

B. Cr-ZTC 24Hrs at 2400°F

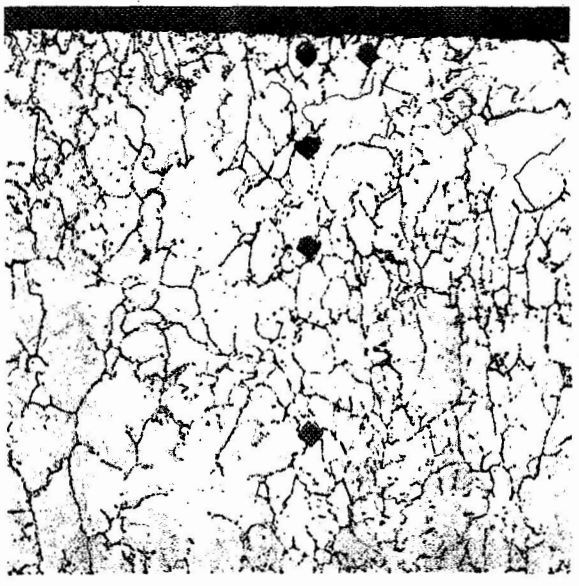

6919 100X

C. Cr-0.2La-ZTC 100Hrs at 2100°F

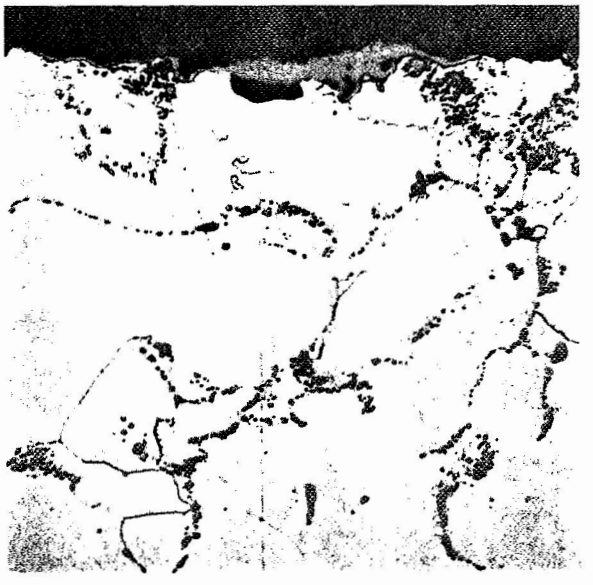

7238 500X

D. Cr-0.2La-ZTC 24Hrs at 2400°F

Figure 15. Effects of 0.2 atomic percent La on the air oxidation of Cr-ZTC alloy. Etched 10% oxalic acid.

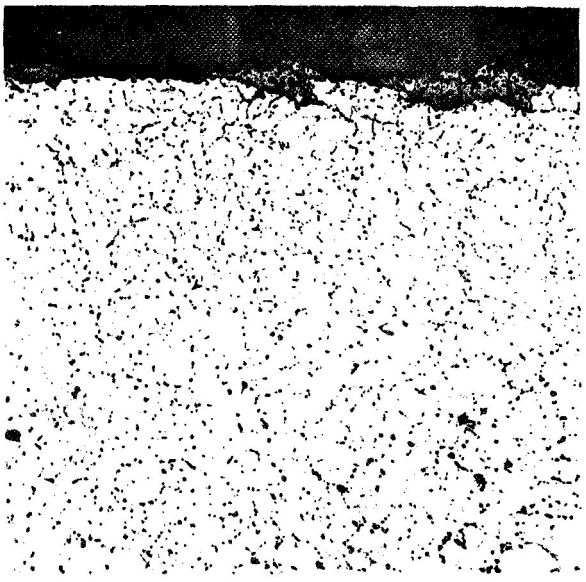

6921 100X

A. Cr-.2La-TiC 24Hrs at 2400°F

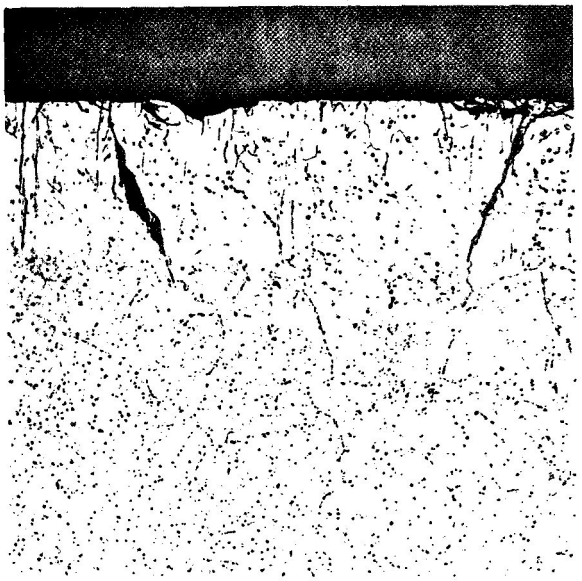

6924 100X

B. Cr-.2Pr-CbC 24Hrs at 2400°F

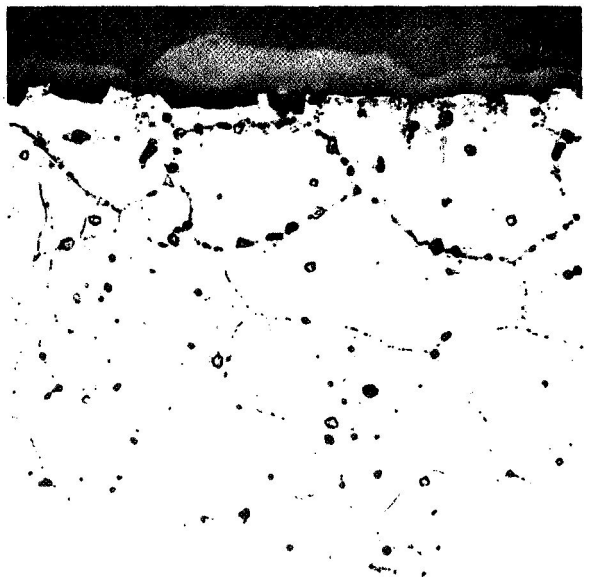

7240 500X

C. Cr-.5La-CbC 24Hrs at 2400°F

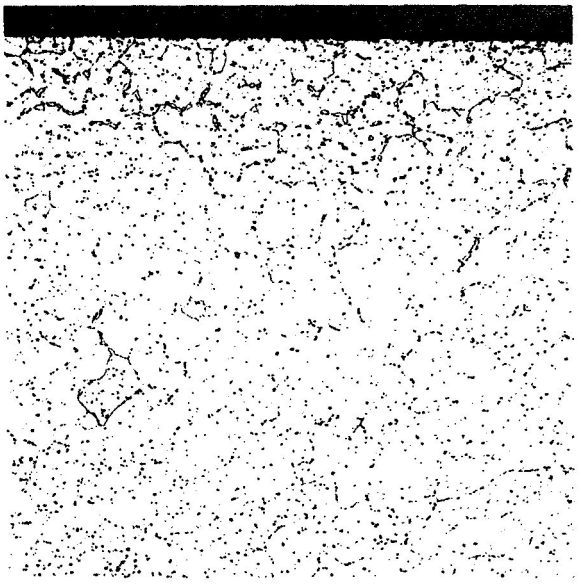

6927 100X

D. Cr-.5La-CbC 100Hrs at 2100°F

Figure 16. Effects of La and Pr additions on the air oxidation of Cr-TiC and Cr-CbC alloys. Etched 10% oxalic acid.

A. 1 Hour at 2100°F, 250X
5:1 Taper M5084

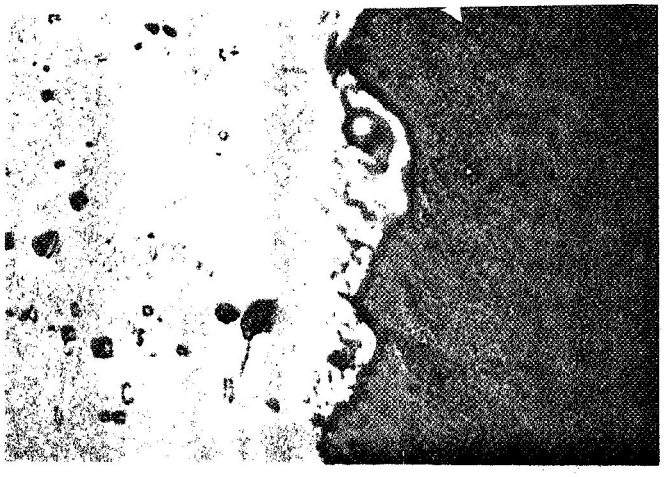

B. 1 Hour at 2100°F, 1000X
5:1 Taper N991

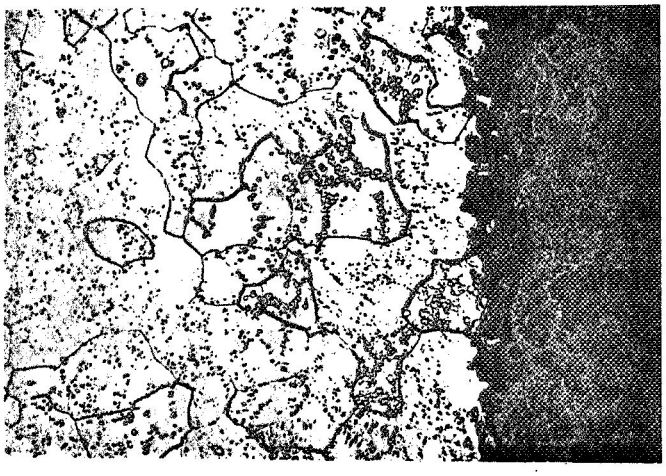

C. 100 Hours at 2100°F, 250X
5:1 Taper M5081

Figure 17. Taper sections through surface scales formed on Cr-.2La alloy at 2100°F in air. Kromic etch.

A. Cr-4Mo-.3La-.6Zr-.4C

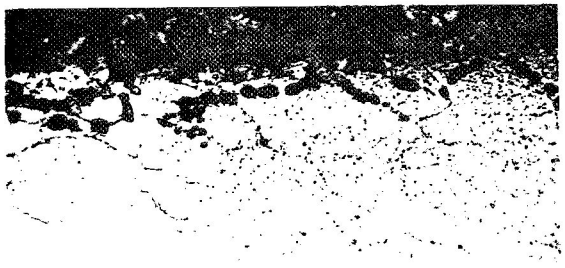

F2141 250X

C. Cr-4Mo- 3La-.4Zr-.2Ti-.4C

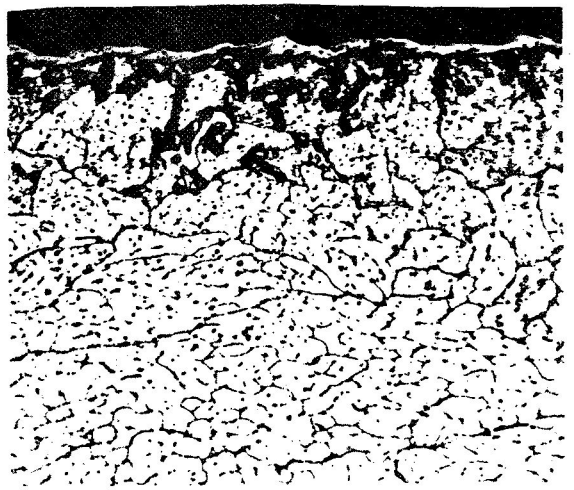

F2138 250X

E. Cr-4Mo-.3La-.6Ta-.4C

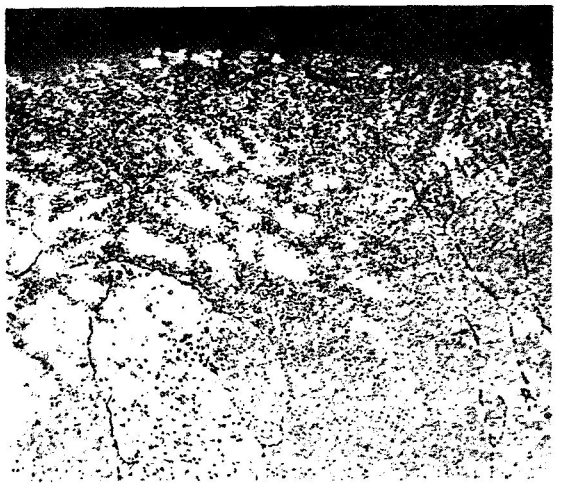

F2143 250X

B. Cr-4Mo-.3La-.6Hf-.4C

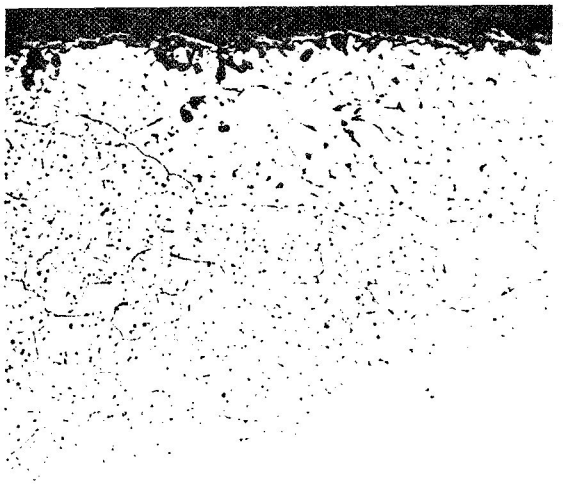

F2145 250X

D. Cr-4Mo-.4La-.6Cb-.4C

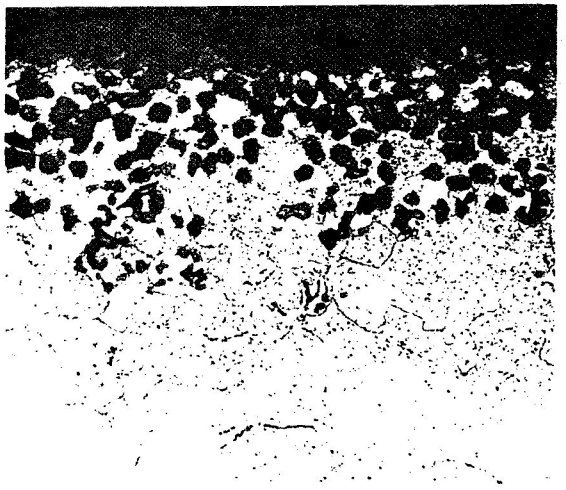

F2142 250X

F. Cr-4Mo-.3La-.3Ta-.3Hf-.4C

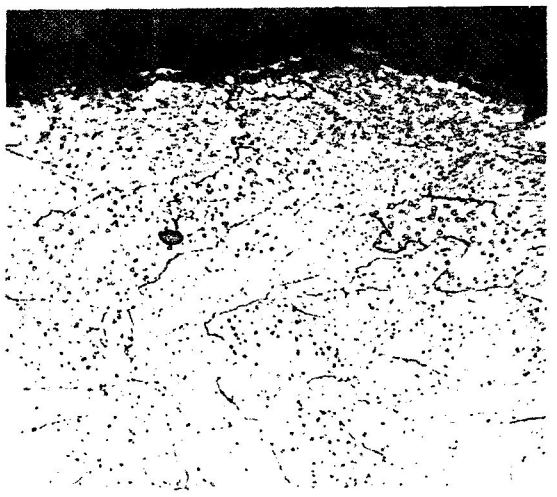

F2144 250X

Figure 18. Cr-4Mo-La alloys with various carbide dispersions after 100-hour air oxidation at 2100°F. Nominal compositions in atomic percent. Etched Kromic acid.

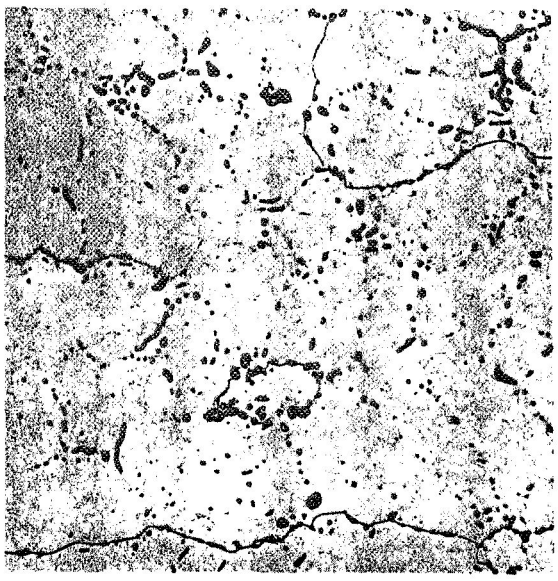

L2955 250X

A. Alloy CI-6 (.202% O_2, <.06% Y)

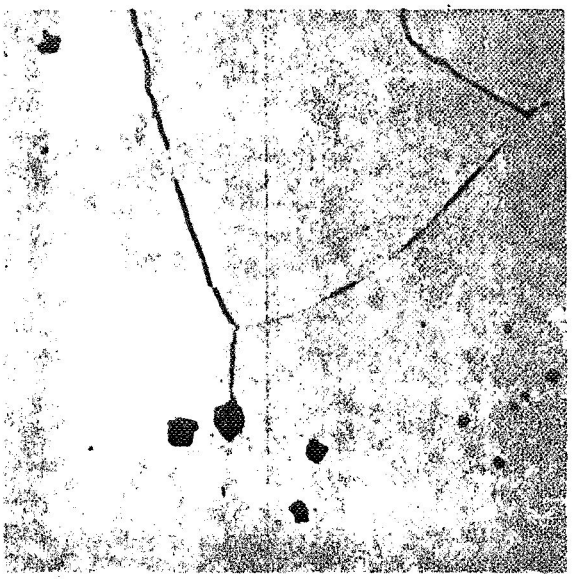

L3781 1000X

B. Alloy CI-5A (.0522% O_2, <.06% Y)

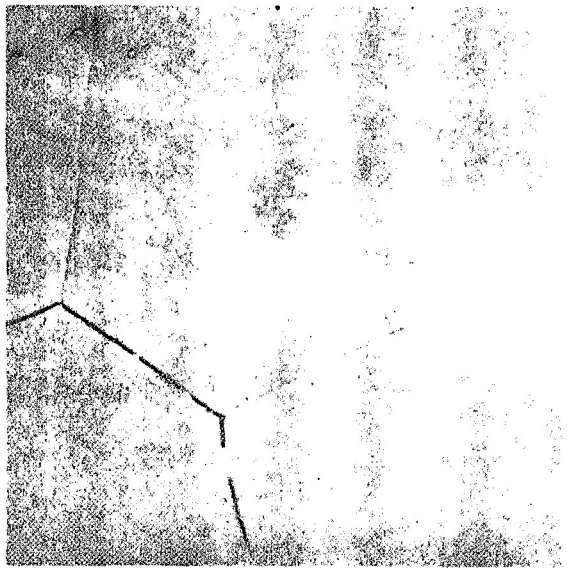

L3784 1000X

C. Alloy CI-7A (.0029% O_2, .10% Y)

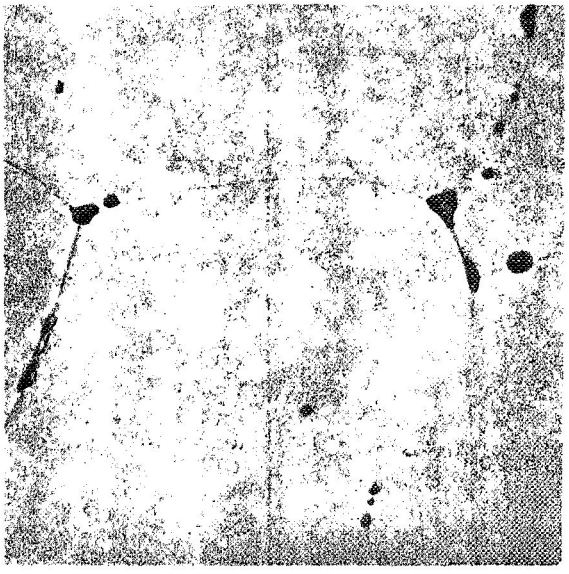

L3780 1000X

D. Alloy CI-5B (.0034% O_2, .19% Y)

Figure 19. Cast structures of induction-melted Cr alloys at indicated oxygen and yttrium levels (weight %). Etched 10% oxalic acid.

A. CI-1 (Cr-.1Y)

E6024 1000X

C. CI-19 (Cr-.05Y-ZTC)

E5054 1000X

E. CI-33 (Cr-.05Y-TiC)

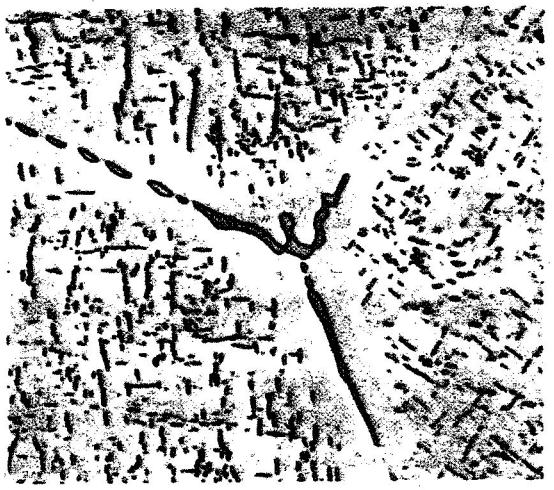

F1089 1000X

B. CI-16 (Cr-4Re-.1Y)

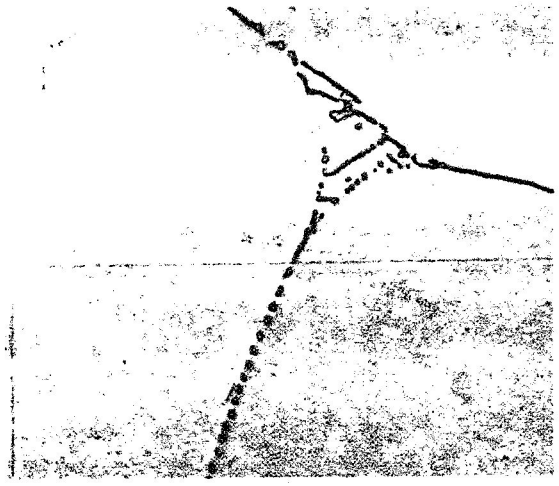

E6647 1000X

D. CI-21 (Cr-.05Y-HZC)

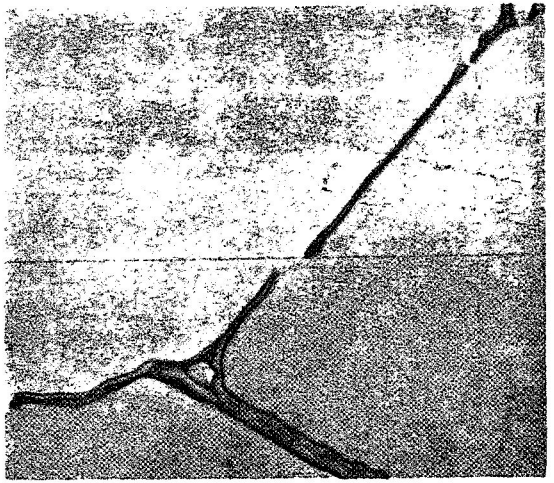

E5162 1000X

F. CI-36 (Cr-.05Y-CbC)

F1091 1000X

Figure 20. Cast microstructures of induction-melted chromium alloys. Etched Kromic acid.

A. CI-1 (Cr-.10Y)

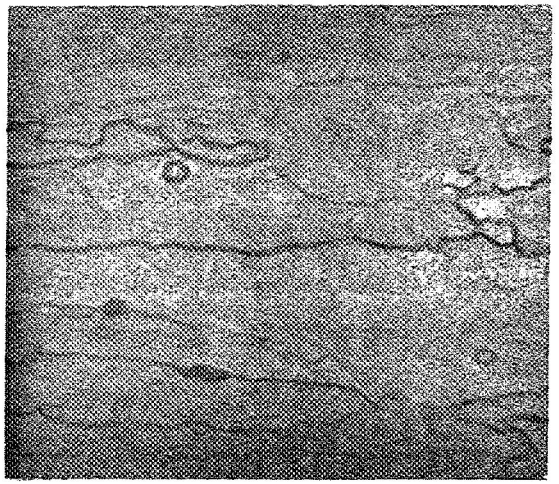

F1493 1000X

C. CI-19 (Cr-.05Y-ZTC)

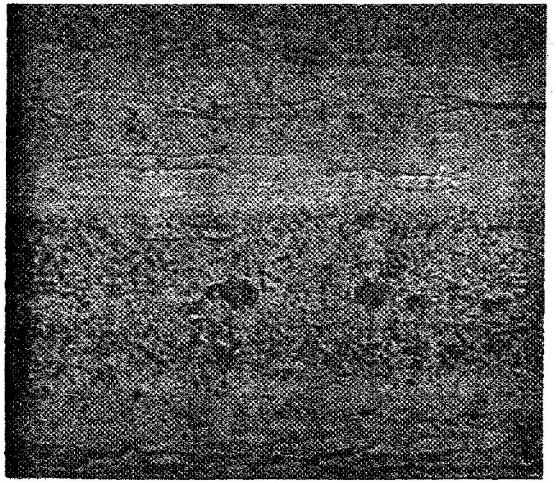

E5306 1000X

E. CI-33 (Cr-.05Y-TiC)

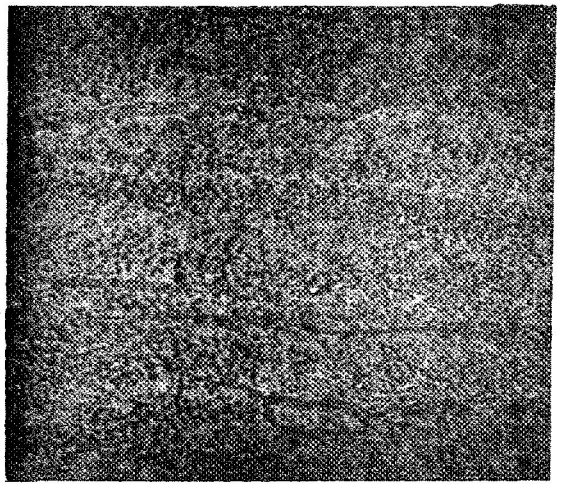

F2332 1000X

B. CA-2 (Cr-35Re)

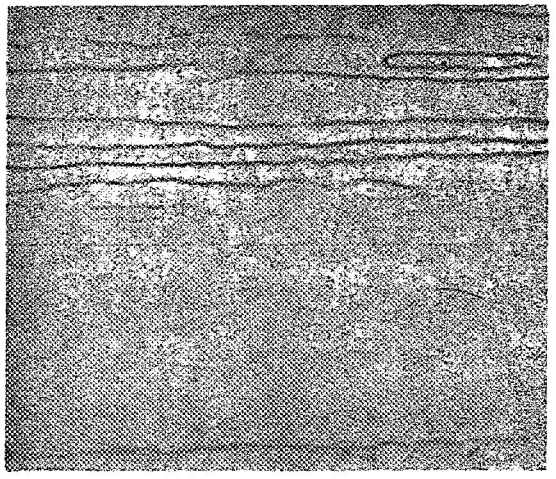

F1476 1000X

D. CI-21 (Cr-.05Y-HZC)

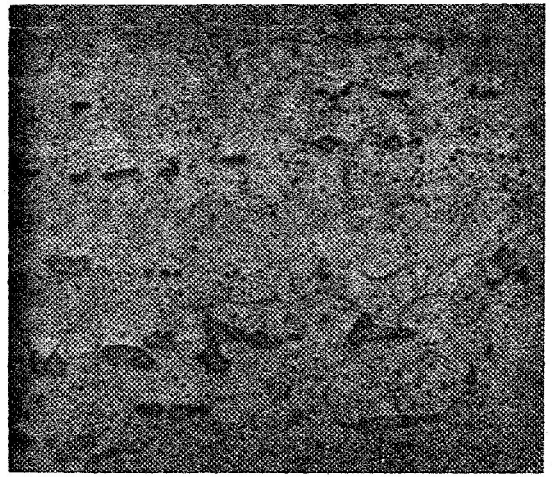

E5734 1000X

F. CI-36 (Cr-.05Y-CbC)

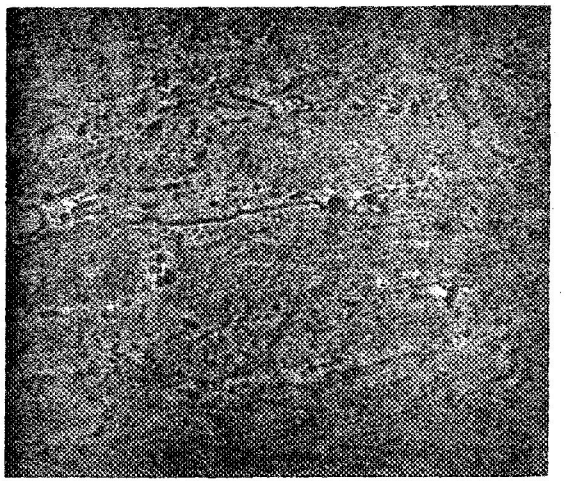

F2334 1000X

Figure 21. Microstructures of swaged chromium alloys. Etched in Kromic acid.

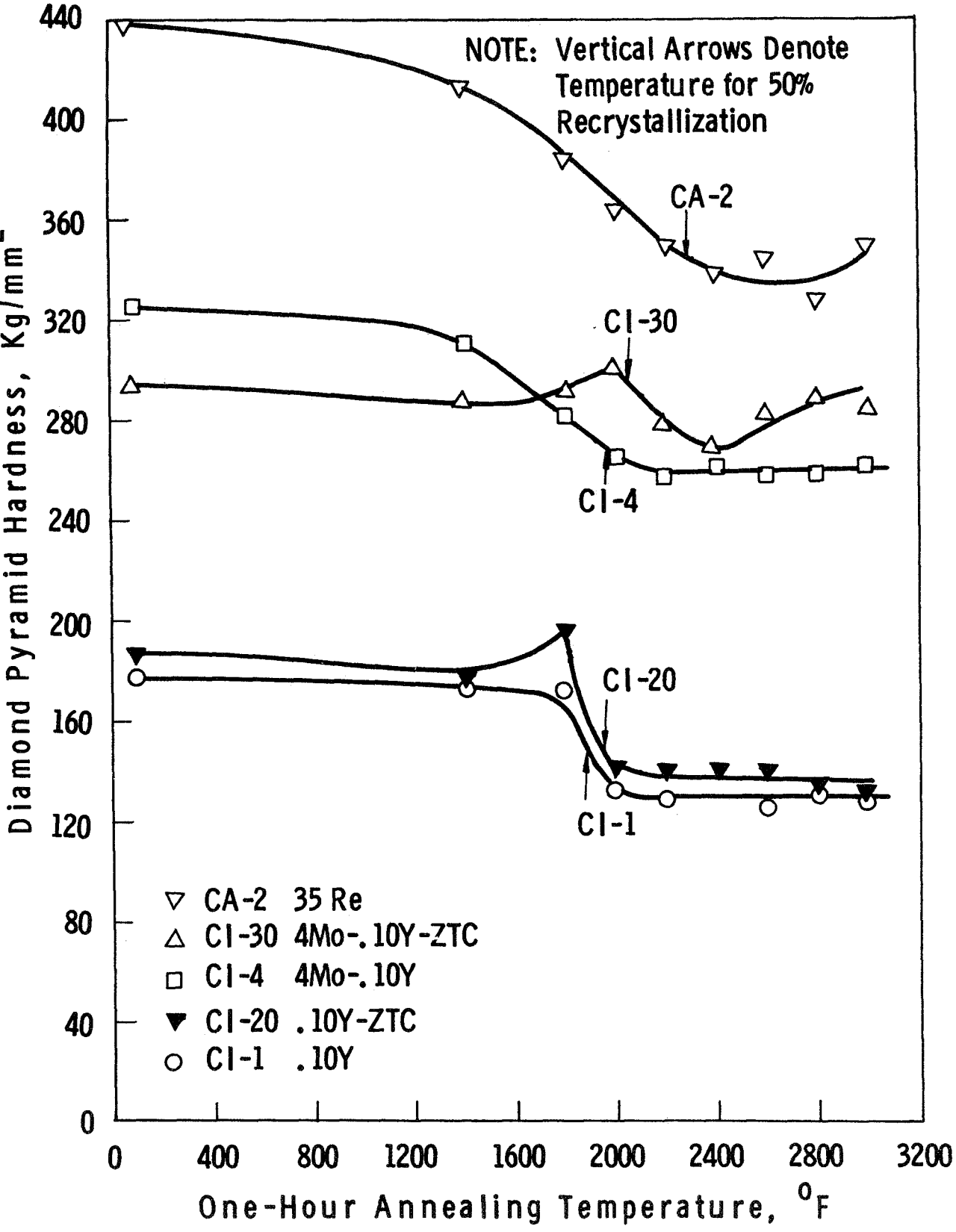

Figure 22. Effect of annealing on the microhardness and recrystallization of representative chromium alloys.

E6028 1000X

A. As Swaged

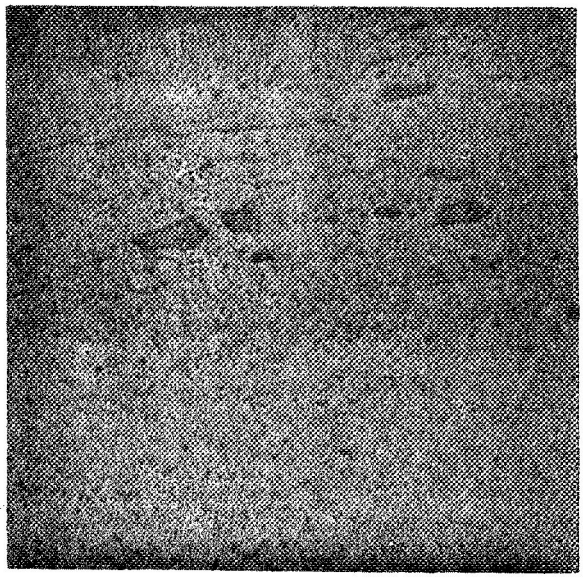

E6029 1000X

B. A + 2000°F, One Hour

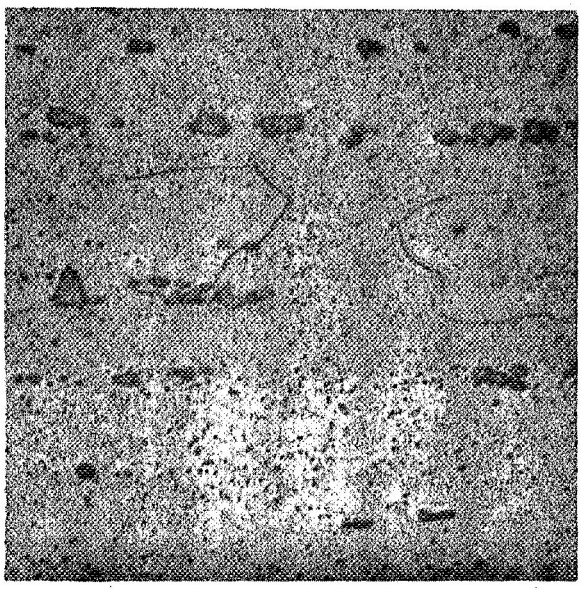

E6032 1000X

C. A + 2200°F, One Hour

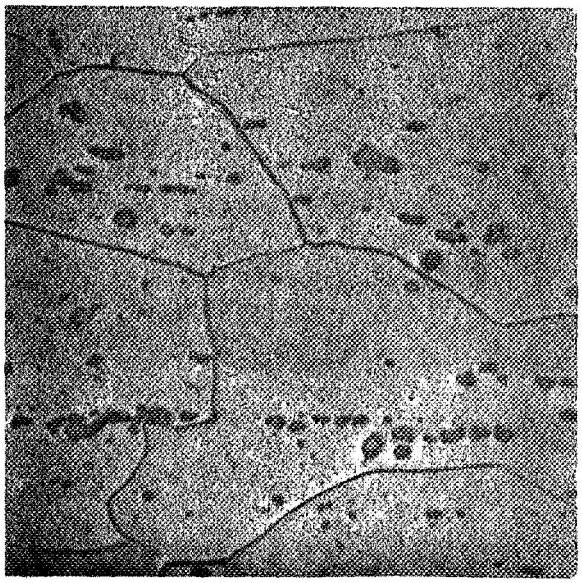

F722 1000X

D. A + 2400°F, One Hour

Figure 23. Effect of indicated annealing treatments on the distribution of carbides in alloy CI-37 (Cr-4Mo-.05Y-HZC). Etched in Kromic acid.

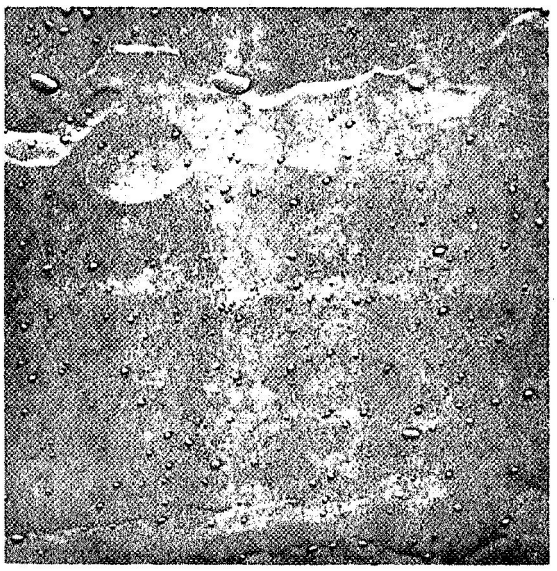

706E 5000X

A. CbC (CI-36)

706E 5000X

B. CbC (CI-36) Banded

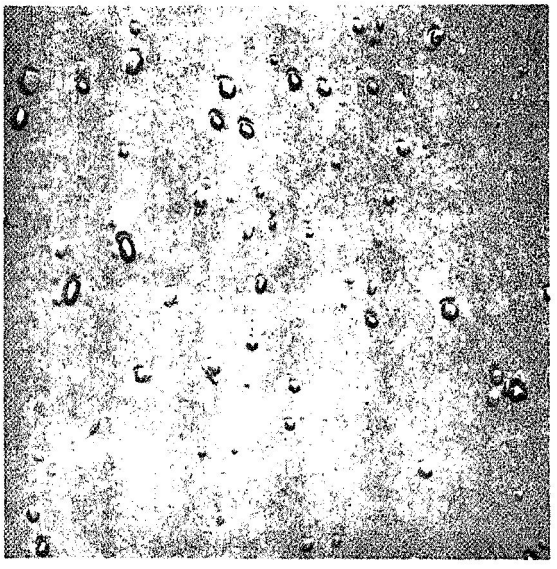

706C 20,000X

C. TaC (CI-41)

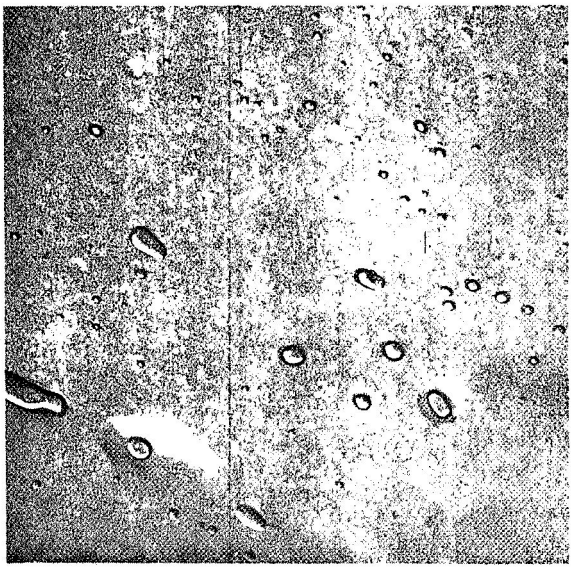

706D 5000X

D. (Hf,Zr)C (CI-37)

Figure 24. Electron micrographs of swaged Cr-4Mo-.05Y alloys containing indicated carbides.

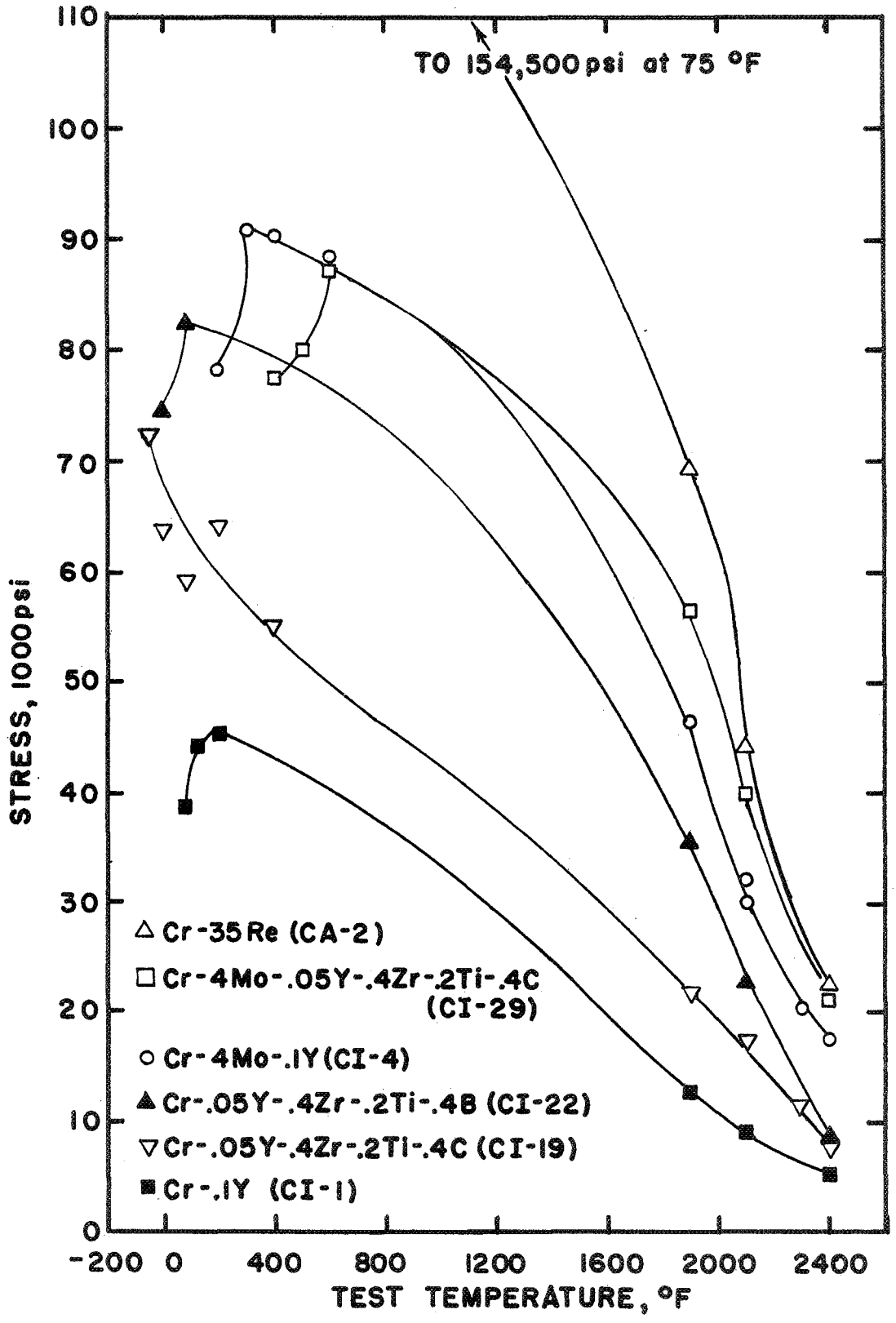

Figure 25. Tensile strengths of representative alloys in the stress-relieved condition.

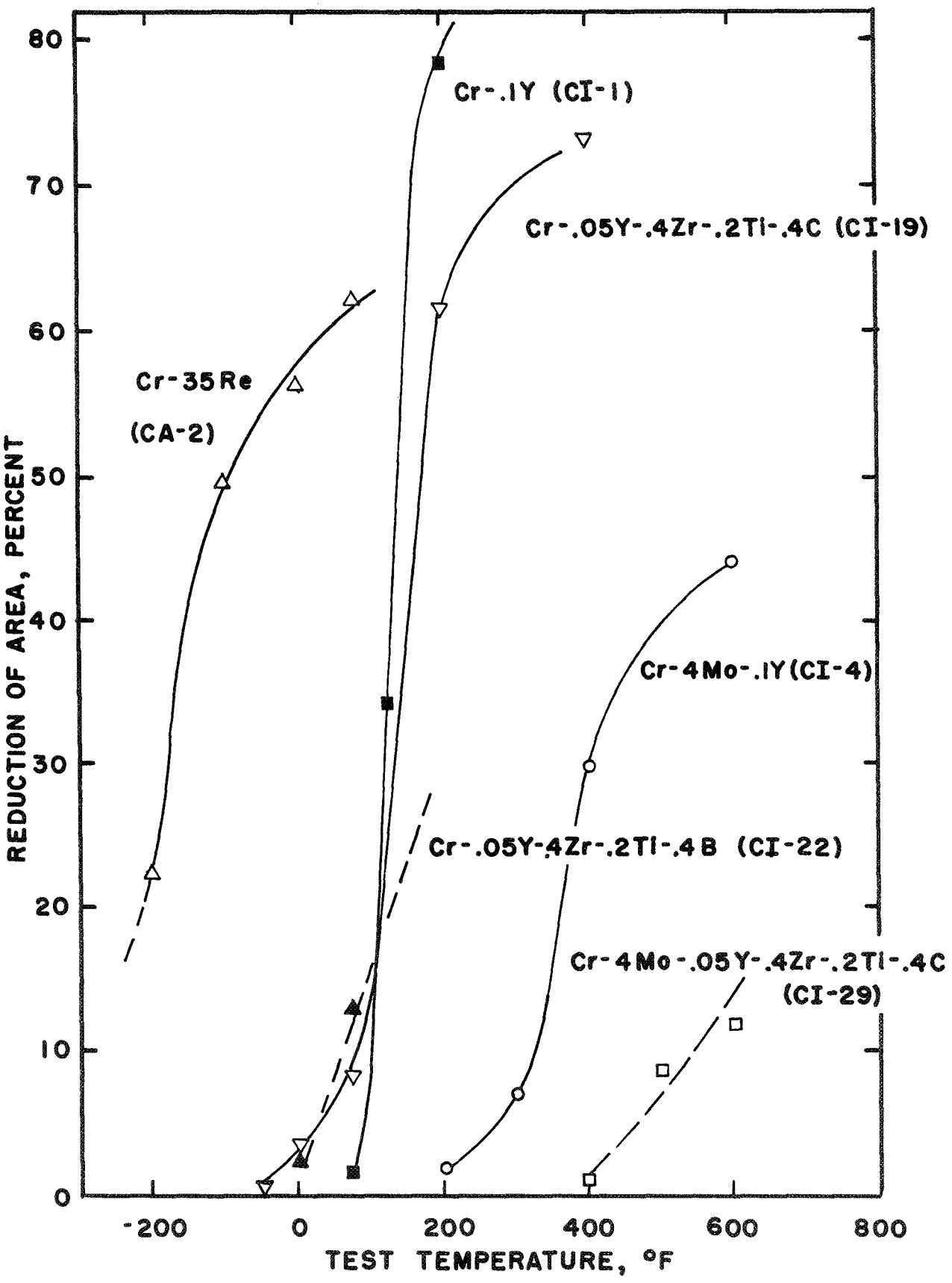

Figure 26. Tensile strengths of representative alloys after one-hour annealing at 2000°F.

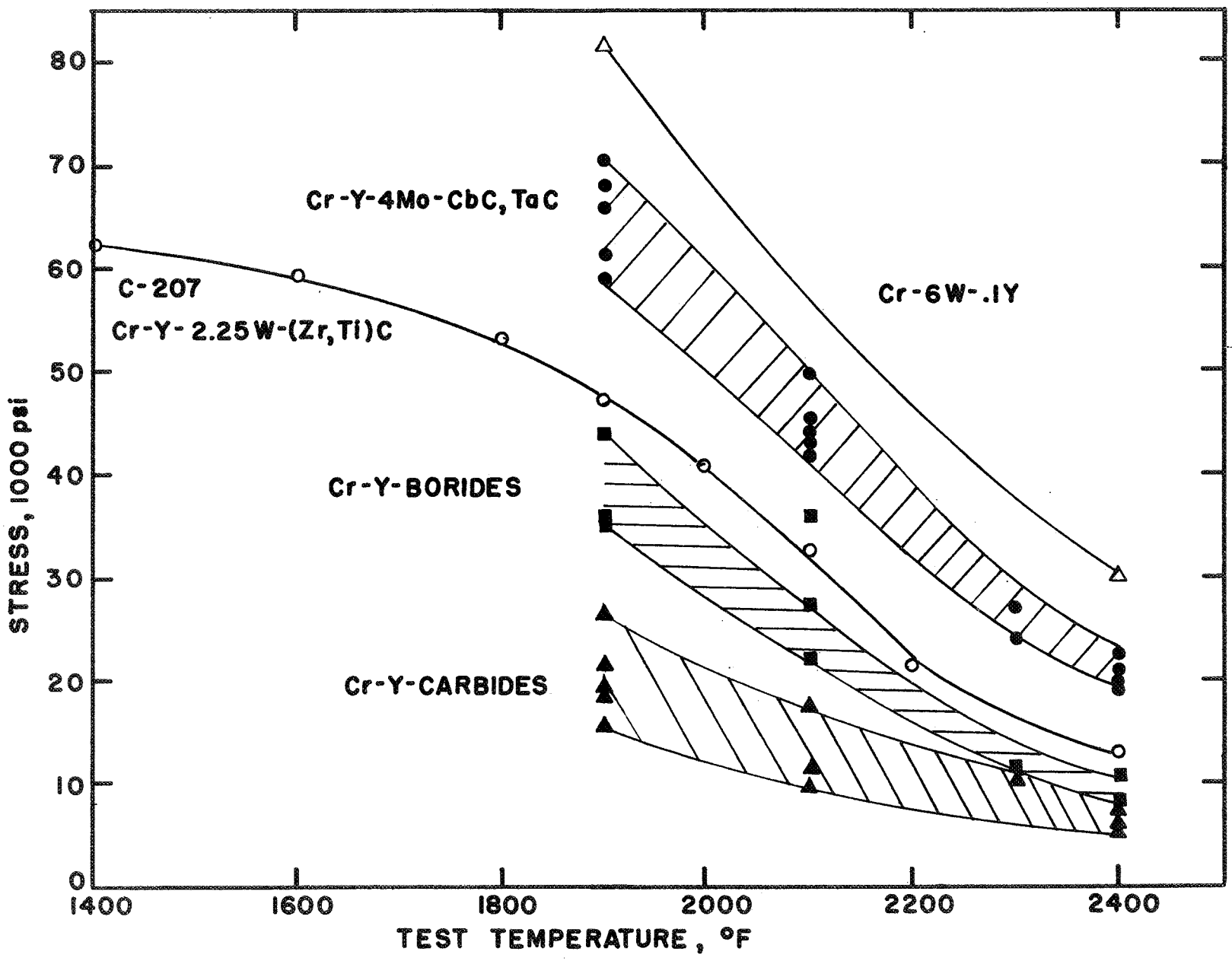

Figure 27. Elevated-temperature tensile strengths of selected chromium alloys in the stress-relieved condition.

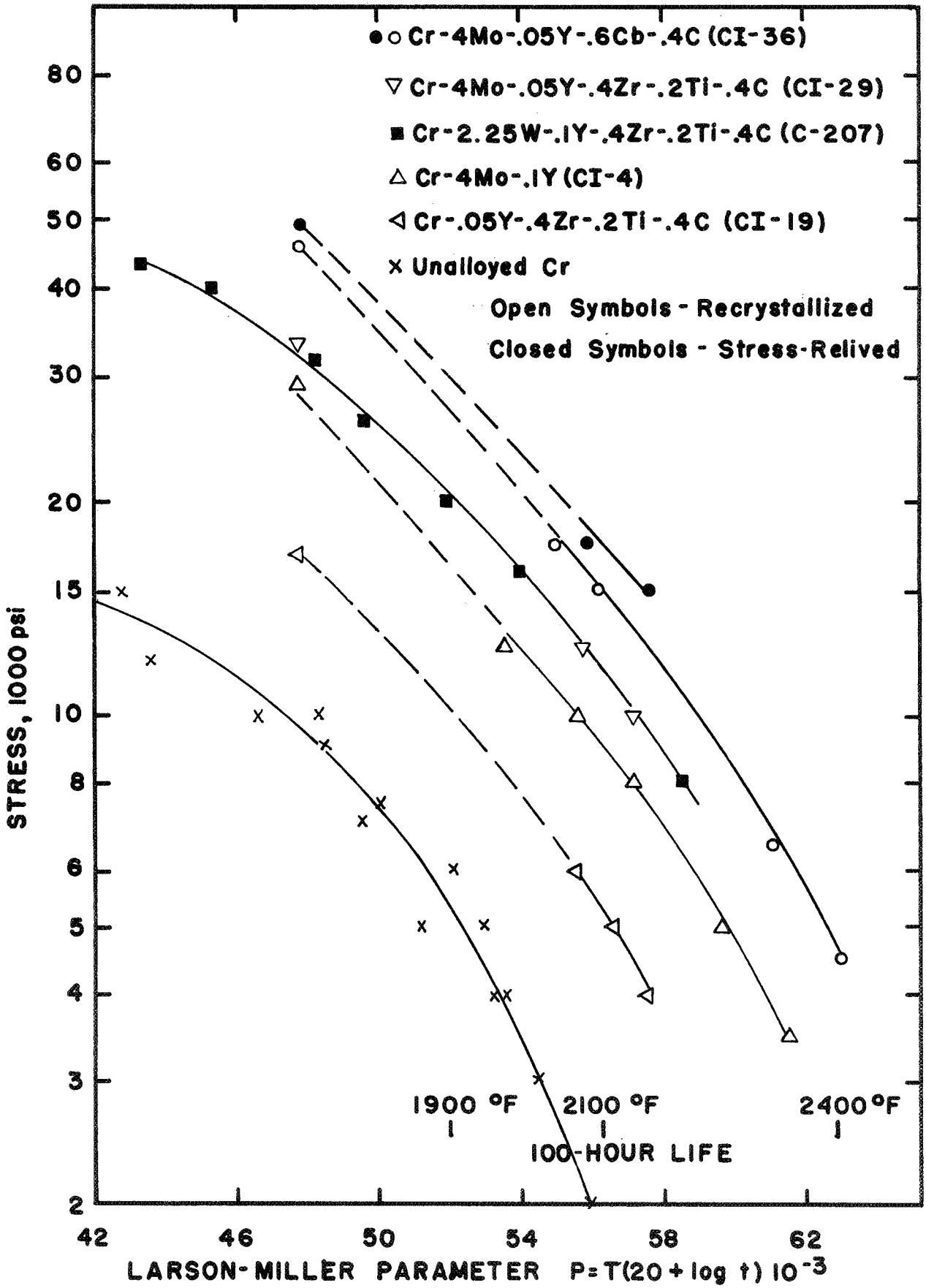

Figure 28. Stress-rupture properties of carbide-strengthened chromium alloys. Tested in helium at 2100° and 2400°F.

A. Adherent oxide, no nitride. CI-49, 25 hours at 2400°F

N1113 250X

B. No nitride, interaction with dispersion. CI-44, 100 hours at 2100°F

N1846 250X

C. Internal precipitation of nitride. CI-7, 100 hours at 2100°F

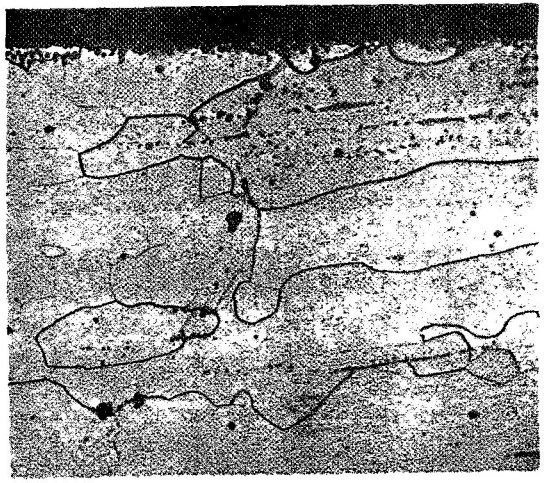

M2269 250X

D. Intergranular nitride. CI-17, 25 hours at 2400°F

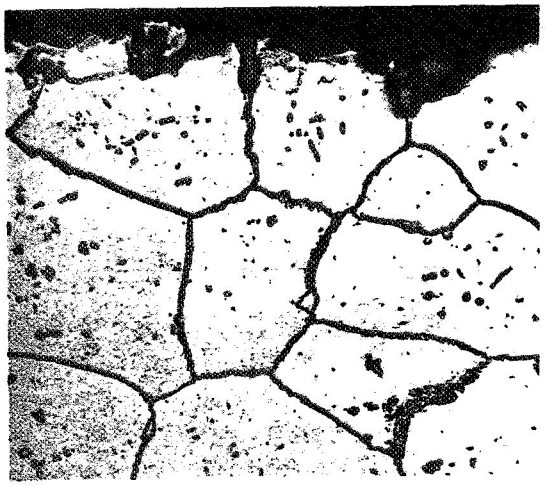

L5254 250X

E. Surface nitride layer. CI-47, 100 hours at 2100°F

N1108 250X

F. Intergranular oxide. CI 31, 100 hours at 2100°F

M2161 250X

Figure 29. Representative oxidation and nitridation characteristics of wrought chromium alloys. Etched Kromic acid.

APPENDIX A

TENSILE PROPERTIES OF WROUGHT CHROMIUM ALLOYS IN THE STRESS-RELIEVED CONDITION[a] ($\dot{\epsilon}$ = .03 PER MINUTE)

Alloy	Nominal Composition (At. %)	Test Temp (°F)	UTS (ksi)	.2% Offset (ksi)	Elong. (%)	R.A. %
CI-1	.1Y	75	38.8	38.0	1.5	1.5
		125	44.2	32.2	19.7	34.2
		200	45.4	28.1	59.2	78.3
		1900	12.4	8.4	67.1	96.5
		2100	9.1	6.0	60.8	94.3
		2400	5.2	3.4	58.2	96.0
CI-2	.2Y	75	42.9	42.0	0.4	1.7
		125	46.1	29.9	24.1	38.6
		200	42.3	31.3	58.7	76.8
		1900	9.3	5.8	63.1	95.1
		2400	4.2	3.4	69.4	95.6
CI-3	.1Y-.05Hf-.03Th	75	43.9	32.8	5.9	6.4
		125	44.3	36.2	38.8	61.5
		200	39.0	34.0	49.1	70.5
		1900	19.9	19.4	22.3	87.7
		2400	5.5	4.1	68.5	78.2
CI-4	4Mo-.1Y	200	78.3	73.3	1.0	1.7
		300	91.0	71.6	6.1	6.9
		400	90.6	69.4	18.4	29.9
		600	88.5	67.0	26.7	44.0
		1900	46.4	37.2	16.8	48.2
		2100	30.1	24.3	32.2	33.8
		2100	32.1	26.9	27.0	68.8
		2300	20.3	18.9	36.4	35.1
		2400	17.6	16.5	31.9	32.8
CI-5	6Mo-.1Y	2400	24.0	22.8	14.2	15.4

APPENDIX A (CONT'D)

Alloy	Nominal Composition (At. %)	Test Temp (°F)	UTS (ksi)	.2% Offset (ksi)	Elong. (%)	R.A. (%)
CI-7	4W-.1Y	400	67.6	67.6	0.2	0.8
		600	90.3	75.4	3.5	4.0
		600	92.1	74.8	7.2	7.1
		800	92.0	71.7	24.1	53.7
		1900	63.6	58.9	20.7	74.3
		2100	39.3	32.8	62.7	63.3
		2400	24.3	22.7	19.5	24.5
CI-8	6W-.1Y	1900	81.0	73.2	19.3	71.5
		2400	30.1	28.5	48.6	66.0
CI-9	4Mo-2W-.1Y	1900	54.5	40.5	8.7	8.7
		2400	23.3	19.9	6.8	8.5
CI-10	6Mo-2W-.1Y	2400	29.2	28.7	28.1	30.5
CI-14	10V-4Mo-.1Y	400	90.4	74.9	5.3	5.0
		600	91.5	72.1	19.2	33.5
		1900	68.9	59.7	22.0	75.1
		2400	22.8	22.0	17.3	22.4
CI-15	10V-4W-.1Y	600	97.3	81.8	6.4	6.2
		800	94.0	75.2	20.9	52.2
		1900	67.2	63.5	20.4	72.1
		2400	27.1	26.4	28.9	40.3
CI-16	4Re-.1Y	400	74.2	65.2	3.8	3.7
		500	81.4	61.0	10.4	10.7
		600	78.7	60.6	26.2	38.1
		1900	34.3	33.1	22.7	91.0
		2400	12.4	11.7	42.3	87.2
CI-17	4Co-.1Y	200	67.9	>67.9	0.1	0.0
		400	78.1	>78.1	0.0	0.0
		1900	21.7	20.5	75.7	81.5
		2400	4.9	4.1	128.0	90.0
CI-19	.05Y-.4Zr-.2Ti-.4C	-50	72.5	>72.5	0.0	0.0
		0	63.8	50.2	3.1	3.3
		75	59.4	38.6	8.0	8.2
		200	64.1	34.6	39.5	61.6
		400	54.9	30.3	43.5	73.0
		1900	21.7	19.2	30.0	87.5
		2100	17.4	15.0	28.1	89.7
		2300	11.3	9.2	49.3	96.0
		2400	7.9	6.3	55.8	95.5

APPENDIX A (CONT'D)

Alloy	Nominal Composition (At. %)	Test Temp (°F)	UTS (ksi)	.2% Offset (ksi)	Elong. (%)	R.A. (%)
CI-20	.1Y-.4Zr-.2Ti-.4C	-50	71.9	70.8	0.5	0.5
		0	61.7	50.3	6.4	6.3
		75	57.6	42.2	22.7	24.6
		1900	15.1	8.7	48.8	72.7
		2100	9.3	7.2	54.6	66.3
		2400	5.9	4.5	59.0	63.2
CI-21	.05Y-.3Hf-.3Zr-.4C	-50	67.7	67.0	0.8	0.8
		0	65.0	49.8	5.7	5.8
		75	71.5	45.5	21.3	24.2
		200	63.5	34.4	57.2	64.8
		400	54.7	33.1	60.8	70.7
		1900	36.5	35.0	30.2	86.5
		2100	11.7	11.3	45.9	88.7
		2400	5.9	5.0	94.2	91.5
CI-22	.05Y-.4Zr-.2Ti-.4B	0	74.9	71.8	2.0	2.4
		75	82.9	56.9	12.9	12.9
		1900	35.7	33.4	17.3	79.7
		2100	22.5	20.1	31.0	83.2
		2400	8.0	6.5	91.5	97.5
CI-23	.05Y-.3Hf-.3Zr-.4B	75	67.0	63.5	1.5	1.8
		125	70.8	55.2	8.4	8.1
		200	72.7	54.6	34.9	51.7
		1900	34.8	33.0	16.7	73.7
		2100	27.6	23.6	28.2	78.2
		2400	8.9	7.8	82.0	95.0
CI-24	.05Y-.4Ta-.2Zr-.4B	75	60.0	58.7	1.6	1.5
		200	66.0	54.8	3.5	3.5
		300	78.6	56.0	26.3	47.0
		1900	44.3	41.5	12.8	78.2
		2100	36.5	36.1	25.0	82.7
		2400	10.6	9.8	73.9	96.0
CI-26	4Mo-.1Y-.4Zr-.2Ti	400	36.9	>36.9	0.0	0.0
		600	76.7	49.3	6.8	6.8
		1900	54.9	44.8	22.8	61.9
		2100	35.1	28.8	48.0	51.5
		2400	20.1	19.5	40.5	43.1

APPENDIX A (CONT'D)

Alloy	Nominal Composition (At. %)	Test Temp (°F)	UTS (ksi)	.2% Offset (ksi)	Elong. (%)	R.A. (%)
CI-27	4Mo-.1Y-.3Hf-.3Zr	400	69.2	64.1	1.7	1.6
		500	74.2	52.2	5.6	5.4
		600	77.1	53.1	20.7	36.0
		1900	52.8	49.5	18.0	64.2
		2400	18.3	16.6	50.6	62.7
CI-28	4Mo-.1Y-.05Hf-.03Th	400	73.5	66.4	5.1	5.4
		600	82.8	64.1	28.0	49.3
		1900	49.7	42.2	17.4	49.5
		2400	18.1	17.4	21.2	24.8
CI-29	4Mo-.05Y-.4Zr-.2Ti-.4C	400	77.7	70.0	1.0	0.7
		500	80.1	67.5	8.6	8.5
		600	87.2	68.1	11.4	11.7
		1900	56.4	52.0	27.8	72.7
		2100	39.9	34.1	24.6	58.2
		2400	20.9	20.7	19.6	29.8
CI-30	4Mo-.1Y-.4Zr-.2Ti-.4C	400	68.6	59.7	1.6	1.8
		600	69.9	59.6	1.5	1.5
		600	84.7	61.2	6.9	7.1
		1900	47.8	41.3	14.9	29.8
		2100	35.4	28.4	22.1	36.5
		2300	24.2	20.5	22.4	25.4
		2400	18.8	15.9	23.9	31.8
CI-31	4Mo-.05Y-.5Zr-.25Ti-.4C	400	51.2	>51.2	0.0	0.0
		600	61.6	53.8	1.6	1.6
		600	69.8	56.4	7.3	7.2
		1900	46.7	32.8	23.9	45.8
		2400	19.8	19.1	18.5	23.4
CI-32	4Mo-.05Y-.3Zr-.15Ti-.4C	400	72.7	70.6	1.2	1.2
		500	78.8	61.4	5.4	5.3
		600	80.3	63.7	10.3	10.6
		1900	56.6	49.8	25.8	82.0
		2400	17.1	14.9	46.5	90.5
CI-33	4Mo-.05Y-.6Ti-.4C	400	77.0	77.0	0.2	0.2
		600	73.9	68.3	1.4	1.6
		600	78.1	67.6	2.1	2.0
		1900	59.0	54.5	27.4	76.2
		2100	42.7	40.5	42.3	86.1
		2400	22.8	22.7	43.8	79.7

APPENDIX A (CONT'D)

Alloy	Nominal Composition (At. %)	Test Temp (°F)	UTS (ksi)	.2% Offset (ksi)	Elong. (%)	R.A. (%)
CI-34	4Mo-.05Y-.6Zr-.4C	400	48.2	>48.2	0.1	0.4
		400	72.2	67.1	1.6	1.8
		600	75.5	63.2	8.9	9.0
		1900	45.5	28.4	32.9	51.7
		2100	31.7	26.1	21.4	39.8
		2400	18.7	17.1	24.5	30.2
CI-35	4Mo-.05Y-.6Hf-.4C	400	90.5	74.4	2.3	3.2
		500	97.1	73.3	5.8	5.8
		600	99.5	71.2	27.3	53.5
		1900	58.2	54.2	19.6	59.2
		2100	40.0	33.9	29.8	74.2
		2400	19.3	18.7	37.9	38.1
CI-36	4Mo-.05Y-.6Cb-.4C	300	102.7	91.6	3.1	3.3
		400	109.0	89.4	6.0	5.9
		600	111.0	79.3	10.8	13.1
		1900	65.7	61.2	30.0	84.6
		2100	49.6	46.3	26.3	91.1
		2400	21.8	21.6	68.0	96.0
CI-37	4Mo-.05Y-.3Hf-.3Zr-.4C	300	93.3	89.0	1.9	2.0
		400	104.0	84.7	4.1	5.8
		500	109.4	81.6	10.7	12.1
		600	104.5	77.2	28.2	48.0
		1900	61.0	57.2	26.2	71.7
		2100	39.2	31.9	41.7	75.7
		2300	23.5	21.0	56.4	56.7
		2400	20.7	19.7	46.2	50.2
CI-38	4Mo-.05Y-.6Zr-.3Ti-.6C	400	72.1	70.4	0.7	0.7
		600	88.0	63.4	5.8	5.7
		800	81.2	60.1	18.6	34.4
		1900	52.5	43.3	25.1	68.2
		2100	36.1	29.2	22.6	40.7
		2400	19.2	15.7	18.0	26.9
CI-39	4Mo-.05Y-.2Zr-.1Ti-.2C	400	72.5	67.0	1.5	1.4
		500	75.8	60.2	6.0	5.8
		600	78.2	58.9	20.8	49.3
		1900	50.3	38.1	38.7	76.2
		2100	38.4	32.9	30.6	79.1
		2400	19.9	19.1	35.4	34.8

APPENDIX A (CONT'D)

Alloy	Nominal Composition (At. %)	Test Temp (°F)	UTS (ksi)	.2% Offset (ksi)	Elong. (%)	R.A. (%)
CI-40	4Mo-.05Y-.4Ta-.2Zr-.4C	600	69.2	54.8	2.5	3.1
		700	79.9	56.1	12.2	21.7
		1900	49.0	42.0	20.8	71.1
		2100	40.8	36.9	24.1	50.3
		2400	20.5	20.4	22.6	36.8
CI-41	4Mo-.05Y-.6Ta-.4C	400	98.1	89.2	3.1	3.0
		500	106.3	85.0	8.7	9.0
		600	102.2	74.1	9.3	10.7
		1900	61.5	56.5	23.1	83.0
		2100	41.8	38.2	Failed out of gage	
		2400	18.7	14.6	66.6	96.5
CI-42	4Mo-.05Y-.4Cb-.2Zr-.4C	300	84.0	83.1	0.5	0.4
		400	92.1	80.7	5.1	5.0
		500	89.5	71.1	11.3	18.0
		1900	59.4	52.8	25.4	68.9
		2400	20.2	19.0	48.1	51.7
CI-43	4Mo-.2La-.4Cb-.2Zr-.4C	300	89.0	81.1	3.2	3.1
		400	89.2	75.3	8.2	8.4
		500	85.6	74.0	21.1	37.2
		1900	58.8	54.2	22.1	76.2
		2100	43.9	41.6	28.1	78.0
		2400	21.0	19.9	53.8	94.5
CI-44	6Mo-.05Y-.4Zr-.2Ti-.4C	600	90.1	>90.1	0.0	0.0
		700	120.1	83.4	5.5	5.4
		800	116.3	80.2	10.8	16.3
		1900	64.8	62.0	16.7	34.2
		2400	27.0	26.9	20.6	23.6
CI-45	4W-.15(La + Y)-.3Ta-.3Hf-.4C	600	96.1	>96.1	0.0	0.0
		700	126.2	92.2	6.0	5.8
		800	120.4	89.4	14.1	20.7
		1900	84.1	76.2	18.4	32.7
		2400	30.6	26.0	22.4	23.3
CI-46	2W-2Mo-.15(La + Y)-.3Ta-.3Hf-.4C	600	93.2	92.0	1.6	1.8
		700	109.4	89.0	7.1	7.4
		800	115.1	87.5	25.4	42.7
		1900	70.9	69.8	16.1	55.4
		2400	19.8	19.2	46.0	60.9

Alloy	Nominal Composition (At. %)	Test Temp (°F)	UTS (ksi)	.2% Offset (ksi)	Elong. (%)	R.A. (%)
CI-47	2W-2Mo-.15(La + Y)-.6Ta-.4C	500	103.1	96.0	5.1	5.0
		600	122.0	96.3	13.6	12.4
		800	107.0	93.9	22.4	56.1
		1900	70.3	66.4	22.0	69.9
		2400	21.0	19.6	50.2	54.6
CI-48	4Re-.15(La + Y)-.3Ta-.3Hf-.4C	75	99.2	80.7	5.2	6.5
		200	98.0	74.8	10.6	13.1
		500	92.6	70.1	14.5	24.7
		600*	77.4	65.3	6.1	5.9
		1900	46.8	44.9	20.8	54.0
		2400	14.6	12.7	38.3	52.0
CI-49	2W-2Mo-.15(La + Y)-.6Hf-.4C	400	98.3	74.8	4.7	5.2
		500	99.1	71.3	14.7	26.3
		1900	46.9	42.7	13.4	35.8
		2400	20.1	18.8	25.4	31.8
CI-50	.15(La + Y)-.6Hf-.4C	0	78.7	78.2	0.8	0.8
		75	75.3	55.4	24.6	28.7
		1900	19.0	18.1	19.7	81.1
		2400	5.5	4.9	75.2	88.6
CI-51	.1Y-.03Th-.6Hf-.4C	-50	80.9	79.8	1.1	1.1
		0	83.2	71.2	7.4	7.2
		75	71.7	45.3	48.4	57.0
		1900	18.6	18.1	29.1	26.4
		2400	5.0	3.5	66.4	86.1
CI-52	20V-5W-.15(La + Y)	400	114.0	102.0	1.6	1.4
		500	132.7	110.6	3.7	3.7
		600	141.5	107.5	18.7	34.9
		1900	73.4	68.7	28.1	44.3
		2100	52.1	48.0	20.3	29.2
		2400	31.0	26.5	13.2	15.2
CI-54	4Mo-.15(La + Y)-.6Ta-.4Hf-.8C	600	90.6	82.1	1.7	1.6
		700	95.3	77.4	5.2	5.0
		800	107.1	74.9	26.9	49.3
		1900	68.2	61.1	32.4	40.8
		2400	20.7	19.3	12.4	20.6

* Defective specimen, failed outside gage.

APPENDIX A (CONCL'D)

Alloy	Nominal Composition (At. %)	Test Temp (°F)	UTS (ksi)	.2% Offset (ksi)	Elong. (%)	R.A. (%)
CI-56	4Mo-.15(La + Y)-.3Ta-.3Hf-.2C-.2B	600	101.7	85.6	3.3	3.3
		700	110.5	80.1	15.2	28.8
		1900	71.0	65.1	23.7	72.1
		2400	22.3	18.8	62.9	96.0
CI-57	4Mo-.15(La + Y)-.8Hf-.2C-.2B-.2Si	1900	58.2	52.1	22.8	70.4
		2100	42.3	34.6	37.6	64.5
		2400	18.1	17.4	40.7	42.0
CI-58	4Mo-.15(La + Y)-.6Cb-.2C-.2N	500	83.4	82.0	1.0	0.9
		600	99.6	79.9	7.3	7.8
		800	106.6	77.3	24.3	44.5
		1900	67.8	62.3	26.2	65.2
		2100	45.2	43.3	31.5	64.5
		2400	21.6	19.5	33.0	59.6
CI-60	4Mo-.15(La + Y)-.3Ta-.3Ti-.4C	400	59.2	-	0.0	0.0
		600	81.4	63.9	3.0	3.4
		700	92.6	62.5	18.4	30.7
		1900	45.2	29.8	33.9	66.0
		2100	34.7	27.2	36.8	58.0
		2400	19.9	19.3	32.2	51.0
CI-61	4Mo-.15(La + Y)-.3Cb-.3Ti-.4C	400	75.8	59.3	3.3	4.1
		500	83.6	59.0	5.4	6.2
		600	81.0	57.3	6.5	9.4
		1900	42.6	29.0	36.7	67.7
		2400	18.6	18.3	49.4	63.7
CA-1	Unalloyed Cr	75	38.4	-	0.0	0.0
		125	39.7	42.2[b]	4.5	4.3
				35.2[b]		
		200	36.2	32.3[b]	54.7	81.8
				26.1[b]		
		400	31.2	23.7[b]	71.1	88.8
				18.2[b]		
		1900	7.0	3.1	92.5	96.5
		2100	4.3	2.4	84.4	97.1
		2400	2.5	1.0	76.0	99.0
CA-2	35Re	-200	199.7	179.3	20.5	22.3
		-100	188.3	154.8	44.5	49.6
		0	168.1	137.1	45.1	56.2
		75	154.5	125.2	48.7	62.1
		1900	69.7	63.2	16.0	28.8
		2100	39.2	35.3	27.3	32.1
		2400	22.3	17.0	39.1	45.8

[a] Unalloyed Cr annealed 1600°F - 1 hour, all others 2000°F - 1 hour.

[b] Upper and lower yield points.

APPENDIX B

TENSILE PROPERTIES OF WROUGHT CHROMIUM ALLOYS IN THE RECRYSTALLIZED CONDITION[a] ($\dot{\varepsilon}$ = .03 PER MINUTE)

Alloy	Nominal Composition (At. %)	Test Temp (°F)	UTS (ksi)	.2% Offset (ksi)	Elong. (%)	R.A. (%)
CI-1	.1Y	75	32.7	-	0.0	0.0
		125	40.6	22.4	6.7	6.4
		200	43.9	17.0	63.8	69.8
		1900	11.5	8.2	64.2	97.5
		2100	8.8	5.9	65.1	96.5
		2400	5.1	3.7	63.4	98.0
CI-2	.2Y	0	36.2	29.3	3.1	3.0
		75	49.3	28.0	13.3	17.8
		200	44.5	21.1	67.1	72.5
		1900	9.6	4.6	58.6	94.5
		2400	4.2	2.7	72.2	95.0
CI-3	.1Y-.05Hf-.03Th	0	43.7	42.5	1.2	0.8
		75	48.8	22.1	9.3	15.3
		1900	13.2	8.9	46.3	86.0
		2400	5.3	4.0	52.1	81.2
CI-4	4Mo-.1Y	400	72.5	55.0	3.2	3.4
		500	73.0	49.0	11.8	12.3
		600	75.2	43.4	23.2	53.5
		1900	38.9	25.1	18.9	28.5
		2100	29.8	23.5	30.0	33.0
		2100	30.0	22.1	24.0	27.8
		2300	21.2	18.0	27.1	34.3
		2400	16.8	15.9	31.5	38.5
CI-5	6Mo-.1Y	1900	48.5	32.2	16.5	21.7
CI-7	4W-.1Y	700	92.5	68.0	5.4	5.2
		800	76.3	52.4	28.4	49.7
		1900	49.6	34.8	32.3	79.0
		2100	39.6	29.4	28.8	73.3
		2400	23.3	21.2	28.6	38.8
CI-8	6W-.1Y	1900	60.2	45.1	24.6	52.7

APPENDIX B (CONT'D)

Alloy	Nominal Composition (At. %)	Test Temp (°F)	UTS (ksi)	.2% Offset (ksi)	Elong. (%)	R.A. (%)
CI-9	4Mo-2W-.1Y	1900	45.0	33.9	18.1	24.6
CI-10	6Mo-2W-.1Y	1900	57.3	41.2	22.6	23.0
CI-14	10V-4Mo-.1Y	600	80.1	60.3	5.1	5.7
		800	71.4	49.7	26.1	45.5
		1900	45.5	31.6	26.7	43.9
		2400	19.2	18.3	30.2	36.1
CI-15	10V-4W-.1Y	400	83.2	73.5	2.1	2.0
		600	98.3	71.4	12.6	19.7
		1900	51.7	37.0	25.3	50.2
		2400	25.1	23.7	20.8	36.4
CI-16	4Re-.1Y	400	61.6	52.1	2.7	2.6
		600	70.3	38.4	19.4	48.3
		1900	29.2	23.1	19.6	75.1
		2400	12.1	10.1	34.3	40.7
CI-17	4Co-.1Y	200	101.5	-	0.0	0.0
		400	87.8	87.8	0.2	0.5
		600	77.2	74.3	1.6	1.6
		1900	18.9	18.5	66.4	91.0
		2400	4.4	3.2	100 +	-
CI-19	.05Y-.4Zr-.2Ti-.4C	-50	72.5	-	0.0	0.0
		0	60.7	47.5	2.1	2.1
		75	59.2	31.2	10.0	11.7
		1900	22.7	14.2	38.0	87.0
		2100	17.0	11.1	58.9	91.3
		2400	7.3	4.6	72.3	97.5
CI-20	.1Y-.4Zr-.2Ti-.4C	-50	48.8	42.6	1.8	1.7
		0	47.2	36.3	5.1	5.0
		75	58.3	23.8	16.4	24.8
		1900	14.3	9.1	52.2	78.0
		2400	5.5	4.0	77.8	90.5
CI-21	.05Y-.3Hf-.3Zr-.4C	0	52.8	33.7	2.7	2.5
		75	52.1	20.0	7.9	7.9
		200	50.7	15.6	37.1	45.0
		1900	15.2	10.8	43.3	84.5
		2100	10.0	9.0	61.4	84.6
		2400	5.5	4.4	73.2	95.5

APPENDIX B (CONT'D)

Alloy	Nominal Composition (At. %)	Test Temp (°F)	UTS (ksi)	.2% Offset (ksi)	Elong. (%)	R.A. (%)
CI-22	.05Y-.4Zr-.2Ti-.4B	0	54.7	40.8	3.7	3.7
		75	64.0	25.8	13.5	15.3
		1900	25.2	13.5	29.0	82.2
		2100	19.1	12.2	52.4	90.6
		2400	8.2	7.4	80.8	97.0
CI-23	.05Y-.3Hf-.3Zr-.4B	0	54.1	-	0.0	0.0
		75	60.2	38.4	3.6	3.4
		125	64.3	32.1	8.4	9.7
		1900	24.0	15.9	26.6	79.6
		2400	8.0	7.4	81.5	96.0
CI-24	.05Y-.3Ta-.4Ta-.2Zr-.4B	0	64.2	-	0.0	0.0
		75	60.8	27.4	7.2	9.1
		75	59.6	33.2	4.8	4.8
		125	61.2	26.9	12.9	19.3
		1900	28.3	19.6	34.4	85.4
		2100	25.5	15.3	43.8	82.6
		2400	10.2	9.0	72.2	98.0
CI-26	4Mo-.1Y-.4Zr-.2Ti	400	60.2	>60.2	0.0	0.0
		600	56.4	46.7	1.8	2.3
		800	72.7	41.8	21.3	38.4
		1900	47.7	30.2	35.3	58.7
		2100	30.4	26.3	42.7	60.9
		2400	18.1	17.5	52.4	56.5
CI-27	4Mo-.1Y-.3Hf-.3Zr	400	62.9	61.8	0.8	0.8
		500	76.2	51.4	4.7	5.1
		600	73.4	52.6	6.9	6.9
		1900	48.2	35.7	33.2	53.7
		2100	29.6	26.0	40.1	63.8
		2400	17.5	16.9	50.9	54.8
CI-28	4Mo-.1Y-.05Hf-.03Th	400	64.9	56.3	1.8	1.8
		500	72.4	50.3	5.6	5.4
		600	69.2	47.7	12.4	13.1
		1900	37.1	27.0	20.3	34.2
		2400	16.2	15.8	18.4	23.8

APPENDIX B (CONT'D)

Alloy	Nominal Composition (At. %)	Test Temp (°F)	UTS (ksi)	.2% Offset (ksi)	Elong. (%)	R.A. (%)
CI-29	4Mo-.05Y-.4Zr-.2Ti-.4C	400	69.3	66.8	0.8	0.8
		500	73.1	57.1	3.8	3.5
		600	75.4	53.2	7.2	7.4
		1900	45.7	36.1	24.0	68.1
		2100	33.6	29.4	33.8	61.2
		2400	19.0	18.4	40.1	52.7
CI-30	4Mo-.1Y-.4Zr-.2Ti-.4C	400	70.2	48.0	3.9	3.9
		500	76.2	47.3	4.8	5.2
		600	73.5	46.2	5.7	6.8
		1900	37.9	28.0	23.8	30.5
		2100	32.1	26.0	23.1	36.7
		2400	19.2	17.9	25.7	33.8
CI-31	4Mo-.05Y-.5Zr-.25Ti-.4C	400	63.8	59.7	1.5	1.4
		600	74.1	46.1	5.5	5.3
		700	69.2	44.3	17.4	28.9
		1900	45.3	31.8	21.6	40.5
		2400	18.8	17.7	25.3	33.8
CI-32	4Mo-.05Y-.3Zr-.15Ti-.4C	400	68.3	55.1	2.4	2.4
		500	79.4	51.3	8.8	8.5
		600	75.1	48.3	23.8	46.2
		1900	50.1	37.2	28.9	50.3
		2400	16.7	16.2	32.4	41.4
CI-33	4Mo-.05Y-.6Ti-.4C	400	79.0	55.6	3.2	3.8
		600	66.0	54.3	2.8	3.3
		600	78.1	56.1	7.1	8.0
		700	70.9	52.6	14.8	22.7
		1900	49.4	36.2	40.6	83.6
		2100	37.0	33.1	45.2	85.0
		2400	21.8	21.6	58.0	88.5
CI-34	4Mo-.05Y-.6Zr-.4C	400	61.9	57.2	1.7	1.5
		600	65.0	46.8	5.1	4.6
		700	63.7	42.0	10.9	13.2
		1900	45.3	27.5	27.7	49.3
		2400	22.2	21.7	36.1	45.8

APPENDIX B (CONT'D)

Alloy	Nominal Composition (At. %)	Test Temp (°F)	UTS (ksi)	.2% Offset (ksi)	Elong. (%)	R.A. (%)
CI-35	4Mo-.05Y-.6Hf-.4C	400	58.1	56.2	0.4	0.4
		400	77.8	50.8	4.3	4.0
		500	77.5	50.2	4.8	5.1
		600	79.1	43.3	10.4	9.3
		1900	45.8	28.3	34.8	63.0
		2100	30.0	26.1	40.7	58.2
		2400	17.5	16.6	50.3	63.2
CI-36	4Mo-.05Y-.6Cb-.4C	300	93.3	88.2	2.0	2.5
		400	97.2	83.4	5.5	5.1
		500	92.1	78.0	10.6	16.4
		1900	61.0	50.5	30.5	86.0
		2100	46.2	43.1	39.8	90.7
		2400	19.0	18.0	60.7	96.5
CI-37	4Mo-.05Y-.3Hf-.3Zr-.4C	400	77.4	54.8	4.1	3.9
		500	79.0	51.3	6.0	5.5
		600	73.0	53.7	5.5	5.5
		600	76.2	49.9	12.9	19.4
		1900	50.3	31.2	36.4	71.5
		2100	35.1	29.0	42.6	65.2
		2400	19.4	18.9	60.0	60.2
CI-38	4Mo-.05Y-.6Zr-.2Ti-.6C	500	69.2	64.3	1.2	1.1
		600	81.0	57.3	5.8	5.4
		700	75.1	52.8	10.7	14.2
		1900	47.1	34.7	22.7	24.9
		2400	20.4	19.1	19.2	21.3
CI-39	4Mo-.05Y-.2Zr-.1Ti-.2C	400	69.7	62.7	1.5	1.4
		500	73.3	58.8	6.4	5.9
		600	74.2	52.6	9.3	13.7
		1900	49.4	33.5	37.0	79.7
		2400	19.6	19.4	34.9	55.5
CI-40	4Mo-.05Y-.4Ta-.2Zr-.4C	300	66.2	>66.2	0.1	0.0
		400	80.7	64.7	4.8	5.0
		600	75.9	53.1	13.6	27.1
		1900	46.2	32.2	30.2	65.5
		2400	22.0	21.7	19.4	34.8

APPENDIX B (CONT'D)

Alloy	Nominal Composition (At. %)	Test Temp (°F)	UTS (ksi)	.2% Offset (ksi)	Elong. (%)	R.A. (%)
CI-41	4Mo-.05Y-.6Ta-.4C	400	84.1	76.4	3.2	3.0
		500	89.8	72.1	8.2	9.0
		600	85.3	69.0	15.5	24.8
		1900	61.9	54.5	22.4	81.2
		2100	47.3	44.8	32.6	88.9
		2400	20.4	18.2	53.1	96.5
CI-46	2W-2Mo-.15(La + Y)-.3Ta-.3Hf-.4C	1900	49.0	33.5	34.3	31.8
		2400	21.3	19.9	21.1	26.9
CI-47	2W-2Mo-.15(La + Y)-.6Ta-.4C	1900	62.2	48.0	27.9	73.6
		2400	23.4	21.7	45.7	72.6
CI-48	4Re-.15(La + Y)-.3Ta-.3Hf-.4C	1900	37.3	25.0	31.4	49.7
		2400	15.1	14.2	41.8	57.7
CI-49	2W-2Mo-.15(La + Y)-.6Hf-.4C	1900	47.8	30.9	27.9	44.8
		2400	19.1	18.3	30.2	36.8
CI-50	.15(La + Y)-.6Hf-.4C	1900	18.0	13.1	45.1	74.2
		2400	5.5	4.5	73.7	91.6
CI-51	.1Y-.03Th-.6Hf-.4C	1900	17.5	10.6	44.7	79.1
		2400	5.0	3.8	86.3	89.4
CI-52	20V-5W-.15(La + Y)	1900	53.7	39.9	23.4	43.8
		2400	27.7	26.4	13.3	17.9
CI-58	4Mo-.15(La + Y)-.6Cb-.2C-.2N	1900	54.0	36.9	46.8	69.8
		2100	38.2	31.8	51.8	57.2
		2400	20.0	19.6	46.9	47.3
CI-60	4Mo-.15(La + Y)-.3Ta-.3Ti-.4C	400	69.5	44.0	3.2	4.2
		600	72.0	41.0	8.7	8.5
		1900	43.7	30.4	36.0	49.8
		2100	36.5	26.1	34.2	42.7
		2400	21.4	20.9	32.2	39.9
CI-61	4Mo-.15(La + Y)-.3Cb-.3Ti-.4C	400	78.4	55.0	3.0	5.1
		600	69.0	43.3	5.7	5.9
		1900	46.8	31.7	38.0	51.6
		2400	20.2	19.6	36.7	42.1

Alloy	Nominal Composition (At. %)	Test Temp (°F)	UTS (ksi)	.2% Offset (ksi)	Elong. (%)	R.A. (%)
CA-1	Unalloyed Cr	75	42.7	-	0.0	0.0
		200	35.3	-	0.0	0.0
		300	29.2	-	0.0	0.0
		400	33.5	24.1[b] 16.6[b]	12.3	12.0
		500	28.1	34.8[b] 18.6[b]	74.7	94.2
		1900	7.2	3.2	93.6	94.4
		2400	2.7	1.3	70.3	98.5
CA-2	35Re	-100	174.6	148.0[b] 137.1[b]	21.6	39.2
		0	157.0	128.4[b] 122.6[b]	28.0	50.1
		75	142.4	112.1[b] 105.0[b]	30.4	71.6
		1900	53.6	48.3	24.7	33.6
		2100	34.2	30.6	34.4	39.8
		2400	21.8	18.1	42.4	50.3

[a] Unalloyed Cr annealed 2000°F - 1 hour, CI-36 at 2500°F - 1 hour, all others 2400°F - 1 hour.

[b] Upper and lower yield points.

REFERENCES

1. R. M. Parke and F. P. Bens, "Chromium Base Alloys" ASTM Symposium on Materials for Gas Turbine Engines", p. 80, ASTM, Philadelphia, 1946.

2. A. H. Sully, Chromium, Academic Press, New York, 1954.

3. J. W. Clark, "Properties of Dilute, Carbide-Strengthened Chromium Alloys" General Electric Report R62FPD285, February 1963.

4. C. T. Sims and J. W. Clark, "Carbide-Strengthened Chromium Alloys" Trans. Met. Soc. AIME 230 (1964) p. 1168.

5. W. H. Chang, "Influence of Heat Treatment on Microstructure and Properties of Columbium-Base and Chromium-Base Alloys", ASD Technical Documentary Report 62-211, Part 4, March 1966.

6. G. R. Wilms and T. W. Rea, "The Tensile Creep Properties of Some Extruded Chromium Alloys" J. Less-Comm. Metals 6 (1964) p. 184.

7. N. E. Ryan and G. R. Wilms, "The Effect of a Tantalum Carbide Dispersion on the High-Temperature Properties of Chromium", J. Less-Comm. Metals 6 (1964) p. 201.

8. N. E. Ryan, "The Formation, Stability, and Influence of Carbide Dispersions in Chromium", J. Less-Comm. Metals 11 (1966) p. 221.

9. J. W. Clark, "Preparation and Properties of a Carbide Strengthened Cr-W-Y Alloy (C-207)" General Electric Report R64FPD119, April 1964.

10. J. W. Clark and W. H. Chang, "New Chromium Alloys" paper presented at AIME High-Temperature Materials Symposium, New York, February 1966.

11. W. H. Smith and A. U. Seybolt, "Effects of Impurities on the Ductility of Chromium" Chapter 13 in Ductile Chromium and Its Alloys ASM, Cleveland, 1957.

12. J. A. McGurty, J. F. Collins, and V. P. Calkins, U. S. Patent 2,955,937, October 1960.

13. J. E. Fox and J. A. McGurty, "Chromium and Chromium-Base Alloys", p. 207 in Refractory Metals and Alloys, Interscience, New York, 1961.

14. C. S. Wukusick, "Research on Chromium-Base Alloys . . .", ASD Technical Documentary Report 63-493, June 1963.

15. G. T. Hahn, A. Gilbert, and R. I. Jaffee, "The Effects of Solutes on the Ductile-to-Brittle Transition in Refractory Metals", p. 23 in Refractory Metals and Alloys II, Interscience, New York, 1963.

16. C. S. Wukusick, "Evaluation of Chromium-Ruthenium Alloys" General Electric Report GEMP-362, June 1965.

17. C. S. Wukusick, "The Rhenium Ductilizing Effect" paper presented at AIME Refractory Metals Symposium, French Lick, Indiana, October 1965.

18. G. T. Hahn and A. R. Rosenfield, "Effects of Second-Phase Particles on Ductility" AFML Technical Report 65-409, January 1966.

19. M. Hansen and K. Anderko, Constitution of Binary Alloys, 2nd Edition, McGraw-Hill, New York, 1958.

20. J. J. English, "Binary and Ternary Phase Diagrams of Cb, Mo, Ta, and W" DMIC Report 152, April 1961.

21. R. F. Domagala, "A Study of the Solubility of Zr in Cr", Trans. ASM 56 (1963) p. 878.

22. H. J. Goldschmidt and J. A. Brand, "The Constitution of the Chromium-Niobium-Silicon System" J. Less-Comm. Metals 3 (1961) p. 34.

23. C. E. Lundin, "Rare-Earth Metal Phase Diagrams" Chapter 16 in The Rare Earths, John Wiley & Sons, New York 1961.

24. R. P. Elliott, Constitution of Binary Alloys, First Supplement, Mc-Graw-Hill, New York, 1965.

25. W. C. Hagel, "Factors Controlling the High-Temperature Oxidation of Chromium" Trans. ASM 56 (1963) p. 583.

26. E. J. Felten, "High-Temperature Oxidation of Fe-Cr Base Alloys with Particular Reference to Fe-Cr-Y Alloys", J. Electrochem. Soc. 108 (1961) p. 490.

27. A. U. Seybolt, "High-Temperature Oxidation of Chromium Containing Y_2O_3", Corrosion Science 6 (1966) p. 263.

28. D. J. Maykuth and A. Gilbert, "Chromium and Chromium Alloys", DMIC Report 234, October 1966.

29. J. W. Pugh, "The Tensile and Stress-Rupture Properties of Chromium", Trans. ASM 50 (1958) p. 1072.

30 D. Caplan and M. Cohen, "The Volatilization of Chromium Oxide" J. Electrochem Soc. 108, (1961) p. 438.

31. C. S. Tedmon, Jr., "The Effect of Oxide Volatilization on the Oxidation Kinetics of Cr and Fe-Cr Alloys", J. Electrochem. Soc. 113 (1966) p. 766.